2014

Behavior of dowels in concrete pavements

Eric Andrew Lorenz
Iowa State University

Behavior of dowels in concrete pavements

by

Eric Andrew Lorenz

A dissertation submitted to the graduate faculty

in partial fulfillment of the requirements for the degree of

DOCTOR OF PHILOSOPHY

Major: Civil Engineering (Structural Engineering)

Program of Study Committee:
Max L. Porter, Co-major Professor
Fouad S. Fanous, Co-major Professor
Halil Ceylan
Kejin Wang
Thomas J. Rudolphi

Iowa State University

Ames, Iowa

2014

DEDICATION

This document is dedicated to my parents, brother, sister, and their families, extended family, friends, and coauthors.

TABLE OF CONTENTS

#

LIST OF FIGURES

LIST OF TABLES

ACKNOWLEDGEMENTS

The research described herein was conducted at Iowa State University in the Department of Civil, Construction and Environmental Engineering through the auspices of the Engineering Research Institute and the Center for Transportation Research and Education (CTRE) and the Center for Portland Cement Concrete Pavement (PCC center). Sponsorship of this research was provided by the Highway Division of the Iowa Department of Transportation (IDOT) and the Iowa Highway Research Board. Funding was provided by American Highway Technology (AHT) and Greenstreak.

I would like to sincerely thank both of my major professors Dr. Max L. Porter and Dr. Fouad S. Fanous for being excellent mentors and role models. I wish to thank and acknowledge my program of study committee: Dr. Halil Ceylan, Dr. Kejin Wang and Dr. Thomas J. Rudolphi. I also recognize and thank Structural Engineering Laboratory Supervisor, Mr. Douglas L. Wood and University Extension Associate Professor, Dr. James K. Cable (retired). Several firms have provided materials services and advice, and require particular recognition and thanks: Doug Gremel from Hughes Brothers, Inc. of Seward, Nebraska; James P. McCallion from RJD Industries, Inc. of Laguna Hills, California; Technical Services, Inc. of Ames, Iowa; Steve Tritsch of American Highway Technology (AHT) of Lenexa, KS and John Busel of the Market Development Alliance of Harrison, NY.

As a special note, this dissertation could not have been completed without the extraordinary care and consideration exhibited by the writing and research inclusive of the American Highway Technology (AHT) report. Great thanks to Dr. Max L. Porter, Mr. Robert J. Guinn, Jr. and Mr. Andrew L. Lundy.

ABSTRACT

Concrete structural elements such as wall sections, bridge abutments and slabs on grade rely on dowels to transfer loads across the joints. As the joint width becomes wider, or if the joint is formed, the effect of aggregate interlock to transfer load is reduced and the loads are transferred by dowels. The dowels can be circular or elliptical shaped and are more commonly made of steel or Fiber Reinforced Polymer (FRP). This research project considered steel dowels with either a circular or an elliptical shape used in a highway or airport pavement. The following linear-elastic analysis, however, can be used for FRP dowels and for other doweled structural elements.

Dowels are spaced along transverse joints in a highway or airport pavement. The dowel's main purpose is to transfer shear load across the joint which separates adjacent concrete slabs. Dowels are approximately eighteen inches (457 mm) long, placed at mid-height of the pavement thickness, positioned parallel to the pavement surface, and embedded symmetrically about the transverse joint centerline. The transverse joint was assumed to open, and its width is dependent on the combination of concrete shrinkage and slab contraction due to colder temperatures.

Wheel loads from a single axle, positioned along the open transverse joint, apply a shear load to each effective dowel along the joint. Effective dowels are those dowels included in the distribution of the wheel loads. The shear load causes the dowels to bear against the concrete and causes the dowels to deflect within the concrete. These deflections are directly related to the bearing stress between the embedded dowel and the concrete (or contact bearing stress). The maximum bearing stress corresponds to the maximum deflection which occurs at the transverse joint face. If the maximum bearing

stress does not exceed some portion of the elastic-limit stress for concrete, the deformed concrete around the deflected dowel will rebound to its original or reference state. Repetitive loading, however, may not allow the deformed concrete around the dowel to rebound to its original state before another set of wheel loads crosses the transverse joint. In this repetitive load case, permanent concrete deformation would be present.

A need exists to reduce the bearing stress around dowels for maximum axle loading, as well as, repetitive axle loading. Therefore, a comparison was made between circular- and elliptical-shaped dowels with equivalent flexural rigidity. This dowel comparison showed that, for a given load, the elliptical shape with a wider cross section had reduced deflections within the concrete and, reduced bearing stress between the dowel and the concrete. Also, the deflections of the dowel within the concrete at the transverse joint face, for the circular and elliptical shapes, compare favorably with measured deflections found through experimental methods.

Two published analytical foundation models for a beam on elastic foundation were used to determine the deflections of the embedded dowel within the concrete. The first foundation model is referred to as the one-parameter (or Winkler) model, and the second foundation model is referred to as the two-parameter model. The deflections along the dowel were found using each model's respective assumed displaced shape (general solution to the differential equation). The first model's general solution, based on the embedded length of the dowel, was divided into separate theories used for analyzing the dowel. The second model's general solution was simplified due to a slight modification.

The contribution of this research project was to simplify beam on elastic foundation theory through matrix formulation and apply these improved analysis methods to dowels embedded in concrete pavements joints. One of these simplifications allows for the analysis of any dowel embedment length greater than about nine inches (229 mm). Dividing the dowel into smaller elements is not required in the solution.

The analytical foundation models represented the concrete with linear-elastic springs. The spring stiffness for each model is given by elastic constants or parameters. Each model predicts slightly different deflection behavior for the embedded dowel based on these parameters. The first model assumes the springs act independently to support the dowel; whereas, the second model assumes interaction between adjacent springs. Modifications were made to the first model to include the effect of pavement thickness which allowed for comparison of both models.

The theoretical bearing stress between the dowel and the concrete was determined based on the fourth derivative of the assumed displaced shape for a particular model. Therefore, the bearing stresses along the dowel-concrete interface are directly related to the corresponding deflections along the dowel within the concrete. The maximum theoretical bearing stress at the transverse joint face was compared to experimental bearing stress. The experimental bearing stress was calculated from the measured deflection of the dowel at the transverse joint face. The maximum bearing stress was limited to some portion of the elastic-limit stress for the concrete medium.

For a given concrete depth below the dowel, as the load on the dowel is increased, the deflections along the dowel within the concrete and the bearing stresses along the dowel-concrete interface will increase. The analyses using the foundation models

(described previously) showed, however, that as the medium depth below the dowel was reduced the dowel deflections within the concrete decreased. A decrease in deflection could be explained by the reduction in cumulative compression over the smaller depth. In addition, the analyses by these models showed that as the concrete medium depth below the dowel decreased the contact bearing stress increased. To verify the deflection behavior of dowels embedded in concrete, experimental testing was undertaken for various size steel dowels having either a circular or an elliptical shape.

Three laboratory test methods were modeled using the stiffness method of structural analysis. Two elemental shear test methods and a cantilever test method were modeled. The elemental shear test methods investigated a single dowel that was embedded in concrete on either side of an open transverse joint and subjected to shear loading. The models, based on the assembled stiffness matrix, were used to determine the deflections along the dowel within the concrete and to verify elastic constants for a particular foundation model.

Additional analysis of the elemental shear test specimens allowed for the inclusion of an elastic medium under a portion of the test specimen to model soil-pavement interaction. This analysis was referred to as the three-parameter model which defines a layered system. In this system, the embedded dowel and surrounding concrete are idealized as beams, connected together with springs and the concrete beam is further supported by an elastic medium.

Key Words: dowel; elastic foundation; linear-elastic analysis; elliptical dowels; concrete pavements; Winkler; one-parameter model; two-parameter model; three-parameter model

CHAPTER 1. INTRODUCTION

1.0 Overview

The following series of papers introduces the reader to the analysis of circular- and elliptical-shaped steel dowels embedded in concrete. The analysis approach idealized the dowel as a beam, and the concrete was assumed to behave as an elastic medium. Therefore, the dowels could be investigated using the stiffness (displacement) method for a beam on elastic foundation (Melerski 2000).

Dowels positioned along a transverse joint are used to transfer shear load between adjacent concrete slab sections. The joints are spaced at regular intervals dividing a highway or airport pavement. The joint width (c) is dependent on the combination of colder temperatures and concrete shrinkage which resulted in contraction of the adjacent slabs. The concrete surrounding the loaded dowels is assumed to behave elastically, provided the bearing stress between the dowel and the concrete is maintained below the elastic-limit stress for the concrete medium.

Load transfer efficiency (AASHTO 1993) is used to rate the performance of a doweled transverse joint. This rating, however, may include permanent deformation of the concrete around the dowel. Permanent deformation, as explained in this series of papers, could be minimized by limiting the bearing stress between the dowel and the concrete. This limit is meant to improve the performance of each joint.

Load transfer between adjacent slabs is accomplished by distributing the wheel loads, positioned along the transverse joint, laterally to effective dowels along that joint (Friberg 1940). This assumed transverse-linear distribution is shown in Figure 1-1. In Figure 1-1, the value of 1.0 corresponds to the wheel loads, W_1 and W_2, which are equal.

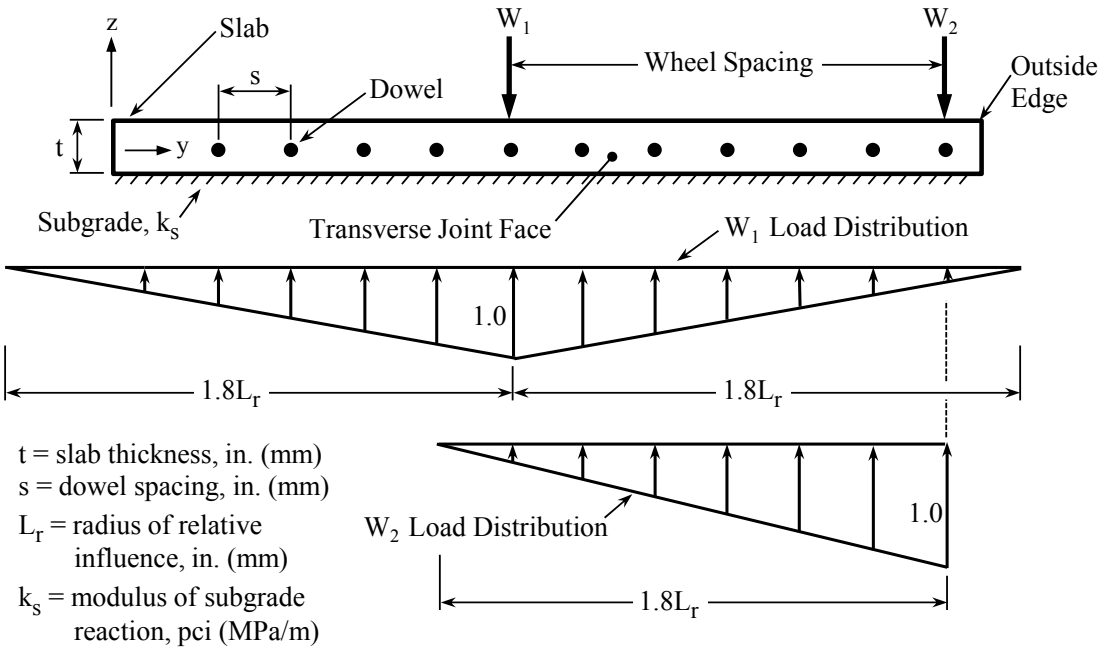

Figure 1-1 Lateral distribution of wheel loads to dowels (Friberg 1940)

Based on this value of 1.0, the wheel loads were proportioned to each dowel using similar triangles. One half of each wheel load is distributed to the dowels according to Yoder, et al. (1975). The shear load on a specified dowel is used to calculate the deflections along the embedded dowel within the concrete. The maximum bearing stress at the transverse joint face is determined from the corresponding deflection value.

The following papers present analytical solutions to differential equations based on matrix formulation. The general solution to the differential equations (or assumed displaced shape) is used to determine the deflected shape of the embedded dowel within the concrete. The constants for the general solution were determined using boundary conditions for the embedded dowel. In addition, the slope, moment, shear, and reaction functions along the embedded dowel can be determined by successive differentiation of the assumed displaced shape function. The size of these derivative functions was reduced using substitution values in vector form from Melerski (2000).

The deflected shape of the embedded dowel, when verified experimentally, can be used to define the more appropriate foundation model. These foundation models, representing the concrete with springs, are the one- and two-parameter foundation models. Each foundation model is defined by elastic constants (or parameters) which give the spring stiffness. The elastic constants are the contact modulus (k) or modulus of foundation (k_o) used in the one-parameter model, and the Winkler constant (k_a) and the load-spreading constant (k_b) used in the two-parameter model. The springs supporting the dowel act independently in the one-parameter model; whereas, interaction between adjacent springs through load spreading defines the two-parameter model.

Analytical solutions are provided using the dowel's embedment length (L_e) throughout the following papers. The analytical solutions, however, apply for any dowel embedment length greater than about nine inches (229 mm). Discretization of the dowel into smaller elements is not required in the solution.

Based on the analytical solutions for the one- and two-parameter models, the element stiffness matrices [k_e] were developed for: 1) the one-parameter model (finite beam theory), 2) the one-parameter model (semi-infinite beam theory), 3) the one-parameter model (with shear deflection along the embedded dowel), and 4) the two-parameter model. Also, the element stiffness matrices were included for two beams connected by springs (composite action) and the three-parameter model. These element stiffness matrices were incorporated into the assembled stiffness matrices [K_e] which modeled laboratory test specimens.

The goal of this research project was to show that the elliptical shape, as compared to the circular shape, was an improved dowel shape for use in highway or

airport pavements. Also, a comparison between the one- and two-parameter models is being introduced to find out which model best represents the concrete around a particular dowel size, shape and material.

1.1 Dissertation Layout

This dissertation is divided into five chapters. Chapters two through four are individual papers ready to submit for publication. Chapters two and three will be submitted as companion papers. The fifth chapter includes the general conclusions.

The second chapter explains how to determine the deflected shape of the dowel within the concrete. These deflections along the embedded dowel were based on the assumed displaced shape for the one- and the two-parameter model. The element stiffness matrices $[k_e]$, developed for each model using the stiffness method of structural analysis, were used to verify the dowel deflections at the transverse joint face. The theoretical deflections were determined for six different steel dowel sizes, having either a circular or an elliptical shape, embedded in concrete. The theoretical deflection at the transverse joint face (or maximum deflection along the embedded dowel), for each dowel, was compared to experimental deflections measured through laboratory testing. Equations that define the elastic constants (or parameters) for each foundation model are given in the second chapter.

The third chapter explains how to determine the theoretical bearing stress between the dowel and the concrete for six separate steel dowel sizes, having either a circular or an elliptical shape, embedded in concrete. The theoretical maximum bearing stress from these dowels was compared to the experimental bearing stress. The maximum bearing stress corresponds to the maximum deflection at the transverse joint face. The

experimental bearing stress was based on the maximum dowel deflection using the one-parameter model. A limit on maximum bearing stress was defined as some portion of the elastic-limit stress for the concrete medium.

The concrete was modeled using both elastic foundation models. These models (incorporated in several equations including elasticity equations from Boussinesq theory) were used to determine the bearing stress and the stress profile throughout the concrete below the dowel. The stress is based on the dowel-concrete reaction or load (q). This reaction is determined from the fourth derivative of the assumed displaced dowel shape for each model. Based on the dowel-concrete reaction, a radial stress distribution along the dowel's bottom-half circumference was verified to be the correct stress distribution for the circular and elliptical shapes. This radial stress replaces the commonly used uniform stress for dowels supported by an elastic medium.

The fourth chapter considered three laboratory test methods (two elemental shear test methods and a cantilever test method) that were modeled using the stiffness method of structural analysis. The assembled stiffness matrices [K_e] were used to verify the deflections of the dowel within the concrete at the transverse joint face as determined by these tests. The deflected shape of the dowel was determined from the assumed displaced shape. Also, the laboratory test methods were used to verify the elastic constants (or parameters) for each foundation model.

The elemental shear test models were used to investigate soil-pavement interaction by incorporating an elastic support under a portion of the test specimen. A rubber material was considered as the elastic support to represent the soil. Equations for the three-parameter model were used in this elastic support analysis. Hetenyi (1950 and

1961) defined this layered system which was incorporated into dowel analysis at Iowa State University. The embedded dowel and surrounding concrete were idealized as beams and connected by linear-elastic springs. The concrete beam was further supported by an elastic medium.

The elastic support was removed from the theoretical development which resulted in two beams connected by springs. Two beams connected by springs are used for composite beam action in laboratory test specimens.

1.2 Literature Review

References are cited respectively in each individual paper or chapter.

1.3 References

AASHTO, 1993. *AASHTO Guide for Design of Pavement Structures*, American Association of State Highway and Transportation Officials, Washington D.C., 624.

Friberg, B.F., 1940. Design of Dowels in Transverse Joints of Concrete Pavements, *Proceedings, American Society of Civil Engineers*, 105, 1076-1116.

Hetenyi, M., 1950. A General Solution for the Bending of Beams on an Elastic Foundation of Arbitrary Continuity, *Journal of Applied Physics*, 1, 55-58.

Hetenyi, M., 1961. *Beams on Elastic Foundation,* The University of Michigan Press, Ann Arbor, Michigan.

Melerski, E.S., 2000. *Design Analysis of Beams, Circular Plates and Cylindrical Tanks on Elastic Foundations*, Rotterdam, Netherlands, A.A. Balkema Publishers.

Yoder, E.G., and Witczak, M.W., 1975. *Principles of Pavement Design*, 2nd Edition, John Wiley & Sons, Inc., New York, NY.

CHAPTER 2. FOUNDATION MODELS FOR DOWELS EMBEDDED IN CONCRETE: PART I – VERIFICATION OF DEFLECTIONS FOR DOWELS IN CONCRETE PAVEMENTS

A paper prepared for submission to the *International Journal of Pavement Engineering*

Eric A. Lorenz[1]*, P.E., Max L. Porter*[2]*, P.E.,*
and Fouad S. Fanous[3]*, P.E.*

Abstract

Shear transfer across doweled joints in concrete pavements on grade has been investigated by several researchers in past years. Improving the analysis of circular- and elliptical-shaped steel dowels embedded in these joints is the topic of a two-part companion paper. This first paper shows how to calculate dowel deflections within the concrete, and the second paper shows how to limit the magnitude of the bearing stress between the dowel and the concrete.

Two published analytical models, which utilized beam on elastic foundation theories, represented the concrete surrounding the dowel. Modifying one of these models to include the effect of pavement thickness allowed for the comparison of both models. Their resulting theoretical deflections were compared to (and verified by) deflection values that were determined through laboratory testing at Iowa State University. These comparisons showed that a dowel with an elliptical shape, having the same flexural rigidity as a comparable circular shape, had reduced deflections within the concrete.

[1] Doctoral Candidate, Civil Engineering, Department of Civil, Construction and Environmental Engineering, Iowa State University, Ames, Iowa 50011

[2] University Professor Emeritus, Civil Engineering, Department of Civil, Construction and Environmental Engineering, Iowa State University, Ames, Iowa 50011

[3] Professor, Civil Engineering, Department of Civil, Construction and Environmental Engineering, Iowa State University, Ames, Iowa 50011

2.1 Introduction

Concrete pavements on grade considered in this paper have joints transverse to traffic flow and spaced at regular intervals. Contraction of adjacent slabs due to concrete shrinkage and temperature change results in joint separation. Dowels, spaced along this joint, will transfer a portion of the single-axle wheel loads from one slab section to the other across the transverse joint. Dowels are approximately eighteen inches (457 mm) long, placed at mid-height of the pavement thickness, positioned parallel to the pavement surface, and embedded symmetrically about the joint centerline.

The idealization of the dowel as a beam on elastic foundation (BEF) assumes that the dowel is supported by an elastic medium. Vertical support from this medium is represented by compression-only springs that are positioned along the top and bottom of the embedded dowel. When calculating the deflection of the dowel within the concrete, these springs can either: (1) work independently to support the dowel (Winkler 1867), or (2) interact with adjacent springs to support the dowel (Zhaohua, et al. 1983). Both analyses were based on the stiffness method of structural analysis for a BEF (Weaver, et al. 1990 and Melerski 2000), and these analyses were used to investigate dowels that were embedded in concrete pavement joints. The first approach was modified, to include the effect of pavement thickness, which allowed for the comparison of both methods. The objective of this paper was to provide deflection results, using these improved analysis methods, for dowels that were embedded in concrete.

2.2 Background

The dowels are surrounded by concrete along the embedment length on both sides of the transverse joint. If the concrete is assumed to be an elastic medium, then

commonly the embedded dowel is modeled as a BEF. The concrete is not perfectly elastic, however, and will undergo some permanent deformation, or plastic set (Huang 1993), from wheel loads that cause the dowels to bear against the concrete. If the bearing stress, resulting from a loaded dowel, is less than the elastic-limit stress for the concrete material, the dowel deflections within the concrete are proportional to the dowel load. Therefore, these dowel deflections are [almost completely] recoverable and linear elasticity applies to the concrete medium (Huang 1993).

2.3 Overview

Two companion papers focus on the contribution of the elliptical shape (Porter, et al. 2001), when compared to the circular shape, for steel dowels used in concrete pavement joints. This focus was achieved by using improved analysis methods for steel dowels of various size and shape that are embedded in concrete. The dowel and concrete material properties remained constant during this analysis. Even with constant properties, the two elastic foundation models – which represent the concrete – show different deflection behavior for a specified dowel embedded in concrete. Both foundation models allow the dowel to be analyzed as a beam supported by an elastic medium. In addition, both models prove that the elliptical shape, having a wider cross section but the same flexural rigidity as a comparable circular shape, will result in reduced dowel deflections within the elastic medium. Therefore, the elliptical-shaped dowel has the potential to improve concrete pavement joints where Figure 2-1 illustrates a doweled pavement joint.

Furthermore, for a loaded dowel, the elliptical shape may prevent oblonging (or enlargement) of the hole in the concrete surrounding the dowel. This deterioration, from

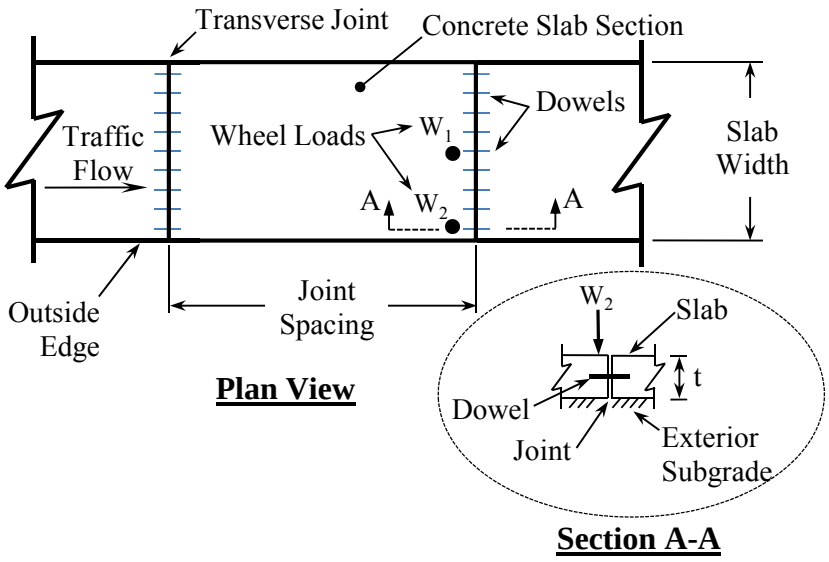

Figure 2-1 Doweled pavement joint

permanent concrete deformation, occurs when the loaded dowel bears against the concrete and either: (1) the bearing stress exceeds the elastic-limit stress for concrete, or (2) repeat loading does not allow the deformed concrete around the embedded dowel to recover to its original state before another set of wheel loads crosses the transverse joint.

2.4 Dowel Shapes

The two companion papers are presenting a shape alternative to the typical 1.0-, 1.25- and 1.5-inch (25.4-, 31.75- and 38.1-mm) diameter, circular steel dowels used in highway and airport pavements. Three elliptical shapes, with flexural rigidities equivalent to each of the previously mentioned circular shapes, are shown to be an improved dowel type. Dowel types refer to dowel size, shape and material. The theory, presented in this paper, is applicable to dowels with either a circular or an elliptical shape, and both shapes are shown in Figure 2-2.

The bearing length (BL) along the dowel's bottom-half circumference is opposite the load as shown in Figure 2-2, and BL is greater for the elliptical shape. A greater BL

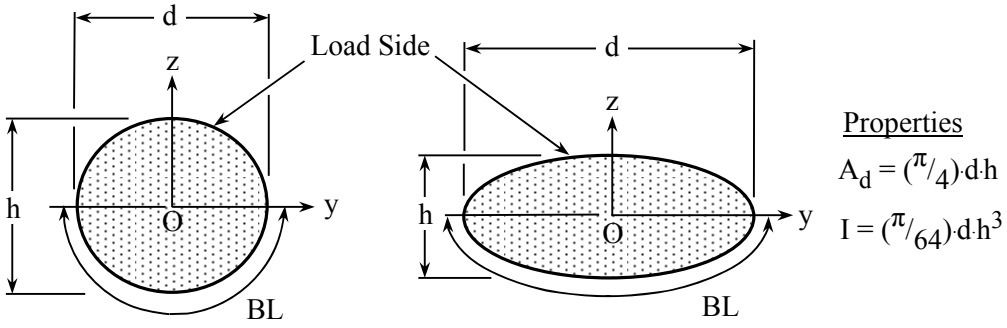

Figure 2-2 Common dowel shapes (circle and ellipse)

provides for reduced dowel deflections within the concrete and reduced contact bearing stress between the dowel and the concrete.

2.5 Concrete Joint Problems

The process of limiting bearing stress to the concrete's elastic-limit stress was introduced in place of the commonly used Load Transfer Efficiency (AASHTO 1993). By limiting the maximum bearing stress, the required number of dowels, the dowel type and the dowel spacing can be determined. These variables are dependent on a specified concrete slab thickness (t) and compressive strength (f_c'), transverse joint width (c), modulus of subgrade reaction (k_s), and single-axle wheel loads positioned along the transverse joint. Load transfer problems may occur due to the following issues as discussed below.

Dowels that maintain positive contact with the surrounding concrete will effectively transfer loads across a transverse joint. The contact may deteriorate, however, because of initial effects and long-term effects. Initial effects (Buch, et al. 1996) include voids below the embedded dowel resulting from improper or incomplete consolidation that leaves water-air pockets present, coatings or loose-fitting sleeves used to prevent bond or corrosion, and concrete that settles away from the bottom of the dowel after

concrete placement (Jeanty, et al. 1988). Long-term effects include permanent concrete deformations resulting from variable subgrades, repeat dowel loading (Buch, et al. 1996), and overloading the dowels.

If the dowels become loose with respect to the surrounding concrete, more of the wheel loads are transferred to the subbase-subgrade. In addition, delayed soil recovery (Zaretskii 1972) does not allow the unloaded soil to rebound to its reference state before another set of wheel loads crosses the transverse joint. Repeat loading therefore, results in further compaction of the subbase-subgrade. This compaction may explain subgrade erosion (Byrum 2013) which includes voids below the concrete slab at the transverse joint. The two companion papers present methods to improve load transfer across doweled joints and consider subgrade erosion.

2.6 Subgrade Analysis

Dowels are spaced along a transverse joint of width c which separates concrete slab sections in highway and airport pavements. These dowels help align the slab sections (see Figure 2-3) during traffic loading and transfer a portion of each wheel load from one slab section to the other as the wheels cross the transverse joint. According to Yoder, et al. (1975), this portion is fifty percent of each wheel load positioned along the transverse joint. This portion of the wheel loads is distributed laterally to the effective dowels according to Friberg (1940).

Figure 2-3 shows the dowel deflection within the concrete at the joint face (z_o). The value of z_o is assumed to be the same at both faces. The dowel is a separate entity within the concrete and z_o will depend on the subgrade stiffness which determines the dowel shear loading (V).

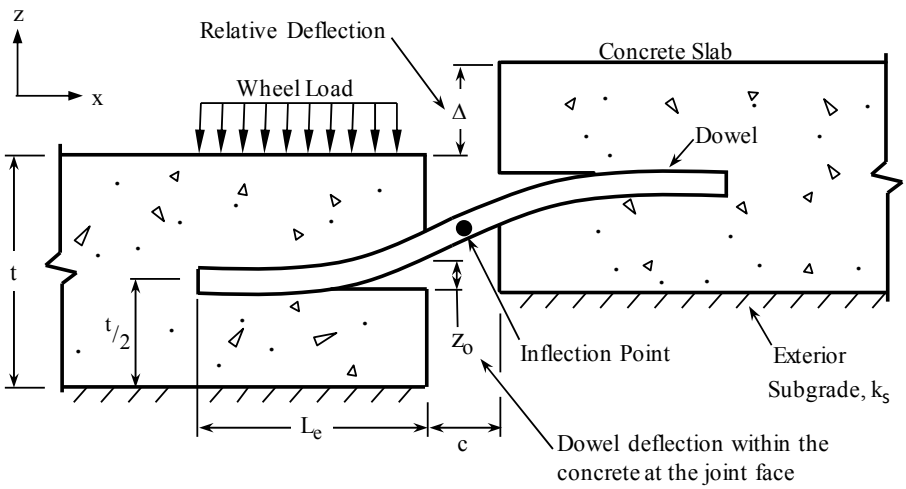

Figure 2-3 Illustration of a doweled concrete joint

The subgrade stiffness is given by the modulus of subgrade reaction (k_s) as indicated in Figure 2-3. The modulus of subgrade reaction was proposed by Vesic, et al. (1970) and is inversely proportional to the slab thickness (t). Equation 2-1 determines k_s below the concrete slab.

$$k_S = \frac{0.91}{t} \cdot \sqrt[3]{\frac{E_S \cdot \left(1 - \mu_c{}^2\right)}{E_c \cdot \left(1 - \mu_S{}^2\right)}} \cdot \frac{E_S}{\left(1 - \mu_S{}^2\right)} \qquad (2\text{-}1)$$

Where:

k_s = modulus of subgrade reaction from Vesic, et al. (1970), pci (MPa/m)

E_c = concrete pavement modulus of elasticity, psi (GPa)

E_s = subgrade modulus of elasticity, psi (GPa)

t = thickness of concrete slab or specimen, in. (mm)

μ_c = concrete Poisson's ratio

μ_s = subgrade Poisson's ratio

The radius of relative influence (L_r) given by Equation 2-2 is a property of the concrete slab which measures the stiffness of the slab in relation to that of the modulus of

$$L_r = \sqrt[4]{\frac{E_c \cdot t^3}{12 \cdot \left(1 - \mu_c{}^2\right) \cdot k_s}} \qquad (2\text{-}2)$$

Where:

L_r = radius of relative influence, in. (mm)

subgrade reaction (k_s). Due to the fourth root in Equation 2-2, L_r is not sensitive to small changes in the k_s value.

According to the Federal Aviation Administration (1995), the soil supporting the slab will have a k_s value ranging from 50 to 300 pci (13 to 81 MPa/m). The modulus of subgrade reaction is influenced by the soil type and amount of soil compaction (Ingram Thesis 2004), the moisture content in the subgrade (Vesic, et al. 1970), the use of a subbase below the concrete slab (Packard 1973), and the location of the wheel load on the slab (Huang 1993).

Frozen subgrade, bedrock subgrade or increasing the thickness of a well-compacted subbase (NAVFAC) may significantly increase the value of k_s. Also, the slab's bending stiffness is reduced at the transverse joint, and wheel loads cause the joint to rotate into the subbase-subgrade. Repeat wheel loading, as mentioned previously, may result in further compaction of the subbase-subgrade and increase k_s along the transverse joint. A larger k_s value reduces the radius of relative influence. A smaller L_r value would result in fewer dowels being loaded, and therefore the maximum dowel load would increase.

2.7 Dowel-Foundation Modeling

As previously mentioned, a dowel embedded in concrete was modeled as a BEF. The concrete elastic foundation which supported the dowel was represented by either of two different analytical models – the one- or the two-parameter model. The differential equations for the deflection within the concrete (z_m) and the reaction along the embedded dowel (q_m) are given in the two companion papers for a dowel supported by both elastic foundation models. These models are defined by constants (A_m, B_m, C_m, and D_m) and a substitution function (N_m). The foundation model was specified by the subscript m, which had a value of one for the one-parameter model (either finite beam or semi-infinite beam theories as a function of x) and a value of two for the two-parameter model.

The one-parameter, single-layer, elastic foundation is referred to as the Winkler Foundation (Winkler 1867) as shown in Figure 2-4. For the Winkler model, only the springs directly beneath the dowel are assumed to support the loaded dowel. This support means the vertical resisting pressure from the concrete was restricted to within the dowel's width. The one-parameter model assumes the dowel's cross section remains relatively unchanged (non-deformed) during loading, and the dowel punches into the supporting medium.

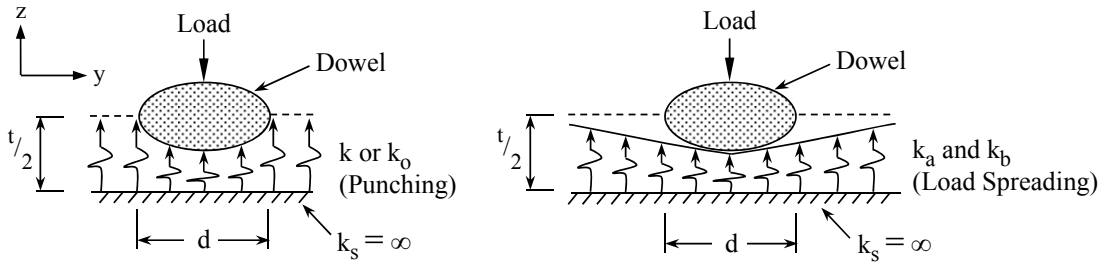

Figure 2-4 One- and two-parameter, elastic foundation models (Selvaduri 1979)

The one-parameter model is defined by one elastic constant given by the contact modulus (k), or the modulus of foundation (k_o), where k is equivalent to $k_o d$. The dowel's width (d) is constant along the embedment length. Vesic (1961) developed an equation for k. This equation was further modified at Iowa State University to incorporate the effect of pavement thickness and is shown later in this paper.

Winkler (1867) assumed that a beam of uniform cross section along its length deflected into an elastic foundation under an applied load. This assumption implies that the foundation reaction, or $q_1(x)$, along the embedded beam is proportional (by the parameter k) to the deflection, or $z_1(x)$, at each point (Hetenyi 1961). The reaction $q_1(x)$ is shown as EI multiplied by the fourth derivative of the assumed displaced shape in Equation 2-3. This equation was used to define a dowel supported on a concrete elastic foundation.

$$EI \cdot \frac{d^4 z_1(x)}{dx^4} - k \cdot z_1(x) = 0 \qquad (2\text{-}3)$$

Where:
$z_1(x)$ = dowel deflections within the concrete, one-parameter model, in. (mm)
E = dowel's modulus of elasticity, psi (GPa)
I = dowel's moment of inertia, in^4 (mm^4)
k = contact modulus, psi (MPa)

In contrast to the previously presented approach, the two companion papers compare another model known as the two-parameter, single-layer, elastic foundation as shown in Figure 2-4. The two-parameter model (Vlasov 1966 and Zhaohua, et al. 1983) considers support from adjacent springs as well as springs directly under the embedded

dowel. This adjacent support means the vertical resisting pressure from the concrete was allowed to spread outside of the dowel's width.

An analogy for the two-parameter model was shown as a thin, tensioned membrane covering the support springs. Viewing the dowel's cross section (see Figure 2-4), as it's placed on top of the membrane, shows the loaded dowel supported by adjacent springs due to the membrane tension (Selvaduri 1979). The two-parameter model assumes the dowel's cross section deforms, and the loaded dowel is carried by a broader area in the elastic medium. When a dowel is supported by a larger area, this model predicts that the deflections of the dowel within the concrete and bearing stress between the dowel and the concrete may be reduced.

The two-parameter model is defined by two elastic constants: k_a (Winkler constant), and k_b (load-spreading constant). Equation 2-4 is the differential equation for the two-parameter model and includes one extra term which defines load spreading in the support medium. The load-spreading constant (k_b) is applied to the beam slope in Equation 2-4 but is also assumed to apply in the perpendicular direction as shown in Figure 2-4. The following theoretical development is, however, only slightly more complex (Zhaohua, et al. 1983) than the one-parameter model. The equations defining the elastic constants for the two-parameter model are presented later in this paper.

$$EI \cdot \frac{d^4 z_2(x)}{dx^4} - k_b \cdot \frac{d^2 z_2(x)}{dx^2} - k_a \cdot z_2(x) = 0 \qquad (2\text{-}4)$$

Where:
$z_2(x)$ = dowel deflections within the concrete, two-parameter model, in. (mm)
k_a = Winkler constant, psi (MPa)
k_b = load-spreading constant, lb. (kN)

The elastic constants (parameters) from both models assume the dowel is embedded in concrete with linear-elastic properties, and these constants are directly related to the concrete's elastic modulus (E_c). Hence, a loaded dowel that results in concrete non-linear behavior (above the elastic limit) must be avoided when evaluating these constants. Loading should result in bearing stress that is below the concrete's elastic-limit stress for both theoretical and experimental work.

Further consideration should be given to crushing of the dowel material, crushing of the concrete around the dowel, deformation of the dowel's cross section, and oblonging (or enlargement) of the hole in the concrete surrounding the dowel. This paper, however, focuses on the behavior of steel dowels embedded in concrete and considers the concrete's limiting properties.

2.8 Concrete Foundations

Concrete is generally assumed to be homogeneous, isotropic and elastic during this analysis. Concrete, however, is made-up of elastic, brittle materials that, when combined, behave in a ductile, non-linear manner under compression (MacGregor 1988). Under flexure, the concrete's stress-strain curve is assumed linear up to a concrete compressive stress of $0.45f_c'$ (elastic limit) and non-linear above this point, although the stress-strain curve is essentially non-linear below this point as well. The initial curved portion is believed to be very similar to the relation in direct compression (Hognestad 1951). During compression, the redistribution of stresses between coarse aggregate and cement paste through micro-cracking (Hsu, et al. 1963) cause the concrete to behave as an anisotropic elastic material. This redistribution of stress occurs not only in the vertical direction as the Winkler Hypothesis assumes.

Some the load-spreading capabilities exhibited by concrete below the dowel may be due to the presence of aggregate. The elliptical dowel shape (steel or Fiber Reinforced Polymer) has a larger bearing area (as does an oversized circular dowel) which results in a broader stress distribution and less punching action. An increase in dowel size, the elliptical shape, the dowel material, and the concrete aggregate may contribute to actual load spreading defined by a two-parameter foundation. First, however, consider the one-parameter model for comparison.

2.9 One-Parameter, Single Layer, Elastic Foundation

The differential equation given by Equation 2-3 relates the reaction $q_1(x)$ to the deflection $z_1(x)$ by a parameter k. Note that the relationship between $q_1(x)$ and $z_1(x)$ is not linear throughout the depth below the dowel. In other words, stress reduces exponentially throughout the depth below the dowel and, as well, the amount of deflection reduces exponentially throughout the depth. The differential equation assumes no exterior loading applied between the ends of the dowel; however, the dowel-concrete reaction $q_1(x)$ is considered a load. The joint loading is applied to the dowel at the transverse joint face and shown in Figure 2-5.

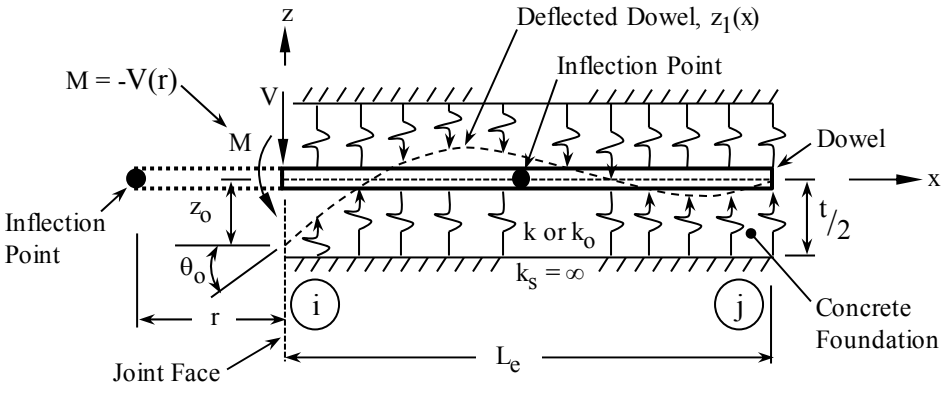

Figure 2-5 Dowel on concrete elastic foundation (one-parameter model)

2.9.1 General Solution

The general solution or assumed displaced shape $z_1(x)$ for a one-parameter model is given by Equation 2-5. This function gives the vertical deflection within the concrete along the dowel's embedment length. The general solution has been simplified using a substitution function (Melerski 2000 pp. 18-19) as shown by $N_1(x)$ in Equation 2-5. Constants A_1, B_1, C_1, and D_1 shown in Equation 2-5 are determined later in this paper for the finite beam theory and must satisfy the boundary conditions for the dowel. The boundary conditions can either be joint loads or support conditions, i.e. pinned, fixed, etc.

$$z_1(x) = N_1{}^T(x) \cdot \begin{pmatrix} A_1 \\ B_1 \\ C_1 \\ D_1 \end{pmatrix} \tag{2-5}$$

Where:
$z_1(x)$ = dowel deflections within the concrete, one-parameter model, in. (mm)
A_1, B_1, C_1, *and* D_1 = constants
$N_1(x)$ = substitution function

Simplifying the general solution into vector form consists of placing $n_1(x)$ through $n_4(x)$ in the substitution function as shown by Equation 2-6. In vector form, the substitution function, or $N_1(x)$, consists of exponential and trigonometric functions that are easily differentiated. Successive differentiation of the substitution function with respect to x, using the chain rule, produces derivative functions (N_1', N_1'', etc.) that are in terms of $n_1(x)$ through $n_4(x)$. The derivative functions are used to give the slope (θ_1), moment (M_1), shear (V_1), and reaction or load (q_1) along the dowel's embedment length

$$N_1(x) = \begin{pmatrix} n_1(x) \\ n_2(x) \\ n_3(x) \\ n_4(x) \end{pmatrix} = \begin{pmatrix} e^{\beta \cdot x} \cdot cos(\beta \cdot x) \\ e^{\beta \cdot x} \cdot sin(\beta \cdot x) \\ e^{-\beta \cdot x} \cdot cos(\beta \cdot x) \\ e^{-\beta \cdot x} \cdot sin(\beta \cdot x) \end{pmatrix} \quad (2\text{-}6)$$

Where:

β = characteristic of the system, in^{-1} (mm^{-1})

$$\beta = \sqrt[4]{\frac{k}{4 \cdot E \cdot I}}$$

k = contact modulus, psi (MPa)

$n_1(x)$, $n_2(x)$, $n_3(x)$, *and* $n_4(x)$ = substitution values

for a one-parameter model. The derivative functions (in vector form) are given in the Appendix section.

2.9.2 Inflection Point within the Transverse Joint

An inflection point (IP), as shown in Figure 2-3, is in the dowel within the transverse joint width (c). The IP was assumed and implies some shear (V) and no moment (M) at that point along with a curvature reversal in the deflected dowel.

According to Ingram (Thesis 2004), using Finite Element Analysis on full-scale highway pavements, an IP does not occur in the dowel spanning the open transverse joint but occurs somewhere in the dowel's embedment length. Theoretical analysis of laboratory test methods (Porter, et al. 2001) has shown that an IP occurred in the dowel at the joint center. Poor contact between the dowel and the concrete (as explained earlier), non-symmetrical joint loading and other casting variables (Porter, et al. 2001) may shift the IP location for dowels used in laboratory tests and full-scale slabs.

An IP in the joint center permits separation of the dowel at the IP with each symmetrical half consisting of a BEF and a cantilever section (with length c/2). Shear

(V) was applied equal and opposite to both cantilevers. A modified analysis for a full-scale slab may conservatively use a cantilever length of c, which indicates a shift in the IP to the transverse joint face.

By using the transfer theorem, V is applied to the dowel at the joint face in Figure 2-5 along with a moment (M) as shown. The magnitude of the moment is dependent on the location of the IP within the joint (r in Figure 2-5) and the actual joint width (c). Using analysis methods as follow, a greater joint width (c) will result in a greater dowel load at the concrete joint face.

2.9.3 BEF Length Classification

A beam on elastic foundation (BEF) is classified as short, medium or long (Hetenyi 1961) by its characteristic length as given by βL_e. This classification is as follows; a short beam – $\beta L_e \leq \pi/4$, a medium beam – $\pi/4 < \beta L_e < \pi$, and a long beam – $\beta L_e \geq \pi$. The theoretical development for the one-parameter foundation model will show that Friberg's (1940) semi-infinite beam theory is applicable for βL_e of π or greater (long beams), and Timoshenko's (1925) finite beam theory is applicable for βL_e greater than $\pi/4$ (medium or long beams). Finite beam theory does not apply for βL_e of $\pi/4$ or less (short beams), however, statics may be used since the beam does not bend (Hetenyi 1961).

2.9.4 Finite Beam Theory

The element stiffness matrix $[k_e]$ was determined for finite beam theory using the stiffness method of structural analysis for a BEF (Melerski 2000 pp. 19-21). The following procedure finds the 4 x 4 element stiffness matrix and constants (A_1, B_1, C_1, and D_1) for finite beam theory. Modifications, as described later, are required for the

semi-infinite beam theory. The [A] and [B] matrices (see Equations 2-7 and 2-8, respectively) were developed using the assumed displaced shape or general solution (see Equation 2-5) and its derivatives for the one-parameter model.

$$A = \begin{bmatrix} 1 & 0 & 1 & 0 \\ \beta & \beta & -\beta & \beta \\ n_1(L_e) & n_2(L_e) & n_3(L_e) & n_4(L_e) \\ \beta \cdot \begin{pmatrix} n_1(L_e) \ldots \\ + -n_2(L_e) \end{pmatrix} & \beta \cdot \begin{pmatrix} n_1(L_e) \ldots \\ + n_2(L_e) \end{pmatrix} & \beta \cdot \begin{pmatrix} -n_3(L_e) \ldots \\ + -n_4(L_e) \end{pmatrix} & \beta \cdot \begin{pmatrix} n_3(L_e) \ldots \\ + -n_4(L_e) \end{pmatrix} \end{bmatrix}^{-1} \tag{2-7}$$

$$B = 2 \cdot \beta^2 \cdot E \cdot I \cdot \begin{bmatrix} -\beta & \beta & \beta & \beta \\ 0 & -1 & 0 & 1 \\ \beta \cdot \begin{pmatrix} n_1(L_e) \ldots \\ + n_2(L_e) \end{pmatrix} & -\beta \cdot \begin{pmatrix} n_1(L_e) \ldots \\ + -n_2(L_e) \end{pmatrix} & -\beta \cdot \begin{pmatrix} n_3(L_e) \ldots \\ + -n_4(L_e) \end{pmatrix} & -\beta \cdot \begin{pmatrix} n_3(L_e) \ldots \\ + n_4(L_e) \end{pmatrix} \\ -n_2(L_e) & n_1(L_e) & n_4(L_e) & -n_3(L_e) \end{bmatrix} \tag{2-8}$$

The element stiffness matrix [k_e] is found by Equation 2-9. This matrix relates joint displacements (deflections and rotations) to member end forces by the expression [k_e]{D} = {F}, where {D} is the joint displacement vector, and {F} is the joint load

$$k_e = B \cdot A \tag{2-9}$$

vector. Displacements are numbered from left to right in Figure 2-5 with positive deflections in the positive z-direction and positive rotations in the counterclockwise direction. Once the joint displacements are determined, the constants for finite beam theory are found using Equation 2-10 (as a vector).

Equation 2-11 (as a vector) gives an alternative method to solve for the constants for finite beam theory which satisfies the boundary conditions – shear (V) and moment (M) when x is zero and zero shear and zero moment when x is L_e (dowel's embedment length). These joint loads constitute the joint load vector {F}. This equation can be used

$$\begin{pmatrix} A_1 \\ B_1 \\ C_1 \\ D_1 \end{pmatrix} = A \cdot D \tag{2-10}$$

Where:
D = the joint displacement vector, in. (mm) and radians

to find the constants without solving for the element stiffness matrix $[k_e]$ or the joint displacement vector {D}.

$$\begin{pmatrix} A_1 \\ B_1 \\ C_1 \\ D_1 \end{pmatrix} = B^{-1} \cdot \begin{pmatrix} V \\ M \\ 0 \\ 0 \end{pmatrix} \tag{2-11}$$

Where:
See Figure 2-5,
V = shear - *negative value*, lb. (kN)
M = moment - *positive value*, in-lb. (kN-m)

Refer to a typical structural analysis text (for the stiffness method), e.g. Weaver, et al. (1990) that shows how to assemble the global stiffness matrix for structures with multiple elements or beams. The assembled global stiffness matrix applies to members embedded in an elastic foundation as with a cantilever dowel that has two elements – a BEF and a free cantilever. The stiffness method is considered a finite element method for beams, i.e. an assemblage of beam elements.

2.9.5 Semi-Infinite Beam Theory

Friberg's semi-infinite beam theory assumes the deflection is zero at x equal to infinity, therefore, constants A_1 and B_1 must be zero in Equation 2-5. Constants C_1 and

D_1 are solved for directly and, equations for a semi-infinite beam as a function of x can be developed. Since the dowel length is not infinite, some residual shear and moment remains at the embedded end as compared to finite beam theory which accounts for the actual beam length. This assumption (infinite length) holds true for a characteristic length (βL_e) of π or greater (Hetenyi 1961).

For a semi-infinite beam on elastic foundation, with the loads applied at Node i in Figure 2-5, the dowel deflection (z_o) and slope (θ_o) within the concrete at the joint face (x is equal to zero) are given in matrix form by Equation 2-12. If the loads were applied to Node j in Figure 2-5, the off-diagonal elements in Equation 2-12 would be negative ($-2\beta^2$), as well as the moment (M).

$$\begin{pmatrix} z_o \\ \theta_o \end{pmatrix} = \frac{1}{E \cdot I} \cdot \begin{pmatrix} 4 \cdot \beta^3 & 2 \cdot \beta^2 \\ 2 \cdot \beta^2 & 2 \cdot \beta \end{pmatrix}^{-1} \cdot \begin{pmatrix} V \\ M \end{pmatrix} \qquad (2\text{-}12)$$

Where:
z_o = dowel deflection within the concrete at the joint face, in. (mm)
θ_o = dowel slope within the concrete at the joint face (radians)

The deflection and slope at the transverse joint face may also be written as $z_1(0)$ and $\theta_1(0)$ which signifies the one-parameter model. Equation 2-12 is from the stiffness method and is in the form $\{D\} = [k_e]^{-1}\{F\}$ which shows the element stiffness matrix $[k_e]$ for the semi-infinite beam theory. This equation was presented to solve for the contact modulus (k) when an experimental deflection within the concrete (z_e) is known.

2.9.6 Elastic Constant (Parameter)

The support medium in the Winkler model (1867) is a one-parameter, elastic foundation and is defined by k – or contact modulus – and is equivalent to $k_o d$, where k_o

is the modulus of foundation. The dowel width (d) is constant along the embedment length. The k_o value defines a spring supporting an area that deflects under a load and has units of force per unit area per unit length. The dowel in Figure 2-5 is supported by an infinite number of such springs as defined by Equation 2-3. The ability to work with this differential equation is dependent on knowing or being able to solve for the k_o value. Several previous investigators have solved for k (or k_o), most notably Vesic (1961), and his work is presented next.

Vesic (1961) developed his theoretical equation for the contact modulus k (see Equation 2-13) describing the behavior of a horizontal beam (of width d) on a soil elastic

$$k = 0.80 \cdot \sqrt[12]{\frac{E_c \cdot d^4}{16 \cdot E \cdot I}} \cdot \frac{E_c}{\left(1 - \mu_c{}^2\right)} \qquad (2\text{-}13)$$

Where:
k = contact modulus (not modified from Vesic (1961)), psi (MPa)
E_c = concrete's modulus of elasticity, psi (MPa)
μ_c = concrete Poisson's ratio

foundation, and Melerski (2000 pp. 82-84) applied this same equation to laterally-loaded, vertical piles (of width d) embedded in soil. In order to apply Equation 2-13 to a soil elastic foundation, change E_c to the soil modulus of elasticity (E_s) and μ_c to the soil Poisson's ratio (μ_s). Vesic derived Equation 2-13 accounting for uniform deflection across the beam width, and Equation 2-13 applies to an infinite depth elastic medium below the beam. Equation 2-13 applies to a total concrete thickness (t) of 36 inches (914 mm) and greater which can be considered an infinite depth.

Researchers at Iowa State University investigated Equation 2-13 for dowels supported on a concrete elastic foundation but with a given finite depth below the dowel. The dowel was centered vertically in the concrete thickness (t). Theoretically, the k value should increase as the medium depth below the dowel decreases and should become infinity as the medium depth approaches zero.

Equation 2-14 accounts for the effect of the concrete pavement thickness on the contact modulus (k). This equation can be used reliably for a total concrete thickness (t) of 5 inches (127 mm) and greater and is applicable to dowels embedded in concrete pavement joints. Equation 2-14 was verified in the second companion paper (see Section 3.6.3). A soft conversion can be made in this equation for use with metric units (mm) by changing the term –t/7 to –t/178.

$$k = \left(1.20 \cdot e^{\frac{-t}{7}} + 0.80\right) \cdot \sqrt[12]{\frac{E_c \cdot d^4}{16 \cdot E \cdot I}} \cdot \frac{E_c}{\left(1 - \mu_c{}^2\right)} \qquad (2\text{-}14)$$

Where:
k = contact modulus (modified), psi (MPa)
t = total thickness of slab or specimen, in. (mm)

2.10 Two-Parameter, Single-Layer, Elastic Foundation

The two-parameter model applies to dowel embedment lengths greater than about nine inches (229 mm) based on the moment and shear along the embedded dowel. Assembling beams into the global stiffness matrix still applies for more than one beam. Considering the dowel embedded in concrete as a BEF, the deflected dowel shape for a two-parameter model is shown in Figure 2-6. This deflected dowel shape differs from the deflected shape in Figure 2-5 for a one-parameter model.

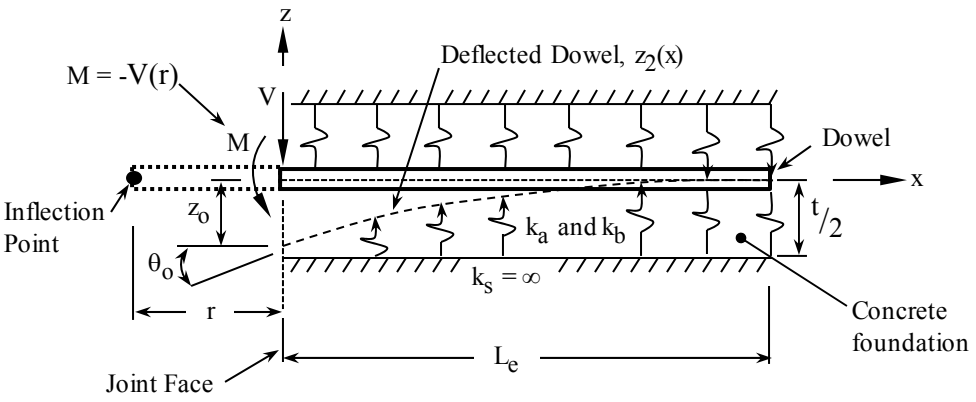

Figure 2-6 Dowel on concrete elastic foundation (two-parameter model)

2.10.1 General Solution

The assumed displaced shape or general solution for the two-parameter model gives the vertical deflection of the dowel within the concrete along the dowel's embedment length (x-direction). The general solution is shown by Equation 2-15.

$$z_2(x) = N_2^T(x) \cdot \begin{pmatrix} A_2 \\ B_2 \\ C_2 \\ D_2 \end{pmatrix} \tag{2-15}$$

Where:
$z_2(x)$ = dowel deflections within the concrete, two-parameter model, in. (mm)
A_2, B_2, C_2, *and* D_2 = constants
$N_2(x)$ = substitution function

The reduction in Equation 2-15 was accomplished by the substitution function as given by Equation 2-16 for a two-parameter foundation. Differentiating the substitution function, using the chain rule, gives derivative functions that are vectors in terms of $n_1(x)$ through $n_4(x)$. The derivative functions are used to find the slope (θ_2), moment (M_2), shear (V_2), and reaction or load (q_2) for the two-parameter foundation model. The

$$N_2(x) = \begin{pmatrix} n_1(x) \\ n_2(x) \\ n_3(x) \\ n_4(x) \end{pmatrix} = \begin{pmatrix} cos(\alpha \cdot L \cdot x) \cdot cosh(\lambda \cdot L \cdot x) \\ cos(\alpha \cdot L \cdot x) \cdot sinh(\lambda \cdot L \cdot x) \\ sin(\alpha \cdot L \cdot x) \cdot cosh(\lambda \cdot L \cdot x) \\ sin(\alpha \cdot L \cdot x) \cdot sinh(\lambda \cdot L \cdot x) \end{pmatrix} \tag{2-16}$$

Where:

$n_1(x)$, $n_2(x)$, $n_3(x)$, *and* $n_4(x)$ = substitution values (as slightly modified from Zhaohua, et al. (1983))

$$L = \sqrt[4]{\frac{k_a}{E \cdot I}} \qquad \psi = tan\left(\frac{\sqrt{4 \cdot k_a \cdot E \cdot I - k_b^{\,2}}}{k_b} \right)^{-1}$$

$$\alpha = sin\left(\frac{\psi}{2} \right) \qquad \lambda = cos\left(\frac{\psi}{2} \right)$$

derivative functions for the two-parameter model are given in the Appendix section. The deflection (z_o) and slope (θ_o) at the transverse joint face for a two-parameter model will not necessarily be equal to those from a one-parameter model.

Development of the stiffness matrix for the two-parameter elastic foundation model follows the same approach as presented for the one-parameter model. The [A] and [B] matrices (see Equations 2-17 and 2-18, respectively) are given for the two-parameter model, and the expression $[k_e] = [B][A]$ represents the element stiffness matrix.

Letting k_b be equal to zero and k_a be equal to k (contact modulus from the one-parameter model) and ψ be equal to $\pi/2$, the two-parameter equations can be used for the one-parameter model (Zhaohua, et al. 1983). By letting k_b be zero and using k_a, the two-

$$A = \begin{bmatrix} 1 & 0 & 0 & 0 \\ 0 & L\cdot\lambda & L\cdot\alpha & 0 \\ n_1(L_e) & n_2(L_e) & n_3(L_e) & n_4(L_e) \\ -L\cdot(\alpha)\cdot n_3(L_e)\ \ldots & -L\cdot(\alpha)\cdot n_4(L_e)\ \ldots & L\cdot(\alpha)\cdot n_1(L_e)\ \ldots & L\cdot(\alpha)\cdot n_2(L_e)\ \ldots \\ +\,L\cdot(\lambda)\cdot n_2(L_e) & +\,L\cdot(\lambda)\cdot n_1(L_e) & +\,L\cdot(\lambda)\cdot n_4(L_e) & +\,L\cdot(\lambda)\cdot n_3(L_e) \end{bmatrix}^{-1} \tag{2-17}$$

$$B = L^2\cdot E\cdot I\cdot \begin{bmatrix} 0 & L\cdot(\lambda^3 - 3\cdot\alpha^2\cdot\lambda) & L\cdot(3\cdot\alpha\cdot\lambda^2 - \alpha^3) & 0 \\ -(\lambda^2 - \alpha^2) & 0 & 0 & -(2\cdot\alpha\cdot\lambda) \\ -L\cdot(\alpha^3 - 3\cdot\alpha\cdot\lambda^2)\cdot n_3(L_e)\ \ldots & -L\cdot(\alpha^3 - 3\cdot\alpha\cdot\lambda^2)\cdot n_4(L_e)\ \ldots & -L\cdot(3\cdot\alpha\cdot\lambda^2 - \alpha^3)\cdot n_1(L_e)\ \ldots & -L\cdot(3\cdot\alpha\cdot\lambda^2 - \alpha^3)\cdot n_2(L_e)\ \ldots \\ +\,-L\cdot(\lambda^3 - 3\cdot\alpha^2\cdot\lambda)\cdot n_2(L_e) & +\,-L\cdot(\lambda^3 - 3\cdot\alpha^2\cdot\lambda)\cdot n_1(L_e) & +\,-L\cdot(\lambda^3 - 3\cdot\alpha^2\cdot\lambda)\cdot n_4(L_e) & +\,-L\cdot(\lambda^3 - 3\cdot\alpha^2\cdot\lambda)\cdot n_3(L_e) \\ (\lambda^2 - \alpha^2)\cdot n_1(L_e)\ \ldots & (\lambda^2 - \alpha^2)\cdot n_2(L_e)\ \ldots & (\lambda^2 - \alpha^2)\cdot n_3(L_e)\ \ldots & (\lambda^2 - \alpha^2)\cdot n_4(L_e)\ \ldots \\ +\,(-2\cdot\alpha\cdot\lambda)\cdot n_4(L_e) & +\,(-2\cdot\alpha\cdot\lambda)\cdot n_3(L_e) & +\,(2\cdot\alpha\cdot\lambda)\cdot n_2(L_e) & +\,(2\cdot\alpha\cdot\lambda)\cdot n_1(L_e) \end{bmatrix} \ldots$$
$$+\,-k_b\cdot \begin{bmatrix} 0 & L\cdot\lambda & L\cdot\alpha & 0 \\ 0 & 0 & 0 & 0 \\ L\cdot(\alpha)\cdot n_3(L_e)\ \ldots & L\cdot(\alpha)\cdot n_4(L_e)\ \ldots & -L\cdot(\alpha)\cdot n_1(L_e)\ \ldots & -L\cdot(\alpha)\cdot n_2(L_e)\ \ldots \\ +\,-L\cdot(\lambda)\cdot n_2(L_e) & +\,-L\cdot(\lambda)\cdot n_1(L_e) & +\,-L\cdot(\lambda)\cdot n_4(L_e) & +\,-L\cdot(\lambda)\cdot n_3(L_e) \\ 0 & 0 & 0 & 0 \end{bmatrix} \tag{2-18}$$

parameter model can be used to determine deflections within the concrete. These deflections will be larger than those given by the one-parameter model when using k.

The constants for a two-parameter model are found by multiplying the inverse of the [B] matrix by the joint load vector {F} as shown in Equation 2-19. The expression {C} = [A]{D} can also be used to solve for constants, where {C} is the vector of constants.

$$\begin{pmatrix} A_2 \\ B_2 \\ C_2 \\ D_2 \end{pmatrix} = B^{-1} \cdot \begin{pmatrix} V \\ M \\ 0 \\ 0 \end{pmatrix} \tag{2-19}$$

2.10.2 Elastic Constants (Parameters)

The elastic constants (k_a and k_b) are defined as follows for the two-parameter model. Solving the following equations will require a cyclic solution (Vallabhan, et al. 1991). First, assume a value for γ, then calculate k_a and k_b with Equations 2-20 and 2-21, respectively, and finally evaluate γ by Equation 2-22. The γ value is considered to be the distribution of vertical displacement with depth in the elastic medium.

$$k_a = \frac{(1-\mu_c)\cdot E_c \cdot d}{(1+\mu_c)\cdot(1-2\cdot\mu_c)\cdot H} \cdot \frac{\gamma\cdot(\sinh(\gamma)\cdot\cosh(\gamma)+\gamma)}{2\cdot\sinh(\gamma)^2} \tag{2-20}$$

$$k_b = \frac{E_c \cdot d \cdot H}{2\cdot(1+\mu_c)} \cdot \frac{1}{\gamma} \cdot \left[\frac{(\sinh(\gamma)\cdot\cosh(\gamma)-\gamma)}{2\cdot\sinh(\gamma)^2}\right] \le \sqrt{4\cdot k_a \cdot E \cdot I} \tag{2-21}$$

Where:
H = depth of medium below the bottom of the dowel, in. (mm)
γ = distribution of vertical displacement with depth

$$\gamma = H \cdot \sqrt{\frac{(1-2\cdot\mu_c)}{2\cdot(1-\mu_c)} \cdot \frac{\int_0^{L_e} \theta_2(x)^2\,dx + \frac{1}{2}\cdot\sqrt{\frac{k_a}{k_b}}\cdot\left(z_2(0)^2 + z_2\left(L_e\right)^2\right)}{\int_0^{L_e} z_2(x)^2\,dx + \frac{1}{2}\cdot\sqrt{\frac{k_b}{k_a}}\cdot\left(z_2(0)^2 + z_2\left(L_e\right)^2\right)}} \tag{2-22}$$

Finally, compare the assumed value of γ with that calculated using Equation 2-22. Due to the size of k_a and k_b, the accuracy of γ should be at least four decimal places. In Equation 2-22, the deflection (z_2) is given by Equation 2-15, and the slope (θ_2) is given by $N_2'(x)$, found in the Appendix section, multiplied by the vector of constants.

2.11 One-Parameter Model with Shear Effect

According to Aydogan (1995), the deflection caused by shear effect can be considered in the overall deflection of a BEF. Shear deflection is dependent on the shear-shape factor (λ_s) of the dowel which is shown by Equation 2-23 (Cowper 1966). This equation can be used for either circular- or elliptical-shaped dowels. Equation 2-23, with Poisson's ratio equal to one half, gives the shear-shape factor of 10/9 for a circular-shaped dowel.

$$\lambda_s = \frac{(40+37\cdot\mu)\cdot h^4 + (16+10\cdot\mu)\cdot h^2\cdot d^2 + \mu\cdot d^4}{12\cdot(1+\mu)\cdot h^2\cdot\left(3\cdot h^2 + d^2\right)} \tag{2-23}$$

Where:
λ_s = shear-shape factor
μ = Poisson's ratio for the dowel
h = dowel's minor axis, in. (mm)
d = dowel's major axis, in. (mm)

Shear deflection for the one-parameter model was considered in this paper. The term for shear effect is applied to the dowel's slope in the differential equation, and the

general solution is in the same form as for the two-parameter model (Aydogan 1995). Therefore, the two-parameter model given by Equations 2-15 through 2-18 can be used for the one-parameter model with shear effect by introducing modifications from Equation 2-24 and by replacing k_b with α_s in Equation 2-18.

$$L = \sqrt[4]{\beta_s} \qquad \psi = tan\left(\frac{\sqrt{4\cdot\beta_s - \alpha_s^2}}{\alpha_s}\right)^{-1}$$

$$\beta_s = \frac{k}{E\cdot I} \qquad \alpha_s = \frac{\lambda_s\cdot k}{A_d\cdot G} \tag{2-24}$$

Where:
A_d = dowel's cross-sectional area, in^2 (mm^2)
G = dowel's shear modulus, psi (MPa)

2.12 Cubic Equation Formulation

In order to check deflections for both models, the stiffness matrices developed from the cubic equation were included in this document (Zhaohua, et al. 1983). Elastic constants from both models are used with the following matrices. For the one-parameter (Winkler) model, displacements were determined using the expression $[k_w]\{D\} = \{F\}$, where $\{D\}$ and $\{F\}$ have been defined previously. The stiffness matrix $[k_w]$ for the one-parameter model is given by Equation 2-25.

For the two-parameter model, displacements were determined using the expression $[k_T]\{D\} = \{F\}$. The stiffness matrix $[k_T]$ for the two-parameter model is given by Equation 2-26. Both stiffness matrices are less complex than those developed

$$k_w = \frac{E \cdot I}{L_e^{\,3}} \cdot \begin{pmatrix} 12 & 6 \cdot L_e & -12 & 6 \cdot L_e \\ 6 \cdot L_e & 4 \cdot L_e^{\,2} & -6 \cdot L_e & 2 \cdot L_e^{\,2} \\ -12 & -6 \cdot L_e & 12 & -6 \cdot L_e \\ 6 \cdot L_e & 2 \cdot L_e^{\,2} & -6 \cdot L_e & 4 \cdot L_e^{\,2} \end{pmatrix} + k \cdot \begin{pmatrix} \frac{13 \cdot L_e}{35} & \frac{11 \cdot L_e^{\,2}}{210} & \frac{9 \cdot L_e}{70} & \frac{-13 \cdot L_e^{\,2}}{420} \\ \frac{11 \cdot L_e^{\,2}}{210} & \frac{L_e^{\,3}}{105} & \frac{13 \cdot L_e^{\,2}}{420} & \frac{-L_e^{\,3}}{140} \\ \frac{9 \cdot L_e}{70} & \frac{13 \cdot L_e^{\,2}}{420} & \frac{13 \cdot L_e}{35} & \frac{-11 \cdot L_e^{\,2}}{210} \\ \frac{-13 \cdot L_e^{\,2}}{420} & \frac{-L_e^{\,3}}{140} & \frac{-11 \cdot L_e^{\,2}}{210} & \frac{L_e^{\,3}}{105} \end{pmatrix} \tag{2-25}$$

previously using differential equations, and the resulting deflections compare closely to the previous approaches.

$$k_T = \frac{E \cdot I}{L_e^{\,3}} \cdot \begin{pmatrix} 12 & 6 \cdot L_e & -12 & 6 \cdot L_e \\ 6 \cdot L_e & 4 \cdot L_e^{\,2} & -6 \cdot L_e & 2 \cdot L_e^{\,2} \\ -12 & -6 \cdot L_e & 12 & -6 \cdot L_e \\ 6 \cdot L_e & 2 \cdot L_e^{\,2} & -6 \cdot L_e & 4 \cdot L_e^{\,2} \end{pmatrix} + k_a \cdot \begin{pmatrix} \frac{13 \cdot L_e}{35} & \frac{11 \cdot L_e^{\,2}}{210} & \frac{9 \cdot L_e}{70} & \frac{-13 \cdot L_e^{\,2}}{420} \\ \frac{11 \cdot L_e^{\,2}}{210} & \frac{L_e^{\,3}}{105} & \frac{13 \cdot L_e^{\,2}}{420} & \frac{-L_e^{\,3}}{140} \\ \frac{9 \cdot L_e}{70} & \frac{13 \cdot L_e^{\,2}}{420} & \frac{13 \cdot L_e}{35} & \frac{-11 \cdot L_e^{\,2}}{210} \\ \frac{-13 \cdot L_e^{\,2}}{420} & \frac{-L_e^{\,3}}{140} & \frac{-11 \cdot L_e^{\,2}}{210} & \frac{L_e^{\,3}}{105} \end{pmatrix} \ldots$$

$$+ k_b \cdot \begin{pmatrix} \frac{6}{5 \cdot L_e} & \frac{1}{10} & \frac{-6}{5 \cdot L_e} & \frac{1}{10} \\ \frac{1}{10} & \frac{2 \cdot L_e}{15} & \frac{-1}{10} & \frac{-L_e}{30} \\ \frac{-6}{5 \cdot L_e} & \frac{-1}{10} & \frac{6}{5 \cdot L_e} & \frac{-1}{10} \\ \frac{1}{10} & \frac{-L_e}{30} & \frac{-1}{10} & \frac{2 \cdot L_e}{15} \end{pmatrix} \tag{2-26}$$

2.13 Results

Tables 2-1 and 2-2 were developed theoretically and show the one- and two-parameter model's maximum deflections at the transverse joint face, respectively. These deflections were compared to experimental deflections at the transverse joint face from

the American Highway Technology (AHT) report (Porter, et al. 2001) in Table 2-3. The experimental deflections were slightly modified to include the effect of slope and flexural deflection in the dowel across the transverse joint. The tables and conclusions were developed using the following properties. The circular and elliptical shapes are compared, in the following tables, using approximately the same flexural rigidity (EI). Since the steel dowel's modulus of elasticity (E) is assumed to be constant, only the moment of inertia (I) is shown in Table 2-1. Equation 2-14 (k modified) was used for deflection calculations in the one-parameter model unless otherwise stated. The dowel deflection values for the one-parameter model in the following tables did not include shear deflection along the embedment length.

Table Properties *(*Porter, et al. 2001*)*
E = 29,000,000 psi (200 GPa) Modulus of elasticity for steel dowels
μ = 0.29 Poisson's ratio for steel dowels
f_c' = 6,000 psi (41.37 MPa) Concrete compressive strength
E_c = 4,415,201 psi (30.4 GPa) Concrete modulus of elasticity
μ_c = 0.18 Poisson's ratio (concrete)
V = -2,127 lb. (-9.46 kN) Shear
M = 133 lb.-in. (15.03 N-m) Moment
L_e = 8.9375 in. (227 mm) Dowel embedment length
c = 1/8 in. (3.2 mm) Transverse joint width
Concrete Thickness
t = 12 in. (305 mm) Tables 2-1 thru 2-3
t = 8 in. (203 mm) Table 2-4 (Not included in Porter, et al. (2001))

Table 2-3 includes the experimental deflection (z_e) within the concrete at the joint face. The experimental results documented in Table 2-3 match closely to the elastic deflections (δ_1 and δ_2 for the one- and two-parameter models, respectively) found using the elasticity equations outlined in Section 3.6.2.

Table 2-1 One-parameter, elastic foundation model (maximum deflections)

Dowel Description h x d, in. (mm)	I, in^4 (mm^4)	k, psi (MPa) Eq. 2-14	$z_1(0)$, in. (mm) Eq. 2-5	Cubic Equation, in. (mm)	Hetenyi *y`(0) in. (mm)
1.00 x 1.00 (25.40 x 25.40)	0.0491 (20,432)	4,044,050 (27,900)	-0.0010 (-0.0259)	-0.0008 (-0.0213)	-0.0013 (-0.0330)
0.88 x 1.41 (22.35 x 35.81)	0.0472 (19,632)	4,549,900 (31,350)	-0.0009 (-0.0240)	-0.0008 (-0.0193)	-0.0009 (-0.0217)
1.25 x 1.25 (31.75 x 31.75)	0.1198 (49,882)	4,044,050 (27,900)	-0.0008 (-0.0205)	-0.0007 (-0.0185)	-0.0008 (-0.0209)
1.13 x 1.66 (28.70 x 42.16)	0.1176 (48,938)	4,452,200 (30,700)	-0.0008 (-0.0192)	-0.0007 (-0.0171)	-0.0006 (-0.0147)
1.50 x 1.50 (38.10 x 38.10)	0.2485 (103,436)	4,044,050 (27,900)	-0.0007 (-0.0170)	-0.0006 (-0.0159)	-0.0006 (-0.0144)
1.34 x 1.98 (34.04 x 50.29)	0.2339 (97,338)	4,458,700 (30,750)	-0.0006 (-0.0160)	-0.0006 (-0.0149)	-0.0004 (-0.0103)

* Radial deflection (ϕ = 0 degrees) from Section 3.5.

Table 2-2 Two-parameter, elastic foundation model (maximum deflections)

Dowel Description h x d, in. (mm)	First and second parameters		γ -value Eq. 2-22	$z_2(0)$, in. (mm) Eq. 2-15	Cubic Equation, in. (mm)
	k_a, psi (MPa) Eq. 2-20	k_b, lb. (kN) Eq. 2-21			
1.00 x 1.00 (25.40 x 25.40)	1,166,700 (8,050)	1,968,500 (8,750)	2.4620	-0.0013 (-0.0338)	-0.0013 (-0.0332)
0.88 x 1.41 (22.35 x 35.81)	1,696,800 (11,700)	2,675,650 (11,900)	2.6152	-0.0010 (-0.0244)	-0.0009 (-0.0239)
1.25 x 1.25 (31.75 x 31.75)	1,400,950 (9,650)	2,592,400 (11,550)	2.2231	-0.0010 (-0.0259)	-0.0010 (-0.0256)
1.13 x 1.66 (28.70 x 42.16)	1,890,600 (13,050)	3,368,300 (15,000)	2.3275	-0.0008 (-0.0199)	-0.0008 (-0.0196)
1.50 x 1.50 (38.10 x 38.10)	1,647,050 (11,350)	3,213,550 (14,300)	2.0461	-0.0008 (-0.0206)	-0.0008 (-0.0203)
1.34 x 1.98 (34.04 x 50.29)	2,198,850 (15,150)	4,162,150 (18,500)	2.1539	-0.0006 (-0.0161)	-0.0006 (-0.0159)

Table 2-3 Experimental deflections compared to the elastic deflections

Dowel Description h x d, in. (mm)	Experimental Values		One-Parameter Model	Two-Parameter Model
	$z_e(0)$*, in. (mm)	k, psi (MPa) (Solved)	δ_1** in. (mm)	δ_2** in. (mm)
1.00 x 1.00 (25.40 x 25.40)	Not tested	Not tested	-0.0012 (-0.0307)	-0.0011 (-0.0283)
0.88 x 1.41 (22.35 x 35.81)	-0.0011 (-0.0282)	3,653,600 (25,200)	-0.0010 (-0.0259)	-0.0010 (-0.0246)
1.25 x 1.25 (31.75 x 31.75)	-0.0013 (-0.0320)	2,220,500 (15,300)	-0.0009 (-0.0233)	-0.0009 (-0.0239)
1.13 x 1.66 (28.70 x 42.16)	-0.0012 (-0.0294)	2,502,700 (17,250)	-0.0008 (-0.0201)	-0.0008 (-0.0210)
1.50 x 1.50 (38.10 x 38.10)	-0.0008 (-0.0199)	3,260,850 (22,500)	-0.0007 (-0.0184)	-0.0008 (-0.0206)
1.34 x 1.98 (34.04 x 50.29)	-0.0009 (-0.0240)	2,596,350 (17,900)	-0.0006 (-0.0160)	-0.0007 (-0.0181)

* As slightly modified from the AHT Report (Porter, et al. 2001).
** Elastic deflections determined from Section 3.6.2, Equation 3-18.

Table 2-4 shows deflection values for an eight-inch (203-mm) pavement thickness. Both Equation 2-13 (k not modified) and Equation 2-14 (k modified) were compared with the two-parameter model deflections. Equation 2-13 does not incorporate pavement thickness. As shown in Table 2-4, smaller deflection values for both models were determined by reducing the pavement thickness.

The deflections of the dowel at the transverse joint face were shown in the tables in this paper. The deflections within the concrete, along the dowel's embedment length, are required to determine which model applies to a given dowel type. The shape of the deflected dowel through experimental methods, therefore, can be used to verify the more appropriate model.

Table 2-4 Maximum dowel deflections in an eight-inch (203-mm) pavement

Dowel Description h x d, in. (mm)	One-Parameter Model		Two-Parameter Model
	k, Not Modified Eq. 2-13	k, Modified Eq. 2-14	$z_2(0)$, in. (mm) Eq. 2-15
	$z_1(0)$, in. (mm) Eq. 2-5	$z_1(0)$, in. (mm) Eq. 2-5	
1.00 x 1.00 (25.40 x 25.40)	-0.0012 (-0.0309)	-0.0009 (-0.0232)	-0.0012 (-0.0313)
0.88 x 1.41 (22.35 x 35.81)	-0.0011 (-0.0287)	-0.0008 (-0.0215)	-0.0009 (-0.0229)
1.25 x 1.25 (31.75 x 31.75)	-0.0010 (-0.0245)	-0.0007 (-0.0183)	-0.0009 (-0.0232)
1.13 x 1.66 (28.70 x 42.16)	-0.0009 (-0.0229)	-0.0007 (-0.0172)	-0.0007 (-0.0181)
1.50 x 1.50 (38.10 x 38.10)	-0.0008 (-0.0203)	-0.0006 (-0.0152)	-0.0007 (-0.0180)
1.34 x 1.98 (34.04 x 50.29)	-0.0008 (-0.0192)	-0.0006 (-0.0143)	-0.0006 (-0.0143)

Figure 2-7 illustrates the deflected shape (inches and millimeters) for the 1.50-inch (38.10-mm) diameter dowel using the one- and two-parameter, elastic foundation models. Also, the deflected shape for the one-parameter model including shear deflection along its length was shown.

The deflections in Figure 2-7 are exaggerated for clarity and show a difference in the assumed displaced shape. This difference may be the reason for the deflected shape of Fiber Reinforced Polymer (FRP) dowels shown in Murrison, et al. (2002) where the FRP dowel deflections match the two-parameter model's deflected shape. The two-parameter model (as shown in Figure 2-7) predicts a greater deflection at the transverse joint face for the circular-shaped dowels; whereas, the deflection at the joint face for the elliptical-shaped dowels is the similar for both models.

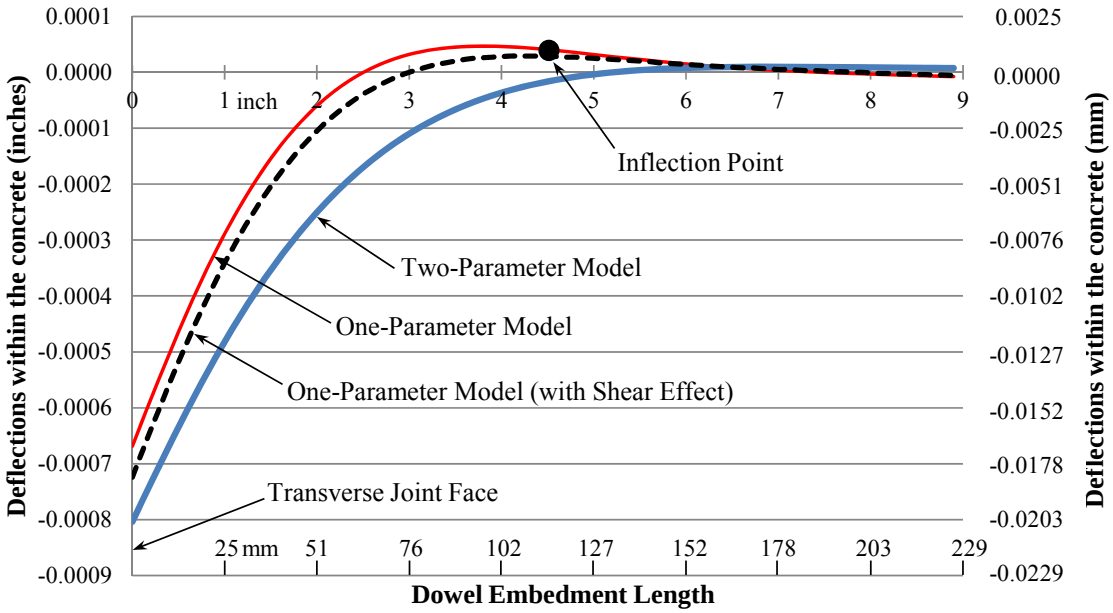

Figure 2-7 Foundation comparison for 1.50-inch (38.10-mm) diameter dowel

Figure 2-8 illustrates the deflected shape (inches and millimeters) for the 1.34- x 1.98-inch (34.04- x 50.29-mm) elliptical-shaped dowel using the one- and two-parameter, elastic foundation models. The deflected shape for the one-parameter model that

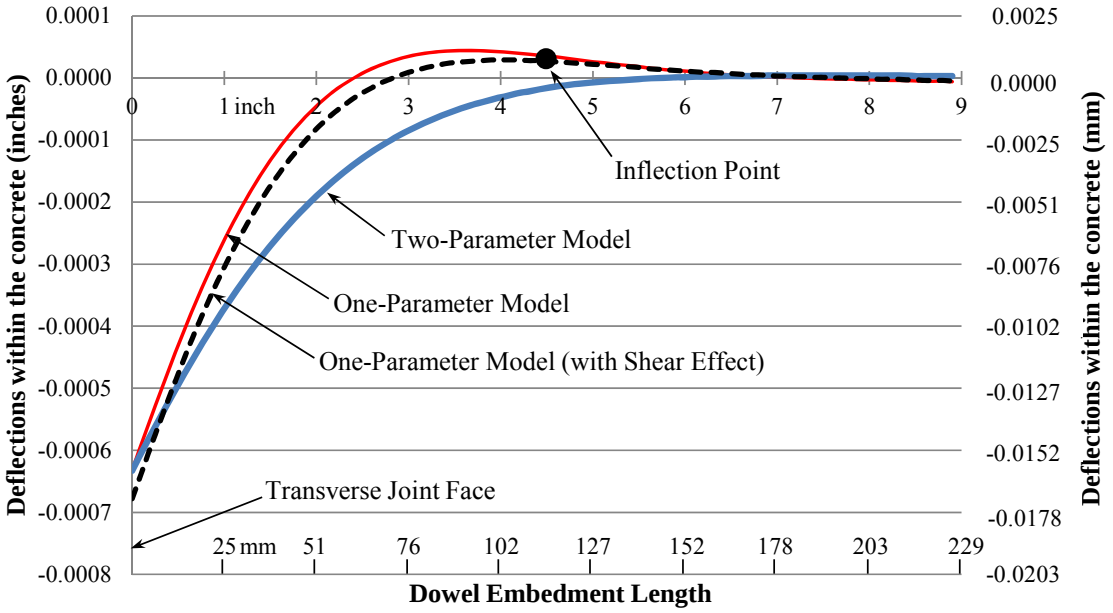

Figure 2-8 Foundation comparison for 1.34- x 1.98-in. (34.04- x 50.29-mm) elliptical dowel

included shear deflection along its length was also shown. The deflected shape for both models is different; however, the maximum deflection at the transverse joint is roughly the same.

Figure 2-7 is typical of the deflected shape comparison for the circular-shaped dowels, and Figure 2-8 is typical of the deflected shape comparison for elliptical-shaped dowels.

Plotting the moment and shear along the dowel's embedment length showed that, for shorter embedment lengths, finite beam theory and the two-parameter model did not converge to zero at the end of the embedded dowel. This discrepancy occurred for embedment lengths less than about nine inches (229 mm). A nine-inch (229-mm) embedment length corresponds to an overall dowel length of 18 inches (457 mm).

2.14 Summary, Conclusions and Recommendations

2.14.1 Summary

The theoretical dowel deflections within the concrete were determined for six different steel dowel sizes, having either a circular or an elliptical shape, embedded in concrete. These deflections were determined using the stiffness method of structural analysis for a beam on elastic foundation. The deflections at the transverse joint face were compared to experimental deflections found through laboratory testing. Dowels that were investigated in this paper are used for highway or airport pavements.

Theoretical analysis was accomplished using two separate foundation models (the one- and two-parameter models) to represent the concrete surrounding the dowel. The deflections along the dowel within the concrete were given as $z_1(x)$ and $z_2(x)$ for the one- and two-parameter models, respectively. One elastic constant defined the one-parameter

model, and two elastic constants defined the two-parameter model. Equations defining these elastic constants (or parameters) were given in this paper.

This paper summarizes calculations for deflections at the transverse joint face for circular- and elliptical-shaped steel dowels embedded in concrete. This analysis was accomplished by:

- Introducing the elliptical shape as an alternative to the circular shape for dowels used in concrete pavement joints which are transverse to traffic flow,
- Comparing two, single-layer, elastic foundation models that were used to represent the concrete for dowels embedded in both sides of an open concrete pavement joint,
- Illustrating the deflected dowel shape for each foundation model. The deflected shape was determined using the stiffness method of structural analysis for a beam on elastic foundation (BEF) along with the assumed displaced shape for both foundation models.

2.14.2 Conclusions

General conclusions are as follows:

- For shorter embedment lengths, plots of the moment and shear along the dowel's embedment length showed that finite beam theory and the two-parameter model did not converge to zero at the end of the embedded dowel. This discrepancy occurred for embedment lengths less than about nine inches (229 mm). A nine-inch (229-mm) embedment length corresponds to an overall dowel length of 18 inches (457 mm) embedded symmetrically about the transverse joint centerline.

The following conclusions were drawn from the investigations of: 1) the dowel deflections of the six different steel dowel sizes, either circular or elliptical shaped, analyzed in this paper using both foundation models, 2) the deflected dowel shapes from Finite Element Analysis (Murrison, et al. 2002) of circular-shaped steel dowels and Fiber Reinforced Polymer (FRP) dowels, and 3) the deflected shape determined by laboratory testing of smaller circular-shaped dowels from Mannava, et al. (1999). Loading is assumed to result in bearing stresses which are less than the concrete's elastic-limit stress (see Chapter 3):

- As the dowel's flexural rigidity (EI) increases for steel and FRP, the two-parameter model may be more appropriate based on the deflected shape,
- The four larger steel dowels used in this research project may be more appropriately represented by the two-parameter model based on the deflected shape,
- The two smaller steel dowels used in this research project may be more appropriately represented by the one-parameter model based on the deflected shape,
- The circular-shaped FRP dowels from Murrison, et al. (2002) should be analyzed using the two-parameter model based on the deflected shape,
- Based on the maximum deflection of all dowel sizes in this research project, the one-parameter model is a good alternative and compares favorably to the two-parameter model.

Three possible reasons that dowels embedded in concrete would be more appropriately modeled using the two-parameter, elastic foundation model instead of the one-parameter, elastic foundation model are:

- Deformation of the dowel's cross section that spreads the load over the supporting medium, i.e. FRP dowels embedded in concrete,
- An elliptical dowel shape – having more contact bearing area than the circular shape with equivalent flexural rigidity,
- The aggregate in concrete may cause the load spreading other than in the vertical direction as the one-parameter (Winkler) model assumes.

Further conclusions are drawn from Tables 2-1 through 2-3 and are summarized below.

- For a given load, and compared to the circular shape with equivalent flexural rigidity, the elliptical shape is an improved alternative for steel dowels used in concrete slab joints based on deflection,
- The elliptical shape, when compared to the circular shape, is determined to have less deflection by the one- and the two-parameter model, and both models determine about the same deflection for the elliptical shape,
- As the dowel's flexural rigidity for the circular and elliptical shape increases, the benefit from the elliptical shape becomes less apparent, and this was determined by the one- and two-parameter models,
- The elliptical shape resulted in lower deflections at the transverse joint face than a comparable circular shape with equivalent flexural rigidity. This lower deflection means the elliptical shape would potentially cause less oblonging of the hole in the concrete surrounding the dowel's cross section,

- The experimental results documented in Table 2-3 match closely to the elastic deflections found using the elasticity equations outlined in Section 3.6.2.

The conclusions from Table 2-4 are as follows:

- As the concrete depth below the dowel is reduced, the resulting dowel deflections within the concrete were smaller for the one-parameter model (k modified) and the two-parameter model. This decreased deflection is due to the reduction in cumulative compression over the smaller depth below the dowel.

The following conclusions are based on Figures 2-7 and 2-8:

- The one- and two-parameter models determine about the same dowel deflections within the concrete at the transverse joint face,
- Shear deflection along the embedded dowel increased the overall deflections determined by the one-parameter model.

2.14.3 Recommendations

The following recommendations are based on this research project:

- Laboratory testing is recommended to determine the deflected shape of dowels embedded in concrete. This shape verifies which foundation model is more representative of a specific dowel size, shape and material,
- Using the one-parameter model for maximum dowel deflections at the transverse joint face is a good alternative when compared to the two-parameter model.

2.15 References

AASHTO, 1993. *AASHTO Guide for Design of Pavement Structures*, American Association of State Highway and Transportation Officials, Washington D.C., 624.

Aydogan, M., 1995. Stiffness-Matrix Formulation of Beams with Shear Effect on Elastic Foundation, *Journal of Structural Engineering*, 121(9), 1265-1270.

Buch, N., and Zollinger, D.G. , 1996. Development of Dowel Looseness Prediction Model for Jointed Concrete Pavements, *Transportation Research Record No. 1525*, 21-27.

Byrum, C.R., 2013. Joint Load Transfer in Concrete Airfield Pavements: Summary Report, Report IPRF-01-G-002-05-2.

Cowper, G.R., 1966. The Shear Coefficient in Timoshenko's Beam Theory, *Journal of Applied Mechanics*, 33(2) (*Transaction of the American Society of Civil Engineers, Vol. 88, Series E*), 335-340.

FAA Advisory Circular, AC 150/5320-6D, 1995. *Airport Pavement Design and Evaluation*, Federal Aviation Administration, Washington, D.C.

Friberg, B.F., 1940. Design of Dowels in Transverse Joints of Concrete Pavements, *Proceedings, American Society of Civil Engineers*, 105, 1076-1116.

Hetenyi, M., 1961. *Beams on Elastic Foundation*, Ann Arbor, Michigan: The University of Michigan Press.

Hognestad, E. *A.*, November 1951. *Study of Combined Bending and Axial Load on Reinforced Concrete Members*, Bulletin 399, University of Illinois Engineering Experiment Station, Urbana, Illinois, 128.

Hsu, T.T.C., Slate, F.O., Sturman, G.M., and Winter, G., February 1963. Micro-cracking of Plain Concrete and the Shape of the Stress-Strain Curve, *Proceedings, Journal of the American Concrete Institute*, 60(2), 209-224.

Huang, Y.H., 1993. Pavement Analysis and Design, Prentice Hall, Englewood Cliffs, New Jersey.

Ingram, D.N.J. *The Effects of the Dowel Bar Shape and Spacing in Portland Cement Concrete Pavements on the Load Transfer Efficiency of the Transverse Joint*, Master's Thesis, Iowa State University, 2004.

Jeanty, P.R., Mitchell, D., and Mirza, M.S., 1988. Investigation of "Top Bar" Effects in Beams, *ACI Structural Journal*, 85(3), 251-257.

MacGregor, J.G., 1988. *Reinforced Concrete Mechanics and Design*, Prentice Hall International Series in Civil Engineering and Engineering Mechanics.

Mannava, S.S., Bush, T.D., and Kukreti, A.R., November-December 1999. Load-Deflection Behavior of Smooth Dowels, *American Concrete Institute: Structural Journal,* 891-898.

Melerski, E.S., 2000. *Design Analysis of Beams, Circular Plates and Cylindrical Tanks on Elastic Foundations*, Rotterdam, Netherlands: A.A. Balkema Publishers.

Murrison, S., Shalaby, A., and Mufti, A.A., June 5-8 2002. Modeling of Concrete Dowel-Slab Interaction. *4th Transportation Specialty Conference of the Canadian Society for Civil Engineering*, Montreal, Quebec, Canada.

Naval Facilities Engineering Command (NAVFAC), Military Handbook (MIL-HDBK-1021/4), *Rigid Design of Airfields*.

Packard, R.G., 1973. *Design of Concrete Airport Pavement*, Portland Cement Association, Skokie, Illinois.

Porter, M.L., Guinn, R.J., and Lundy, A.L., October 2001. *Dowel Bar Optimization: Phase I and II, Final Report*, American Highway Technology (AHT), Center for Transportation Research and Education, Iowa State University.

Selvaduri, A.P.S., 1979. *Elasticity Analysis of Soil-Foundation Interaction*. Elsevior Scientific Publishing Company, Amsterdam, Holland.

Timoshenko, S., and Lessels, J.M., 1925. *Applied Elasticity*, Westinghouse Technical Night School Press, East Pittsburgh, Pennsylvania.

Vallabhan, C.V.G., and Das, Y.C., 1991. Modified Vlasov Model for Beams on Elastic Foundations. *Journal of Geotechnical Engineering*, 117(6), 956 - 966.

Vesic, A.S., 1961. Bending of Beams Resting on Isotropic Elastic Solid. *Journal of the Engineering Mechanics Division, American Society of Civil Engineers*, Vol. 87 (EM2), 35-53.

Vesic, A.S., and Saxena, S.K., 1970. Analysis of Structural Behavior of AASHO Road Test Rigid Pavements, *National Cooperative Highway Research Report 97*, Highway Research Board, Washington, D.C.

Vlasov, V.Z., 1966. *Beams, Plates and Shells on Elastic Foundations*, (Translated from Russian), Israel Program for Scientific Translation, Jerusalem, Israel.

Weaver, W., and Gere, J.M., 1990. *Matrix Analysis of Framed Structures*, 3rd Edition, Von Nostrand Reinhold International Company.

Westergaard, H.M., 1938. A problem of Elasticity Suggested by a Problem in Soil Mechanics: Soft Material Reinforced by Numerous Strong Horizontal Sheets, *Contributions to the Mechanics of Solids, Stephen Timoshenko 60th Anniversary Volume*, MacMillan, New York, 268-277.

Winkler, 1867. Die Lehre vonder Elastizitat und Festigkeit (Prag), 182. (Cited in Hetenyi 1961, pp. 1).

Yoder, E.G., and Witczak, M.W., 1975. *Principles of Pavement Design*, 2nd Edition, John Wiley & Sons, Inc., New York, NY.

Zaretskii, Y.K., 1972. *Theory of Soil Consolidation*, (Translated from Russian), Israel Program for Scientific Translations, U.S. Department of the Interior and the National Science Foundation, Washington, D.C.

Zhaohua, F., and Cook, R.D., 1983. Beam Elements on Two-Parameter Elastic Foundations, *Journal of Engineering Mechanics*, Vol. 109(6), 1390-1403.

CHAPTER 3. FOUNDATION MODELS FOR DOWELS EMBEDDED IN CONCRETE: PART II – LINEAR-ELASTIC ANALYSIS AND BEARING STRESS

A paper prepared for submission to the *International Journal of Pavement Engineering*

Eric A. Lorenz[1]*, P.E., Max L. Porter*[2]*, P.E.,*
and Fouad S. Fanous[3]*, P.E.*

Abstract

Shear transfer across doweled joints in concrete pavements on grade has been investigated by several researchers in past years. Improving the analysis of circular- and elliptical-shaped steel dowels embedded in these joints is the topic of a two-part companion paper. The first paper shows how to calculate dowel deflections within the concrete, and this second paper shows how to limit the magnitude of the bearing stress between the dowel and the concrete.

Two published analytical models, which utilized beam on elastic foundation theories, represented the concrete surrounding the dowel. Modifying one of these models to include the effect of pavement thickness allowed for the comparison of both models. Their resulting theoretical bearing stress distributions were compared to the elastic-limit stress for the concrete. These comparisons showed that a dowel with an elliptical shape, having the same flexural rigidity as a comparable circular shape, had reduced bearing stress along the embedment length.

[1] Doctoral Candidate, Civil Engineering, Department of Civil, Construction and Environmental Engineering, Iowa State University, Ames, Iowa 50011

[2] University Professor Emeritus, Civil Engineering, Department of Civil, Construction and Environmental Engineering, Iowa State University, Ames, Iowa 50011

[3] Professor, Civil Engineering, Department of Civil, Construction and Environmental Engineering, Iowa State University, Ames, Iowa 50011

3.1 Introduction

Dowels are subject to continuous cycles of fatigue loading as they transmit shear loads between adjacent slabs in a concrete pavement. These slabs are separated by transverse joints of width c spaced at regular intervals. As the continued load cycling occurs, the bearing between the dowel and the concrete can cause "oblonging" or permanent deformation of the concrete surrounding a typical circular-shaped dowel. For dowels embedded in concrete pavement joints, the elliptical shape (Porter, et al. 2001) was compared to the circular shape with equivalent flexural rigidity. The goal of the elliptically-shaped dowels was to reduce the maximum contact bearing stress between the dowel and the concrete and reduce oblonging.

Transverse joints (either construction or contraction joints) are used in concrete pavements on grade as a method to control crack formation in the slab sections. Drying shrinkage, in combination with colder temperatures, cause the adjacent slabs on either side of the joint to shorten. The joint opens, and the dowels, spaced along this joint, transfer fifty percent of each wheel load (Yoder, et al. 1975) from one slab section to the next. A balanced joint means the remaining fifty percent of each wheel load is transferred from the slab sections to the subgrade.

Load transfer between slab sections was accomplished by distributing the portion of each wheel load, positioned along the transverse joint, laterally to the effective dowels (Friberg 1940). The shear load (V) on a specified dowel varies according to the axle weight and the position of the axle along the joint which spans the lane width. The resulting maximum bearing stress along the embedded dowel occurs at the transverse joint face and corresponds to the maximum dowel deflection. If the maximum bearing

stress exceeds the concrete's elastic-limit stress due to overloading, or if repetitive loading does not permit the concrete to rebound to its original or reference state after each load, the concrete around the dowel will permanently deform.

This paper calculates the bearing stress around circular- and elliptical-shaped steel dowels. Also, a limit on the maximum bearing stress (and repeated bearing stress) was proposed to minimize the deterioration of the concrete surrounding the dowel.

3.2 Bearing Stress

The wheel loads are distributed laterally to the dowels spaced along the joint as mentioned previously. The corresponding shear load (V) for each dowel is applied through the dowel's inflection point in the transverse joint center. The shear load (V) and calculated moment (M) at the transverse joint face (as shown in Figure 3-1) are used to

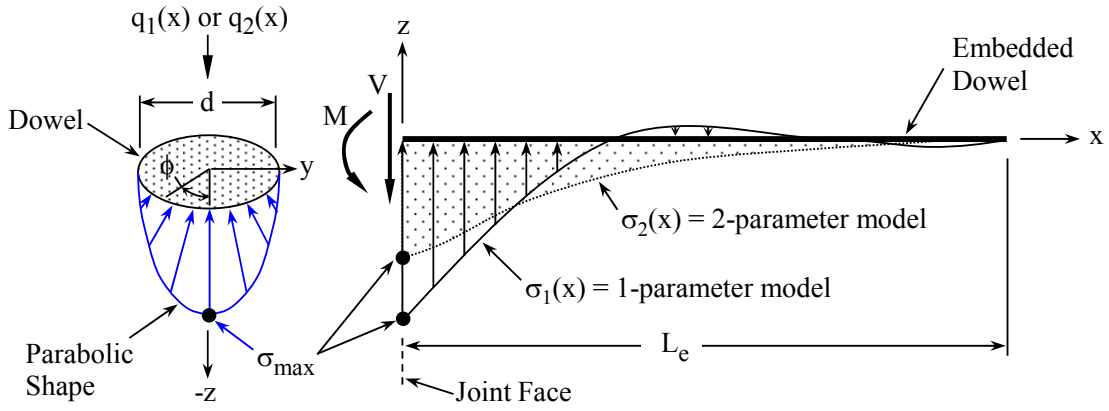

Figure 3-1 Bearing stress along an embedded dowel

determine the dowel-concrete reaction (q), which is distributed along the dowel's embedment length. The dowel-concrete reaction is termed either $q_1(x)$ or $q_2(x)$ for a one- or two-parameter, elastic foundation model, respectively. The dowel-concrete reaction occurs on the same side as the radial stress distribution; however, this reaction was considered as a load in equations and figures throughout this paper.

A radial stress distribution (Marcus 1951) was determined from $q_1(x)$ or $q_2(x)$ at a particular location of x along the dowel's embedment. The radial stress replaces the commonly used uniform stress distribution across the dowel's width. The contact bearing stress, or bearing stress between the dowel and the concrete, corresponds to the peak radial stress.

The radial stress varies according to the radial angle ϕ along the dowel's bottom-half circumference with this stress distribution having an assumed parabolic shape. The maximum value or peak occurs when ϕ is zero as shown in Figure 3-1. Also, the peak radial stress (or bearing stress) was shown to vary along the dowel's embedment length according to the assumed displaced shape (z_1 or z_2 as defined by Equations 2-5 and 2-15 respectively) and its fourth derivative (q_1 or q_2) with a maximum value occurring at the transverse joint face.

Figure 3-1 shows the distribution of bearing stress along the dowel's embedment length (L_e) and across the dowel's width (d) for both the one- and two- parameter models (see Chapter 2). Both stress distributions along the embedded dowel in Figure 3-1 have the same shape as their respective displaced shapes, and their respective dowel-concrete reaction shapes.

The stress distribution at the transverse joint face varies according to elasticity equations (Boussinesq ca. 1885, Westergaard 1938, and Spangler 1951) which show the stress reduces exponentially throughout the depth in the concrete below the dowel. The stress at the contact between the dowel and the concrete, according to the elasticity equations, is the same as the peak radial stress (or bearing stress).

One set of wheel loads positioned along the transverse joint is used to determine the dowel-concrete reaction (q_1 or q_2) and to determine the maximum bearing stress for each dowel. Repeat wheel loading however, as explained next, may be very detrimental to the concrete surrounding the dowels.

3.2.1 Repetitive Dowel Loading

Wheel loading along the transverse joint in a concrete pavement is cyclic (or variable cyclic), dynamic and sometimes sustained (or static). Wheels typically follow a similar path within the lane width, commonly referred to as wheel paths. Repeat loading within the wheel paths, in this paper, is assumed to be variable cyclic loading from normal weight vehicles, including axle loads from the same vehicle. Repeat loading may not allow the dowel deflection within the concrete to completely rebound to its reference state [before] another set of wheel loads crosses the transverse joint. In this repeat load case, linear-elastic analysis may not apply since permanent concrete deformation would be present.

3.2.2 Variability of Elastic Constants

The elastic constants (Sections 2.9.6 and 2.10.2) or parameters for the two foundation models are based on the elastic range of the supporting concrete medium as well as the dowel. These constants are k or k_o for a one-parameter model, and k_a and k_b for a two-parameter model. Loading that causes the bearing stress to exceed the concrete's elastic-limit stress should not be used to evaluate these parameters. The elastic constants, however, may change over time from repeating stresses that do not exceed the concrete's elastic-limit stress.

The elastic constants may change due to a reduction in the concrete's elastic modulus (E_c) resulting from repeat compressive loading (MacGregor 1988). The equation for k (see Equation 2-14) indicates that a lower elastic modulus will result in a reduction in k. A reduction in k will increase the dowel deflections. Even though the deflections increase, the reduction in the concrete's elastic modulus (and k) will cause the dowel-concrete reaction (q_1) to decrease slightly. For a given repeat dowel load, below the elastic limit, there may be an increase in dowel deflections within the concrete without permanent concrete deformation around the dowel.

Due to the possibility of a reduction in the concrete's elastic modulus from repeat loading, the secant modulus was selected over the initial tangent modulus. The secant modulus is roughly ten percent smaller than the initial tangent modulus (MacGregor 1988). The elastic modulus for concrete was calculated by the expression $57{,}000(f_c')^{1/2}$ from MacGregor (1988).

3.2.3 Limit on Maximum Bearing Stress

A limit on maximum bearing stress for dowels embedded in concrete requires that the maximum load on the dowel must be reduced or maintained below some level during repeat loading. This level is being limited to some portion of the concrete's elastic-limit stress. A reduction in load applied to the dowels is equivalent to reducing the bearing stress, which can be achieved by one of the following: 1) increasing the slab thickness, 2) leaving the slab thickness constant and increasing the concrete's compressive strength (f_c'), reducing the subgrade's stiffness by reducing the modulus of subgrade reaction (k_s), or spacing the dowels closer together, or 3) leaving the slab thickness and dowel spacing constant and using larger dowels or using elliptical-shaped dowels.

A stiffer subgrade below the pavement corresponds to an increase in the k_s value and occurs when one of the following is present: 1) increasing the thickness of a well-compacted subbase (NAVFAC), 2) frozen subgrade, or 3) dense rock or bedrock subgrade. With concrete properties, concrete thickness and wheel loads remaining constant, a stiffer foundation will increase the shear load on a specified dowel. Increasing the shear load will increase the bearing stress between the dowel and the concrete.

The limit on maximum bearing stress (or a smaller bearing stress which is repeated) was determined to be the end of the assumed linear portion of the stress-strain curve as shown in Figure 3-2. The corresponding stress was $0.45f_c'$ (McCormac, et al. 2009) which was referred to as the concrete's elastic limit. Below a stress of $0.45f_c'$ the concrete is assumed to have elastic properties predicted by Hooke's law. If the concrete is stressed above its elastic-limit stress, permanent concrete deformation from non-linear behavior leads to voids around the dowel. These voids result in increased differential slab deflections with more of each wheel load transferred to the subgrade as vehicles cross the joint.

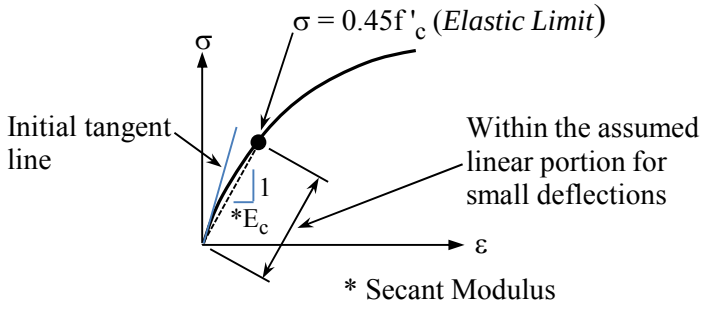

Figure 3-2 Concrete stress-strain curve and the limit on maximum bearing stress

Equation 3-1 below gives the limit on maximum bearing stress considering a factor of safety (FS). The FS is greater than one. The primary use of the FS is to prevent repeat loading from stressing the concrete near its elastic limit, since the initial linear portion is more curved than linear for the concrete medium as shown in Figure 3-2.

$$\sigma_{limit} = \frac{0.45 \cdot f'_c}{FS} \tag{3-1}$$

Where:
f'_c = concrete's compressive strength, psi (MPa)
FS = factor of safety (greater than one)

3.2.4 Dowel-Concrete Reaction (Load)

The dowel-concrete reaction or load (q_m) is determined for the two different elastic foundation models and is directly related to the bearing stress. The subscript m signifies the foundation model; one is used for the one-parameter model (semi-infinite beam and finite beam theories as a function of x), and two is used for the two-parameter model. Equations 3-2 and 3-3 give the dowel-concrete reaction (load) for each of these models, respectively. Equations for $z_1(x)$ and $z_2(x)$ have been given previously (see Chapter 2).

$$q_1(x) = k \cdot z_1(x) \tag{3-2}$$

Where:
k = contact modulus in the one-parameter model, psi (MPa)
See Section 2.9.6 for "k not modified" and "k modified" equations
$z_1(x)$ = deflections along the dowel within the concrete,
one-parameter model, in. (mm)

$$q_2(x) = 2k_a \cdot z_2(x) \tag{3-3}$$

Where:

k_a = Winkler constant in the two-parameter model, psi (MPa)
See Section 2.10.2 for elastic constants in the two-parameter model

$z_2(x)$ = deflections along the dowel within the concrete, two-parameter model, in. (mm)

The one-parameter model can be defined by either semi-infinite beam (Friberg 1940) or finite beam (Timoshenko, et al 1925 and Timoshenko 1976) theories as a function of x according to Equation 3-2. The semi-infinite beam theory is equal to the finite beam theory for beams with characteristic length (βL_e) equal to π or greater. The first companion paper (Chapter 2) presented an equation in matrix form for the deflection (z_o) and slope (θ_o) of embedded dowels at the transverse joint face which satisfies the semi-infinite beam theory criteria.

Equation 3-4 gives the dowel-concrete reaction (q_o) for the semi-infinite beam theory when x is zero at the transverse joint face. The deflection (z_o) is equivalent to q_o divided by k. When the subscript m is equal to o (lower case o), this signifies the semi-infinite beam theory (x equal to zero) and q_o will be equal to $q_1(0)$, from Equation 3-2, for βL_e equal to π or greater.

$$q_o = 2 \cdot \beta \cdot (V - M \cdot \beta) \tag{3-4}$$

Where:

β = characteristic of the system, in^{-1} (mm^{-1})
V = shear at the joint face, lb. (kN)
M = moment at the joint face, in-lb. (kN-m)

The dowel-concrete reaction has been inverted and shown as a varying load applied along the embedded dowel's length in Figure 3-3. This distributed load is for the one-parameter model using either finite beam or semi-infinite beam theory as a function of x. When the distributed load $q_1(x)$ is applied to the dowel in Figure 3-3 the resulting deflections will be the same as given by the function $z_1(x)$. Therefore, only the deflection at the transverse joint face or $z_m(0)$ is required to determine the maximum bearing stress.

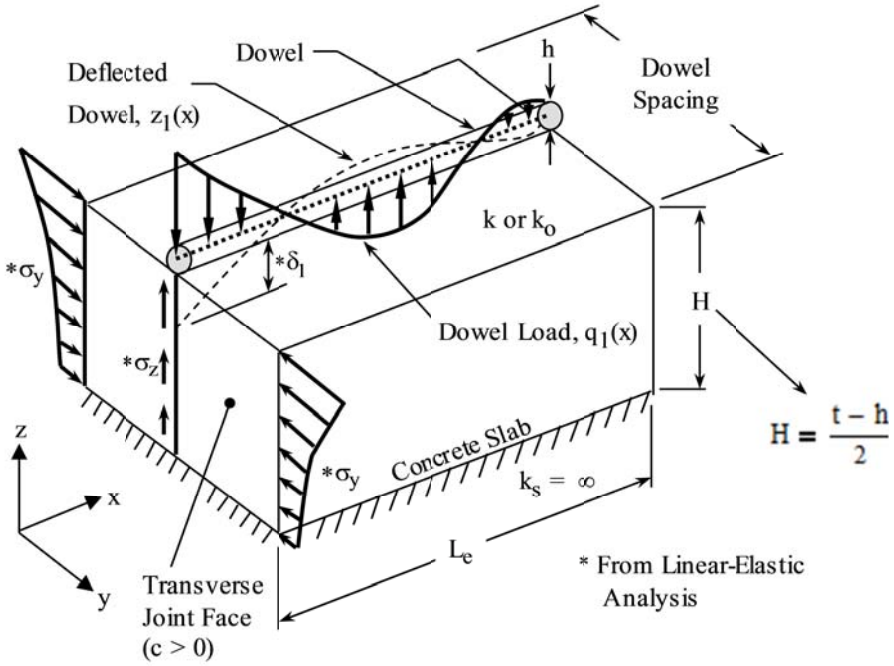

Figure 3-3 Isolating the dowel within the concrete (one-parameter model)

3.3 Uniform Stress Distribution

Past dowel research has always assumed a uniform stress distribution across the dowel's width as shown in Figure 3-4. Friberg (1940) assumed a uniform stress distribution below a dowel supported by an elastic mass and Hetenyi (1961) assumed uniform stress below a beam supported by an elastic foundation. The bearing stress at any point along the dowel's embedment length was calculated using Equation 3-5 which

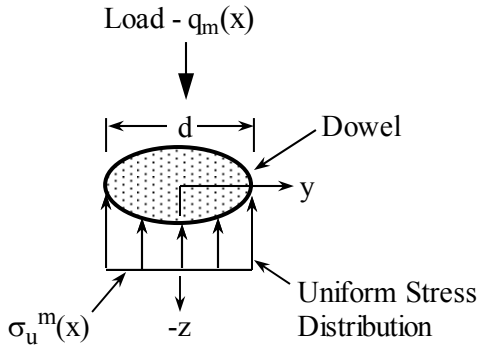

Figure 3-4 Uniform stress below the dowel at the joint face

assumes a uniform stress distribution across the dowel's width. Equation 3-5 applies to either a circular- or an elliptical-shaped dowel in the elastic range.

$$\sigma_u{}^m(x) = \frac{q_m(x)}{d} \tag{3-5}$$

Where:
$q_m(x)$ = dowel-concrete reaction (load) along the dowel's embedment length, lb/in (kN/m)
Typical for the following equations unless noted otherwise;
m = 1 for the one-parameter model (either finite beam or semi-infinite beam theories as a function of x)
= 2 for the two-parameter model
= o (lower case o) for the semi-infinite beam theory when x is equal to zero

Results in this paper verified that the compatibility between the load (q_m) and a uniform stress distribution was not satisfied. Therefore, a radial stress distribution (Marcus 1951), with an assumed parabolic shape, was chosen that varies along one half the dowel's circumference opposite the load. The radial stress distribution was verified to be compatible with the dowel-concrete reaction $q_m(x)$.

3.4 Radial Stress Distribution

The contact modulus (k), see Equation 2-14, and $k_o d$ are equivalent, and either may be used in the one-parameter model. The bearing stress below the dowel, however, is not uniform and not equal to the results from Equation 3-5. To transition from the uniform stress distribution to a radial stress distribution, consider Figure 3-5.

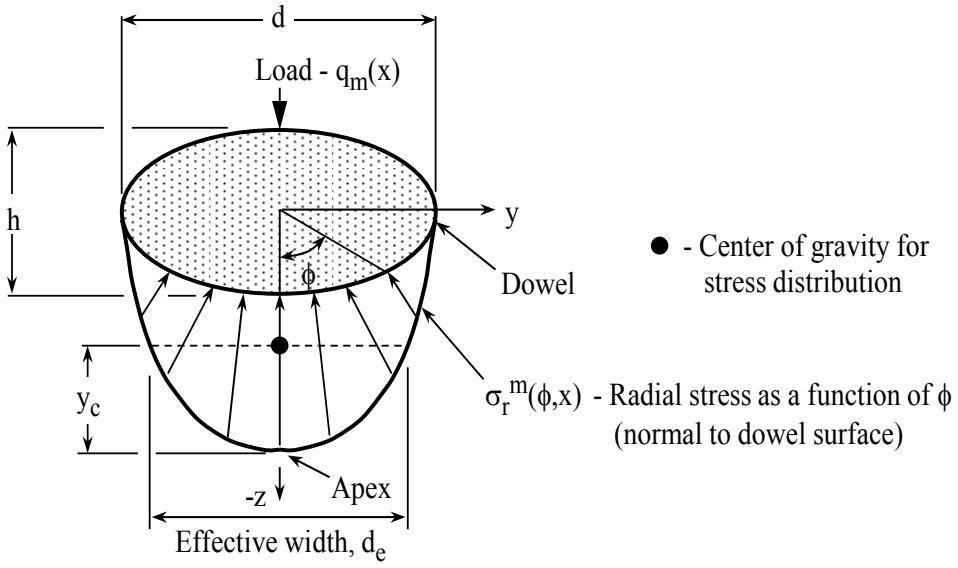

Figure 3-5 Radial stress distribution (parabolic shape) below a dowel

The effective width (d_e) in Figure 3-5 was determined at a point between the apex and the extreme bottom of the dowel or peak stress region at a distance y_c up from the apex. The width d_e is at the center of gravity of the radial stress distribution and is given by Equation 3-6.

Marcus (1951) indicated that the radial stress distribution along the dowel's bottom-half circumference is a function of the vertical load applied to the dowel. Researchers at Iowa State University considered the dowel-concrete reaction (q_m) as the

$$d_e = d \cdot \left(\frac{s+1}{2 \cdot s+1} \right)^{\frac{1}{s}} = 0.775 \cdot (d) \tag{3-6}$$

Where:
d_e = width of the parabolic-shaped stress distribution at the center of gravity, in. (mm)
s = 2 for a second degree parabolic stress distribution

vertical load applied to the dowel. The radial stress distribution (as a function of ϕ) at any location x along the dowel's embedment length is given by Equation 3-7.

$$\sigma_r{}^m(\phi, x) = \frac{4}{\pi} \cdot \left(\frac{q_m(x)}{d} \right) \cdot cos(\phi) \tag{3-7}$$

Where:
$\sigma_r{}^m$ = radial stress, psi (MPa)
$q_m(x)$ = dowel-concrete reaction along the dowel's embedment, lb/in (kN/m)
ϕ = radial angle (radians)

Equation 3-7 can be used for either a circular- or an elliptical-shaped dowel, and the stress distribution has an assumed second degree parabolic shape. The radial stress is a function of the radial angle (ϕ) and is normal to the dowel's surface for both the circular and elliptical shapes. The maximum radial stress, according to Equation 3-7, occurs at the joint face when x is zero and at the bottom of the dowel when ϕ is zero as shown in Figure 3-5.

3.4.1 Radial Stress with a Parabolic Shape

Considering the one-parameter model with either finite beam or semi-infinite beam theories and the two-parameter model, the following equation was developed. Bearing stress, with an assumed parabolic shape, can be determined at any point along the dowel's embedment length using Equation 3-8. The maximum value occurs at the

$$\sigma_m(x) = \frac{q_m(x)}{d_e} = 1.291 \cdot \left(\frac{q_m(x)}{d} \right) \tag{3-8}$$

Where:
σ_m = bearing stress along the dowel's embedment length, psi (MPa)
x = distance along the dowel, in. (mm)
$q_m(x)$ = dowel-concrete reaction along the dowel's embedment length, lb/in (kN/m)

transverse joint face where x is zero. This equation gives an average stress based on the parabolic shape. Equation 3-8 can be used for the radial stress distribution when it's multiplied by cos(ϕ) where ϕ is the radial angle as shown in Figure 3-5.

Equations 3-7 and 3-8 resulted in 27 and 29 percent more bearing stress, respectively, than given by Equation 3-5. The increase in bearing stress is due to the use of radial stress distribution when compared to uniform stress distribution. The radial stress distribution will be verified later in this paper as the correct distribution for the circular- and elliptical-shaped dowels.

3.4.2 Horizontal and Vertical Components of Radial Stress

Radial stress given by Equation 3-7 has two components that have been investigated at Iowa State University. Both components of radial stress vary according to the radial angle ϕ and the angle θ(ϕ) as shown in Figure 3-6, and θ(ϕ) applies to both the circular and the elliptical shapes. When considering only the circular shape, replace θ(ϕ) with ϕ in the following two equations.

The horizontal stress is zero at the bottom and the mid-height of the dowel with a maximum at the quarter point up from the bottom of the dowel (when ϕ is ±π/4) according to Equation 3-9.

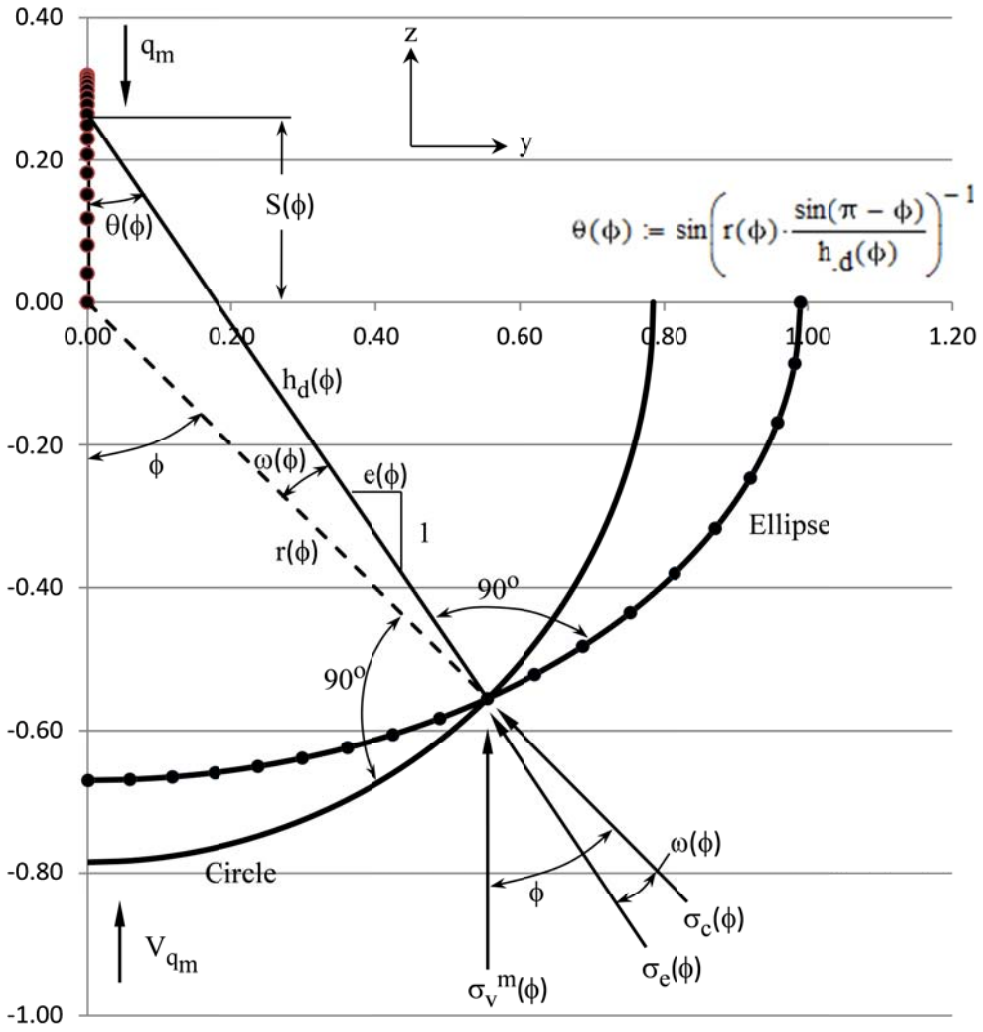

Figure 3-6 Graphical depiction of parabolic stress distribution at location x

$$\sigma_h^m(\phi, x) = \sigma_r^m(\phi, x) \cdot sin(\theta(\phi)) \tag{3-9}$$

The horizontal components on either side of the dowel cancel; however, they confine the dowel and limit deformation of the cross section within the concrete during loading.

The vertical stress given by Equation 3-10 was integrated, considering radial coordinates, along the dowel's bottom-half circumference to find the sum of vertical stress. This sum (V_{q_m} in Figure 3-6) is equal to the loads $q_1(x)$ or q_o, or $q_2(x)$ depending on the foundation model chosen.

$$\sigma_v{}^m(\phi, x) = \sigma_r{}^m(\phi, x) \cdot cos(\theta(\phi)) \tag{3-10}$$

3.4.3 Verification of Radial Stress Distribution

A graphical depiction of the radial stress distribution is shown in Figure 3-6. One quarter of the cross section for the circular- and elliptical-shaped dowels was shown with the origin at zero in Figure 3-6. The load $q_m(x)$ was applied along a line passing through the origin and the exact location varied with the radial angle ϕ and the distance from the origin given by $S(\phi)$. The law of cosines was used to verify the line length for $h_d(\phi)$ which had a slope $e(\phi)$. The line length for $h_d(\phi)$ was constant and equal to d/2. The slope of the line for $h_d(\phi)$ is given in Equation 3-11 where d is the dowel's major axis and h is the dowel's minor axis. The line $h_d(\phi)$ was perpendicular to the elliptical shape at one end, and the load $q_m(x)$ was applied at the other end.

$$e(\phi) = -\left(\frac{d}{h}\right) \cdot \frac{1}{tan(\phi)} \tag{3-11}$$

Where:
h = the dowel's minor axis, in. (mm)
d = the dowel's major axis, in. (mm)

The stresses were shown at the intersection of the circle and the ellipse in Figure 3-6. The stress $\sigma_c(\phi)$ was perpendicular to the circular shape and in line with $r(\phi)$, and the stress $\sigma_e(\phi)$ was perpendicular to the elliptical shape and in line with $h_d(\phi)$.

The radius in polar coordinates, for the circular and elliptical shapes, was given as a function of the radial angle ϕ by Equation 3-12. The radius is constant for the circular shape but not for the elliptical shape. Finally, the vertical stress along the dowel's

$$r(\phi) = \frac{h \cdot d}{2 \cdot \sqrt{d^2 \cdot cos(\phi)^2 + h^2 \cdot sin(\phi)^2}} \tag{3-12}$$

bottom-half circumference was integrated. The value of $V_{q_m}(x)$ from Equation 3-13 was equal to the dowel-concrete reaction $q_m(x)$, which was applied as a load.

$$V_{q_m}(x) = \int_0^{\frac{\pi}{2}} \sigma_v{}^m(\phi, x) \cdot \sqrt{d^2 \cdot cos(\phi)^2 + h^2 \cdot sin(\phi)^2}\, d\phi \tag{3-13}$$

Where:

$V_{q_m}(x)$ = resultant of vertical stress distribution, lb/in. (kN/m)

3.5 Radial Stress for an Arch on Elastic Foundation

Hetenyi (1961) published work for a circular arch on elastic foundation. The arch was a prismatic beam of constant cross-sectional thickness and a unit length (into the page) defined by a radius (r) and radial angle (ϕ). The equations were modified to include arches with either a circular or an elliptical shape, and r was replaced with r(ϕ) as shown in Figure 3-7. The value of k (see Equation 2-14) was equal to the k value from a

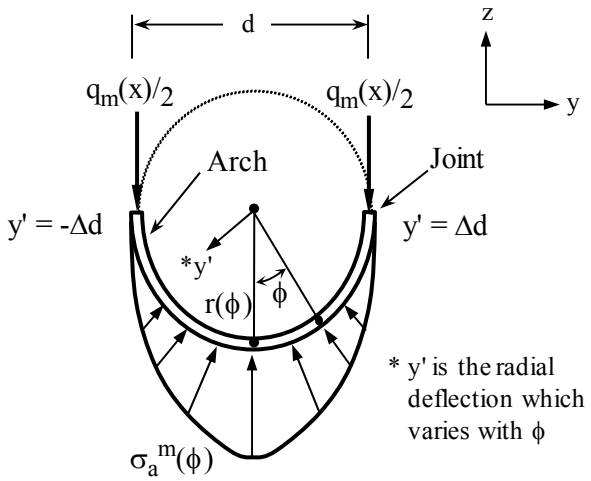

Figure 3-7 Circular arch on elastic foundation

solid-dowel section. The k value was equivalent to k_o (modulus of foundation) since the unit length was one (into the page). The radial stress (σ_a^m) depends on the foundation model (m) and is equivalent to $y`(\phi)k_o$ where $y`(\phi)$ is the radial deflection. The value of m is based on the one-parameter model; one is used for either the finite beam theory or the semi-infinite beam theory as a function of x, and o (lower case o) is used for the semi-infinite beam theory when x is zero. The purpose of the arch in this research was to compare the radial and horizontal stress and deflections from Hetenyi to those found using other methods. Also, the deformation of the dowel's cross section within the concrete was investigated.

Only the bottom half of the arch was used. The flexural rigidity was set very high resulting in a rigid arch which modeled the solid-dowel cross section. The arch consisted of two joints or nodes where boundary conditions were applied to solve for constants (C_0, $C_1 \ldots C_4$). One joint occurs when ϕ is $\pi/2$ and the second joint occurs when ϕ is $-\pi/2$. The dowel-concrete reaction, or $q_m(x)$, was divided in two and applied symmetrically to each joint as a ring compression force. Each joint was permitted to move radially ($y`$) a distance Δd (the joint on the left side of Figure 3-7 moves $-\Delta d$) to represent dowel deformation within the concrete.

The radial stress according to Hetenyi (1961) was modified to accommodate the elliptical shape by researchers at Iowa State University and given by Equation 3-14. To determine the horizontal stress distribution, the radial stress was multiplied by $\sin(\theta(\phi))$ where $\theta(\phi)$ is shown in Figure 3-6. The radial stress from Equation 3-14 and the

$$\sigma_a{}^m(\phi) = k_o \cdot N_1{}^T(\phi) \cdot \begin{pmatrix} C_0 \\ C_1 \\ C_2 \\ C_3 \\ C_4 \end{pmatrix} \tag{3-14}$$

Where:
k_o = modulus of foundation, pci (MPa/m)

$$N_1(\phi) = \begin{pmatrix} 1 \\ \cosh(\alpha'(\phi)\cdot\phi)\cdot\cos(\beta'(\phi)\cdot\phi) \\ \sinh(\alpha'(\phi)\cdot\phi)\cdot\cos(\beta'(\phi)\cdot\phi) \\ \cosh(\alpha'(\phi)\cdot\phi)\cdot\sin(\beta'(\phi)\cdot\phi) \\ \sinh(\alpha'(\phi)\cdot\phi)\cdot\sin(\beta'(\phi)\cdot\phi) \end{pmatrix}$$

$$\eta(\phi) = \sqrt{\frac{r(\phi)^4 \cdot k}{E \cdot I} + 1}$$

$$\alpha'(\phi) = \sqrt{\frac{\eta(\phi) - 1}{2}}$$

$$\beta'(\phi) = \sqrt{\frac{\eta(\phi) + 1}{2}}$$

corresponding horizontal stress matched very closely to the results for radial and horizontal stresses from other methods given throughout this paper.

If the arch was allowed to deform, the radial deflection (y`) was assumed to be Δd and -Δd in Figure 3-7. Due to this deformation, the bearing stress beneath the arch and the arch deflections within the concrete decrease for a given load. The deformation of the dowel, however, may not occur due to the confining (horizontal or y direction) stress from the concrete. As the load $q_m(x)$ increases, more confining stress will be required

than would be available through the concrete medium, and the concrete may deteriorate by tensile splitting (Vintzeleou, et al. 1986).

3.6 Linear-Elastic Analysis

Differential equations do not determine the variation in deflection and stress throughout the depth below the dowel. Elasticity equations were used in this paper to determine deflection and stress profiles at the transverse joint face for any given concrete depth (H) below the dowel. Figure 3-8 shows this depth and illustrates the two-parameter model's deflected shape and load (q_2) along the embedded dowel. Also, elasticity equations were used to determine changes in deflections and bearing stress between the dowel and the concrete as the depth (H) approaches zero for both foundation models.

Linear elasticity, when applied to a concrete medium, must satisfy three fundamental criteria before the theory is valid (Spangler 1951):

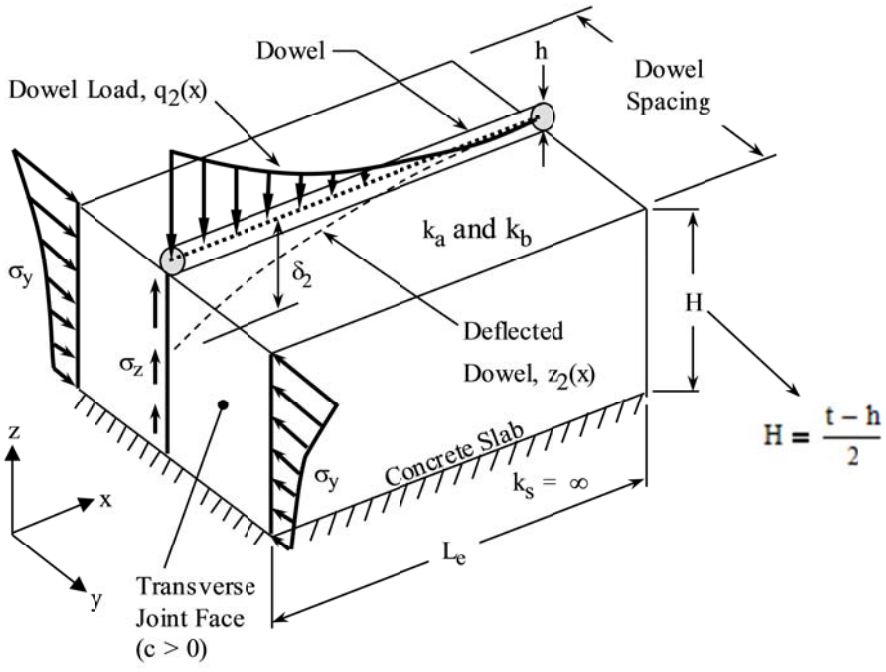

Figure 3-8 Isolating the dowel within the concrete (two-parameter model)

- The total vertical pressure under the dowel must be equal to the applied load $q_1(x)$ or $q_2(x)$ – stress equilibrium.
- There must not be any cracks in the concrete medium – strain compatibility.
- The boundary conditions should comply with those assumed in the mathematical derivation – thus, no discontinuities or joints.

The 3rd criterion will not be satisfied for dowels embedded in concrete along a joint (with c greater than zero) or discontinuous edge. Therefore, stress analysis based on elasticity equations such as Boussinesq (ca. 1885) and Westergaard (1938) may not be directly applicable to jointed pavement slabs.

3.6.1 Exponential Stress Distribution

A modified Boussinesq equation (Spangler 1951) as given by Equation 3-15 can be used to account for this non-compatibility (where the concrete medium was not

$$\sigma_z^{\,m}(z) = \int_0^{L_e} \int_{-\frac{d}{2}}^{\frac{d}{2}} \frac{(n-2)\cdot q_m(x)\cdot z^{n-2}\cdot\sqrt{a}}{2\cdot\pi\cdot d\cdot\left(\sqrt{x^2+y^2+a\cdot z^2}\right)^n}\, dy\, dx \tag{3-15}$$

Where:

$\sigma_z^{\,m}(z)$ = stress in z-direction as a function of z – where $z \geq 0.001$, psi (MPa)

$a = \dfrac{1-2\cdot\mu_c}{2-2\cdot\mu_c}$ Poisson's effect

n = 5.0 = concentration (dispersion) factor

μ_c = concrete Poisson's ratio

L_e = dowel's embedment length, in. (mm)

d = dowel's width perpendicular to loading, in. (mm)

x, y, z = distance along each axis, in. (mm)

Typical for the following equations unless noted otherwise;

m = 1 for the one-parameter model (either finite beam or semi-infinite beam theories as a function of x)

= 2 for the two-parameter model

continuous below dowel). The n value shown in Equation 3-15 is the concentration or dispersion factor that defines the load spreading on a horizontal plane below the actual load (Spangler 1951). Boussinesq concluded that n was 5.0, and Westergaard used a value of 3.0 for n. The n value in Equation 3-15 can be solved for by experimental or theoretical methods. For this paper, n was assumed to be 5.0 which allowed Equation 3-15 to match other methods used to calculate the bearing stress.

Depending on the model chosen, using a value of one or two for the subscript m signifies the one- or two-parameter model, respectively. A value of o (lower case o) for the subscript m is acceptable when calculating contact bearing stress; however, the exponential stress profile throughout the depth below the dowel at the transverse joint face will not be correct.

The stress below a dowel at the face of a transverse joint is given by three components (σ_x, σ_y and σ_z) in the direction of each axis. These stresses in the x-, y- and z-directions are exponential, and the stresses in the y- and z-directions are shown in Figures 3-3 and 3-8. The stress in the x-direction (σ_x) is zero since the transverse joint width is greater than zero. Peak stresses for σ_y and σ_z occur between the dowel and the concrete at the transverse joint face. The dowel-concrete reaction $q_1(x)$ was applied as a load from the one-parameter model as shown in Figure 3-3, and $q_2(x)$ was applied as a load from the two-parameter model as shown in Figure 3-8.

The distribution in stress and deflection throughout the depth in the concrete below the dowel (depth as a function of z) can be determined using elasticity equations. The elasticity equation shown in Equation 3-15 combines Boussinesq and Westergaard theory into a modified equation (Spangler 1951) for stress below the dowel. The values

of $q_1(x)$ and $q_2(x)$ are a maximum at the transverse joint face and vary along the dowel's embedment length to zero at the embedded end. Dividing $q_1(x)$ or $q_2(x)$ by the dowel's width (d) distributes the load. Integrating the distributed load (pressure) over the dowel's length and width allows the stress to be determined at any depth z below the dowel within the concrete at the transverse joint face. The stress profile below the dowel reduces exponentially throughout the concrete depth at the transverse joint.

Equation 3-15, without integration limits and d in the denominator, determines the vertical stress distribution along any horizontal plane for a point load on the surface of an isotropic, homogenous and elastic medium. The analysis used by Westergaard includes a term for Poisson's effect (a) which allows stresses to match more closely (Bowles 1996); whereas, Boussinesq concluded that stress is independent of Poisson's effect. Theoretical work combining a modified Boussinesq equation (Spangler 1951) with Westergaard theory, which modifies the stress using Poisson's effect and which includes a differential equation – $q_m(x)$, has been completed at Iowa State University.

Using the modified Equation 3-15, as discussed in the previous paragraph, the Boussinesq bulb-shaped stress contours (as defined by Spangler (1951)) can be determined below the point load $q_m(x)$ throughout the concrete depth (H). Vertical stresses directly below the point load (z less than about 2 inches or 51 mm) are very large and were not considered.

3.6.2 Elastic Deflections

Linear-elastic theory can be used to determine the elastic settlement for shallow foundations (Das 1999). This theory applies to a foundation or footing that maintains contact with the surface of a soil medium having a finite depth. A dowel encased in

concrete is modeled as a beam on elastic foundation where compression-only springs are positioned along the top and bottom of the dowel along the dowel's embedment length.

The deflected dowel shape is shown as $z_1(x)$ in Figure 3-3 or as $z_2(x)$ in Figure 3-8. The elastic deflection (δ_1 or δ_2) was determined at the transverse joint face by linear-elastic theory as given by Equation 3-16 (Das 1999). The elastic deflection (δ_m) is based

$$\delta_m = \frac{1}{E_c} \cdot \int_0^H \sigma_z{}^m(z) - \mu_c \cdot \left[\sigma_x{}^m(z) + \sigma_y{}^m(z) \right] dz \tag{3-16}$$

Where:
δ_m = total elastic deflection at the joint face, in. (mm)
E_c = concrete's modulus of elasticity, psi (GPa)
H = depth of concrete medium below the dowel, in. (mm)
$\sigma_x{}^m(z)$ = stress in the x-direction, $\sigma_x = 0$ when $c > 0$, psi (MPa)
$\sigma_y{}^m(z)$ = stress in the y-direction, psi (MPa)
$\sigma_z{}^m(z)$ = stress in the z-direction, psi (MPa)

on Hooke's law and should apply to a dowel encased in concrete. The concrete medium is considered a single layer with a given Poisson's ratio (μ_c) and elastic modulus (E_c). Incorporating equations for stress into Equation 3-16 allows the deflection to be determined at the transverse joint face.

The deflection profile at the transverse joint face can be shown to reduce exponentially throughout the depth below the dowel using Equation 3-16. This profile can be determined by integrating Equation 3-16 over small intervals (zero to Point 1, Point 1 to Point 2, and so on) throughout the depth H below the dowel. The sum of the deflection from each interval is the total deflection. Also, using Equation 3-15 (m equal to one or two), the stress can be determined at the mid-depth of each interval. This mid-

depth stress is divided by the concrete's elastic modulus (E_c) and multiplied by the interval length to find the deflection within that interval. Both procedures will give the same deflection profile.

Equation 3-17 gives the stress in the horizontal (or y direction) for either foundation model and can be inserted into Equation 3-16. Equations 3-16 and 3-17 do not apply for subscript m equal to o (lower case o). Equation 3-15 should be used with m equal to one or two when incorporating this equation into Equation 3-16. Stress in the y-direction at the joint face varies exponentially with depth (z) as shown in Figure 3-3. Equation 3-17 was modified from Spangler (1951) to include Poisson's effect (a).

$$\sigma_y{}^m(z) = \int_0^{L_e} \int_{-\frac{d}{2}}^{\frac{d}{2}} \frac{q_m(x)}{2\cdot\pi\cdot d}\cdot\left[\frac{(n-2)\cdot y^2\cdot z}{\left(\sqrt{x^2+y^2+a\cdot z^2}\right)^n} \ldots + -\left(1-2\cdot\mu_c\right)\cdot\left[\frac{y^2-x^2}{\sqrt{x^2+y^2+z^2}\cdot\left(\sqrt{x^2+y^2}\right)^2\cdot\left(\sqrt{x^2+y^2+z^2}+z\right)} \ldots + \frac{x^2\cdot z}{\left(\sqrt{x^2+y^2+z^2}\right)^3\cdot\left(\sqrt{x^2+y^2}\right)^2}\right]\right] dy\ dx \tag{3-17}$$

Where:
$\sigma_y{}^m(z)$ = stress in the horizontal or y-direction as a function of z, psi (MPa)
z = distance along the z axis, $z \geq 0.001$ inches (mm)

The horizontal stress (y direction stress) can also be thought of as a confining stress or a stress that prevents deformation of the dowel's cross section during loading. As shown in Equation 3-16, the confining stress reduces vertical deflections. For the circular shape, Equation 3-17 results in horizontal stress that is equivalent to the horizontal stress found by Equation 3-9, and the horizontal stress determined by Hetenyi

(1961) theory using Equation 3-14 multiplied by sin(θ(ϕ)). Equation 3-17 predicts slightly larger horizontal stress for the elliptical shape compared to results from Equations 3-9, and Equation 3-14 multiplied by sin(θ(ϕ)).

The stress in the x and y directions can be ignored when calculating vertical deflections. The stress in the z direction (from Equation 3-15) is substituted into Equation 3-16 and shown by Equation 3-18. Equation 3-18 does not apply for subscript m equal to o (lower case o). Elastic deflections given by Equation 3-18 compare

$$\delta_m = \frac{1}{E_C} \cdot \int_0^H \left(\frac{2}{3}\right) \cdot \sigma_z^m(z)\, dz \tag{3-18}$$

Where:
δ_m = total elastic deflection at the joint face, in. (mm)

favorably with experimental deflections shown in Table 2-3. A factor of two thirds was used to match differential equation deflections for the one- and two-parameter models.

3.6.3 Modifying the Contact Modulus (One-Parameter Model)

The contact modulus (k) was given by Vesic (1961) assuming an infinite depth medium below the dowel. The concrete below the dowel, however, was not considered an infinite depth. Equation 2-13 was the original equation by Vesic (k not modified) that included a factor of 1.10 in the denominator (0.90 divided by 1.10 was rounded to 0.80) to account for uniform deflection across the dowel's width. Also, a modified equation for k was shown that accounts for a given finite concrete depth below the dowel.

Results from Equation 3-18 and results from the two-parameter model (see Section 2.10) show that the dowel deflections will decrease, for a given load, as the medium depth decreases. The differential equations for deflection for the one-parameter

model do not change with a change in medium depth. To reduce the deflections for the one-parameter model as the medium depth below the dowel decreases, the k value was assumed to increase. Also, as the medium depth approaches zero depth, the k value should become infinity. This signifies an increase in reactive pressure between the dowel and concrete for smaller concrete depths.

The differential equations for the one-parameter model vary based on the fourth root of k and are not overly sensitive to small changes in the k value. Based on these principles, a procedure was developed to modify Vesic's original equation to be applicable to a given finite depth medium as follows.

Equation 3-19, using the one-parameter model, equates Equation 3-18 (without the two-thirds factor) with z_o (see Equation 2-12), or in other words, the deflections are set equal. The n value was assumed to be 5.0 for deflection calculations since the stresses matched closely. Equation 3-19 was used to calculate different k values for a range of

$$\delta_1 = \frac{V - M \cdot \beta}{2 \cdot \beta^3 \cdot E \cdot I} \tag{3-19}$$

concrete thicknesses using the 1.50-inch (38.10-mm) diameter steel dowel. Properties for the dowel and concrete are listed in the Results section of this paper. The increase in k can be shown by F (magnifier) plotted against the specimen thickness (t) in Figure 3-9. The dowel was assumed to be at the mid-height of the specimen thickness. The curve in Figure 3-9 varies for each specific dowel size, shape and material; however, the slight variation in magnifier changes the k value very little. Therefore, this curve was used for all dowels in this research project.

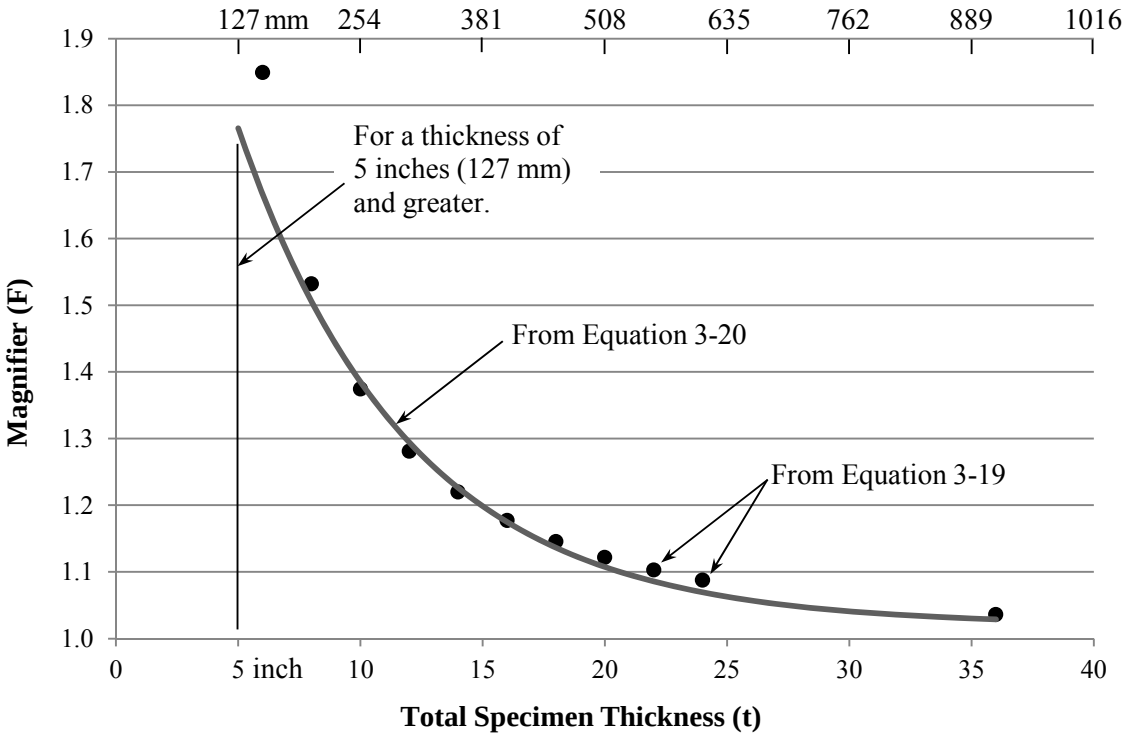

Figure 3-9 Contact modulus magnifier versus specimen thickness

The exponential curve in Figure 3-9 can be used in conjunction with Vesic's original equation to magnify k for a thickness of 5 inches (127 mm) to 36 inches (914 mm) by multiplying the results of Vesic's original equation by F for a specified concrete thickness. The resulting equation for F (magnifier) is given by Equation 3-20. A soft conversion can be made in this equation for use with metric units (mm) by changing the term –t/7 to –t/178.

$$F = 1.50 \cdot e^{\frac{-t}{7}} + 1.02 \qquad (3\text{-}20)$$

Where:
t = total slab or specimen thickness, in. (mm)

Equation 3-20 was used to develop a modified k equation (see Equation 2-14) which is applicable for a concrete thickness of 5 inches (127 mm) and greater. Figure 3-9 can be used for the modulus of foundation (k_o), since k_o is equal to k divided by d.

Figure 3-9 was shown for a range of concrete thicknesses (t) from 5 inches (127 mm) to 36 inches (914 mm) which is inclusive of highway or airport pavement thicknesses. One exponential function cannot show the magnifier approaching infinity, and therefore a lower limit for the concrete thickness was set at 5 inches (127 mm).

As the concrete thickness increases above 36 inches (914 mm) the magnifier (F) approaches one. This thickness corresponds to a 17.25-inch (438-mm) depth below the dowel for a 1.50-inch (38.10-mm) diameter dowel. The original equation by Vesic (Equation 2-13), which is not modified, can be used for a concrete thickness greater than 36 inches (914 mm).

3.7 Results

The following tables were developed using the properties listed below from the American Highway Technology report (Porter, et al. 2001). Tables 3-1 and 3-2 were developed theoretically and show the maximum bearing stress between the dowel and the concrete at the transverse joint face. The subscript m was one for the one-parameter model (finite beam theory), and m was two for the two-parameter model. The "k modified" equation given by Equation 2-14 was used for the one-parameter model unless otherwise indicated.

Table Properties *(Porter, et al. 2001)*

E = 29,000,000 psi (200 GPa) Modulus of elasticity for steel dowels

μ = 0.29 Poisson's ratio for steel dowels

μ_c = 0.18 Poisson's ratio (concrete)

V = -2,127 lb. (-9.46 kN) Shear

M = 133 lb.-in. (15.03 kN-m) Moment

c = 1/8 in. (3.2 mm) Transverse joint width

$f_c^{'}$ = 6,000 psi (41.37 MPa) Concrete compressive strength

E_c = 4,415,201 (30.44 GPa) Concrete modulus of elasticity

Concrete Thickness

t = 12 in. (305mm) Tables 3-1 thru 3-3

t = 8 in. (203 mm) Table 3-4 (Not included in Porter, et al. 2001)

Table 3-3 was developed from deflections (as slightly modified) given in the AHT report (Porter, et al. 2001). Equation 3-8 (in conjunction with Equation 3-2) was used to calculate the bearing stress. Included in this table was the elastic-limit stress using a factor of safety (FS) equal to one.

Table 3-1 Maximum bearing stress for the one-parameter model (m = 1)

Dowel Description h x d, in. (mm)	Reaction or Load	Maximum Bearing Stress at the Joint Face			
	$q_1(0)$, lb/in. (kN/m) Eq. 3-2	$\sigma_r(0,0)$, psi (MPa) Eq. 3-7	$\sigma_1(0)$, psi (MPa) Eq. 3-8	Hetenyi, psi (MPa) Eq. 3-14	$\sigma_z(0)$, psi (MPa) Eq. 3-15
1.00 x 1.00 (25.40 x 25.40)	4,129 (723)	5,258 (36.25)	5,331 (36.76)	5,258 (36.25)	5,289 (36.46)
0.88 x 1.41 (22.35 x 35.81)	4,305 (754)	3,887 (26.80)	3,941 (27.18)	3,887 (26.80)	3,910 (26.96)
1.25 x 1.25 (31.75 x 31.75)	3,268 (572)	3,328 (22.95)	3,375 (23.27)	3,328 (22.95)	3,348 (23.09)
1.13 x 1.66 (28.70 x 42.16)	3,367 (590)	2,583 (17.81)	2,619 (18.06)	2,583 (17.81)	2,598 (17.91)
1.50 x 1.50 (38.10 x 38.10)	2,703 (473)	2,295 (15.82)	2,327 (16.04)	2,295 (15.82)	2,309 (15.92)
1.34 x 1.98 (34.04 x 50.29)	2,817 (493)	1,811 (12.49)	1,836 (12.66)	1,811 (12.49)	1,822 (12.56)

Table 3-2 Maximum bearing stress for the two-parameter model (m = 2)

Dowel Description h x d, in. (mm)	Reaction or Load	Maximum Bearing Stress at the Joint Face		
	$q_2(0)$, lb/in. (kN/m) Eq. 3-3	$\sigma_r(0,0)$, psi (MPa) Eq. 3-7	$\sigma_2(0)$, psi (MPa) Eq. 3-8	$\sigma_z(0)$, psi (MPa) Eq. 3-15
1.00 x 1.00 (25.40 x 25.40)	3,103 (543)	3,951 (27.24)	4,006 (27.62)	3,975 (27.41)
0.88 x 1.41 (22.35 x 35.81)	3,264 (572)	2,948 (20.32)	2,989 (20.61)	2,965 (20.45)
1.25 x 1.25 (31.75 x 31.75)	2,855 (500)	2,908 (20.05)	2,948 (20.33)	2,925 (20.17)
1.13 x 1.66 (28.70 x 42.16)	2,963 (519)	2,273 (15.67)	2,304 (15.89)	2,286 (15.76)
1.50 x 1.50 (38.10 x 38.10)	2,672 (468)	2,268 (15.64)	2,300 (15.86)	2,282 (15.73)
1.34 x 1.98 (34.04 x 50.29)	2,783 (487)	1,790 (12.34)	1,815 (12.51)	1,801 (12.42)

Table 3-3 Experimental results (one-parameter model, m = o)

Dowel Description h x d, in. (mm)	*Experimentally Determined Values			σ_{limit}, psi (MPa) Eq. 3-1 (FS = 1)
	q_o, lb/in. (kN/m) Eq. 3-4	k, psi (MPa) (Solved)	σ_o psi (MPa) Eq. 3-8	
1.00 x 1.00 (25.40 x 25.40)	Not tested	Not tested	Not tested	2700 (18.62)
0.88 x 1.41 (22.35 x 35.81)	4,063 (712)	3,653,600 (25,200)	3,720 (25.65)	2,700 (18.62)
1.25 x 1.25 (31.75 x 31.75)	2,796 (490)	2,220,500 (15,300)	2,887 (19.91)	2,700 (18.62)
1.13 x 1.66 (28.70 x 42.16)	2,898 (508)	2,502,700 (17,250)	2,254 (15.54)	2,700 (18.62)
1.50 x 1.50 (38.10 x 38.10)	2,556 (448)	3,260,850 (22,500)	2,200 (15.17)	2,700 (18.62)
1.34 x 1.98 (34.04 x 50.29)	2,448 (429)	2,596,350 (17,900)	1,596 (11.01)	2,700 (18.62)

*Developed from the AHT Report (Porter, et al. 2001).

Table 3-4 shows the bearing stress at the transverse joint face including the effect of a reduced pavement thickness. A pavement thickness of eight inches (203 mm) was used. Equations for k (modified and not modified) are from Section 2.9.6. Bearing stress for both the one- and two-parameter models is compared.

Table 3-4 Maximum bearing stress for an eight-inch (203-mm) pavement

Dowel Description h x d, in. (mm)	One-Parameter Model Eq.'s 3-2 and 3-8		Two-Parameter Model Eq.'s 3-3 and 3-8
	$\sigma_1(0)$, psi (MPa) (k not modified)	$\sigma_1(0)$, psi (MPa) (k modified)	$\sigma_2(0)$, psi (MPa)
1.00 x 1.00 (25.40 x 25.40)	5,006 (31.51)	5,549 (38.26)	5,264 (36.29)
0.88 x 1.41 (22.35 x 35.81)	3,701 (25.51)	4,103 (28.29)	3,921 (27.04)
1.25 x 1.25 (31.75 x 31.75)	3,171 (21.86)	3,511 (24.21)	3,869 (26.69)
1.13 x 1.66 (28.70 x 42.16)	2,460 (16.96)	2,725 (18.79)	3,027 (20.87)
1.50 x 1.50 (38.10 x 38.10)	2,187 (15.08)	2,420 (16.69)	3,006 (20.73)
1.34 x 1.98 (34.04 x 50.29)	1,726 (11.90)	1,910 (13.17)	2,378 (16.40)

Figure 3-10 compares the exponential stress distribution below a 1.50-inch (38.10-mm) diameter dowel at the transverse joint face for the one- and two-parameter models using Equation 3-15. The interval depth was from z equal to 0.001 inches (or mm) to H. A modified Equation 3-15, without integration limits and d in the denominator, was used to calculate the Boussinesq stresses below a point load ($q_m(x)$) for the one-parameter model (m was equal to lower case o using semi-infinite beam theory).

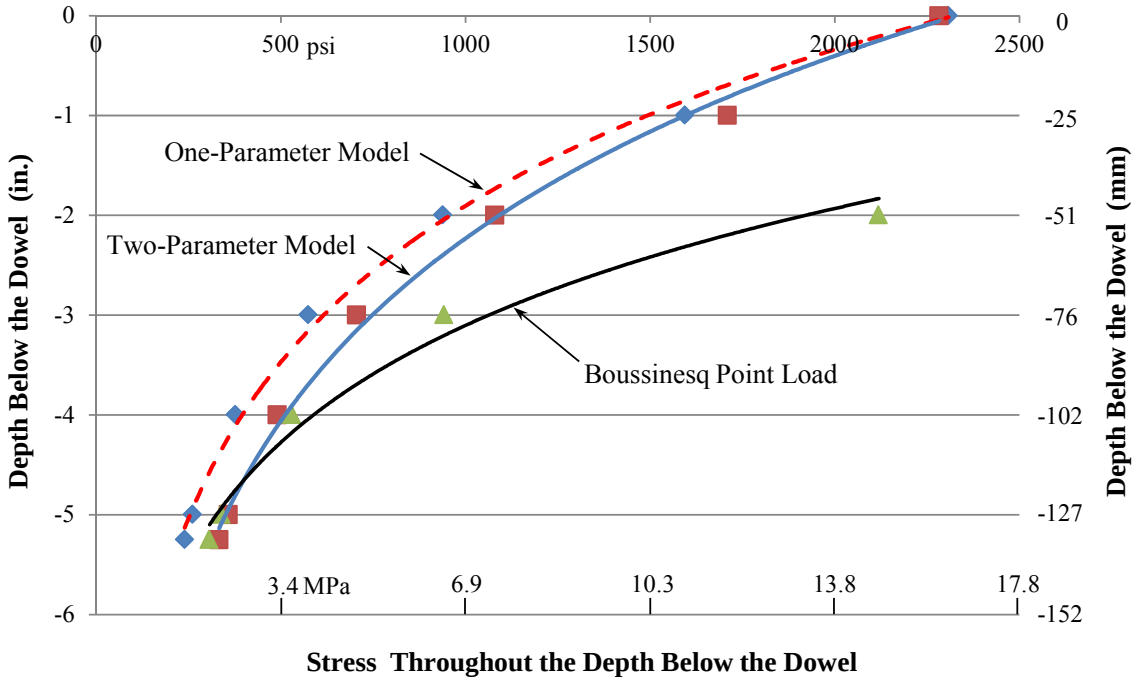

Figure 3-10 Stress distribution through the concrete depth below a 1.50-inch (38.10-mm) diameter steel dowel

Stresses are increased below the point load as shown in Figure 3-10 (and are very large for z less than 2 inches or 51 mm) but match the two-parameter model's stresses near the bottom of the test specimen. Assuming the concrete medium depth below the dowel is greater than H, the stresses from the modified Equation 3-15 approach the one-parameter model's stresses at a greater depth.

3.8 Summary, Conclusions and Recommendations

3.8.1 Summary

The theoretical bearing stress between the dowel and the concrete was determined for steel dowels having either a circular or an elliptical shape embedded in concrete. Six separate dowel sizes were analyzed. The theoretical bearing stress from these dowels was compared to the experimental bearing stress found at the concrete face within a transverse joint.

The concrete was modeled using two separate elastic foundation models – either the one- or the two-parameter model. Both models (incorporated in several methods including elasticity equations from Boussinesq theory) were used to predict the bearing stress which is based on the dowel-concrete reaction or load (q). This reaction is based on the fourth derivative of the assumed displaced dowel shape for each model and given by equations in this paper.

3.8.2 Conclusions

Overall conclusions from this paper are:

- Deflections at the transverse joint face from the first companion paper (see Chapter 2) are used to determine the maximum bearing stress for the one-parameter model (either finite beam or semi-infinite beam theories as a function of x) and the two-parameter model. For the semi-infinite beam theory, a simplified equation for q_o (reaction at the transverse joint face when x is zero) is used to find the maximum bearing stress without deflection values,
- Modifications were made to the contact modulus; however, only small differences in the bearing stress are apparent when using the k (modified) as compared to using the k (not modified) equations for the one-parameter model,
- Based on the bearing stress at the transverse joint face, the one-parameter model is a good alternative and compares well with the two-parameter model,
- Based on a reduced bearing stress, the elliptical-shaped dowel (when compared to the circular-shaped dowel) reduces tensile field splitting below the dowel.

In particular, additional specific conclusions are drawn from the subsequent visuals in this paper which are as follows.

The following conclusions were determined from Tables 3-1 through 3-3.

- The elliptical shape results in less bearing stress than the circular shape with equivalent flexural rigidity. This shape improvement was determined by both the one- and two-parameter foundation models,
- The improvement shown by the elliptical shape (over the circular shape) becomes less apparent as the dowel size increases for a given dowel load,
- The one-parameter stresses (Table 3-1) are close to the bearing stress found by using experimental deflections to calculate the bearing stress in Table 3-3,
- From the six dowel sizes analyzed, theoretical bearing stress for the three smaller dowels exceeds the limit on maximum bearing stress (without a factor of safety) for the one- and two-parameter models, therefore a smaller shear load would be required,
- Theoretical bearing stress for the four larger dowels is about the same when comparing the results from the one- and two-parameter models.

The following conclusions were determined from Table 3-4.

- For the one-parameter model using the k modified equation, as the depth (H) decreases, there was an increase in the bearing stress,
- For the two-parameter model, as the depth (H) decreases, there was an increase in the bearing stress. This increase resulted from loss of load-spreading around the dowel as k_a (Winkler constant) increased and k_b (load-spreading constant) decreased,

- Using larger dowels with a reduced concrete thickness, the bearing stress calculated from the one-parameter model may underestimate the bearing stress when compared to the two-parameter model.

The following conclusion was determined from Figure 3-10.

- The stress at the dowel-concrete contact is similar between the one- and the two-parameter models. Throughout the depth below the dowel, the two-parameter model's stresses are larger than stresses calculated using the one-parameter model. The Boussinesq concentrated load method overestimates the contact stress below the dowel.

3.8.3 Recommendations

The following recommendations are from this research project:

- Laboratory testing is recommended to make use of a bearing pressure indicator between the dowel and the concrete to determine the bearing stress at the transverse joint face,
- Strain gages mounted to the concrete below the dowel at the transverse joint face can be used to determine the stress profile below the dowel.

3.9 References

Boussinesq, ca. 1885 (Cited in Bowles 1996).

Bowles, J.E., 1996. *Foundation Analysis and Design*, 5th Edition, McGraw-Hill International Edition.

Das, B.M., 1999. *Principles of Foundation Engineering*, 4th Edition, Brooks/Cole Publishing Company.

Friberg, B.F., 1940. Design of Dowels in Transverse Joints of Concrete Pavements, *Proceedings, American Society of Civil Engineers*, 105, 1076-1116.

Hetenyi, M., 1961. *Beams on Elastic Foundation*, The University of Michigan Press, Ann Arbor, Michigan.

MacGregor, J.G., 1988. *Reinforced Concrete Mechanics and Design*, Prentice Hall International Series in Civil Engineering and Engineering Mechanics.

Marcus, H., 1951. Load Carrying Capacity of Dowels at Transverse Pavement Joints, *Journal of the American Concrete Institute, Proceedings*, 48(2), 169-184.

McCormac, J.C., and Brown, R.H., 2009. *Design of Reinforced Concrete*, 8th Edition, John Wiley & Sons, Inc..

Naval Facilities Engineering Command (NAVFAC), Military Handbook (MIL-HDBK-1021/4), *Rigid Design of Airfields*.

Porter, M.L., Guinn, R.J., and Lundy, A.L., 2001. *Dowel Bar Optimization: Phase I and II, Final Report, American Highway Technology (AHT)*, Center for Transportation Research and Education, Iowa State University.

Spangler, M.G., 1951. *Soil Engineering*, International Textbook Company.

Timoshenko, S., and Lessels, J.M., 1925. *Applied Elasticity*, Westinghouse Technical Night School Press, East Pittsburgh, Pennsylvania.

Timoshenko, S., 1976. *Strength of Materials – Part II*, 3rd Edition, Robert E. Krieger Publishing Company, Huntington, New York.

Vintzeleou, E.N., and Tassios, T.P., March 1986. Mathematical Models for Dowel Action Under Monotonic and Cyclic Conditions, *Magazine for Concrete Research*, 38(134), 13-22.

Westergaard, H.M., 1938. A problem of Elasticity Suggested by a Problem in Soil Mechanics: Soft Material Reinforced by Numerous Strong Horizontal Sheets, *Contributions to the Mechanics of Solids, Stephen Timoshenko 60th Anniversary Volume*, MacMillan, New York, 268-277.

Yoder, E.G., and Witczak, M.W., 1975. *Principles of Pavement Design*, 2nd Edition, John Wiley & Sons, Inc., New York, NY.

CHAPTER 4. LABORATORY TEST METHODS FOR CONCRETE PAVEMENT DOWELS

A paper prepared for submission to the *International Journal of Pavement Engineering*

Eric A. Lorenz[1]*, P.E., Max L. Porter*[2]*, P.E.,*
and Fouad S. Fanous[3]*, P.E.*

Abstract

Load transfer across an open transverse joint in a concrete pavement is accomplished using dowels spaced along this joint. A specified dowel was idealized as a beam and the concrete supporting the dowel was represented by either of two different elastic foundation models. Both analytical models use springs to support the dowel, and each model determines a slightly different deflected shape for a dowel embedded in concrete. The springs from each model have their stiffness given by elastic constants or parameters.

Three separate laboratory test methods are presented in this paper to verify these elastic constants. The assembled stiffness matrices for all three tests, two elemental shear test methods and one cantilever test method, were developed using the stiffness method of structural analysis. These matrices were used to determine the deflections of the dowel within the concrete and compare them to experimental values. The element stiffness matrix for two beams connected by springs was derived from differential equations and included in two of the assembled stiffness matrices.

[1] Doctoral Candidate, Civil Engineering, Department of Civil, Construction and Environmental Engineering, Iowa State University, Ames, Iowa 50011

[2] University Professor Emeritus, Civil Engineering, Department of Civil, Construction and Environmental Engineering, Iowa State University, Ames, Iowa 50011

[3] Professor, Civil Engineering, Department of Civil, Construction and Environmental Engineering, Iowa State University, Ames, Iowa 50011

4.1 Introduction

Dowels that are spaced along a transverse joint in a highway or airport pavement will transfer a portion of the single-axle wheel loads across the joint. This portion is distributed laterally to the effective dowels (Friberg 1940). The behavior of each loaded dowel in a doweled pavement joint can be accurately represented by laboratory tests. These tests are required to select the appropriate dowel type and dowel spacing to resist the loads. Dowel types include dowel size, shape and material. The laboratory tests in this paper were modeled using the stiffness method of structural analysis (Weaver, et al. 1990 and Melerski 2000). These tests consisted of a single steel dowel, with either a circular or an elliptical shape, spanning a joint width in a concrete specimen. The joint width (c) is dependent on temperature and shrinkage changes in full-scale slabs on grade as discussed later in this paper.

The deflected shape of a dowel embedded in concrete is defined by elastic constants (parameters) from either of two elastic foundation models – the one- or the two-parameter model (Sections 2.9 and 2.10, respectively). The dowel's deflected shape within the concrete, found through laboratory testing, identifies which model is more appropriate. Two laboratory test methods referred to as elemental shear tests were developed previously to determine the elastic constant for a specified dowel. A third test method (the cantilever test) is described in this paper. The laboratory test methods being investigated are: 1) the Iosipescu Shear test (Walrath, et al. 1983), 2) the AASHTO T253 test (AASHTO 1996), and 3) the cantilever test (Harrington Thesis 2006).

The objective of this paper is to explain how to develop the assembled stiffness matrix $[K_e]$ for each laboratory test method which allows comparison of each method.

This paper recommends the cantilever test over the elemental shear tests due to its simplicity. Modifications, however, are being recommended throughout this paper to improve the performance of the elemental shear tests. In addition, the elemental shear tests can include an elastic support under a portion of the test specimen to investigate soil-pavement interaction.

All three test methods (without an elastic support) have a different testing configuration but are theoretically equivalent. These tests will result in the same deflected shape of the embedded dowel and elastic constant for the one-parameter model when absent of casting variables (Porter, et al. 2001) and non-symmetrical loading problems (Section 2.9.2). The cantilever test can be used to verify the elastic constants for the one- and two-parameter models without these unwanted variables. This paper discusses ways to reduce problems associated with casting variables and non-symmetrical loading in test specimens.

4.2 Analysis

The slab (as shown in Figure 4-1) is a soil-pavement interaction problem that considers only elastic settlement of the subgrade without secondary or time-dependent settlement. With only elastic settlement, the subgrade depth can be idealized as a finite thickness (t_s) underlain by a rigid soil subgrade layer ($k_s = \infty$). The k_s value (see Equation 2-1) refers to the soil subgrade modulus in pounds per cubic inch (MPa/m). This subgrade modulus may include a base course overlying the subgrade.

4.2.1 Maximum Shear Load

Concrete slab sections, shown in Figure 4-1, are separated by a transverse joint of width c. A single axle with two wheel loads (W) is positioned along the open joint and a

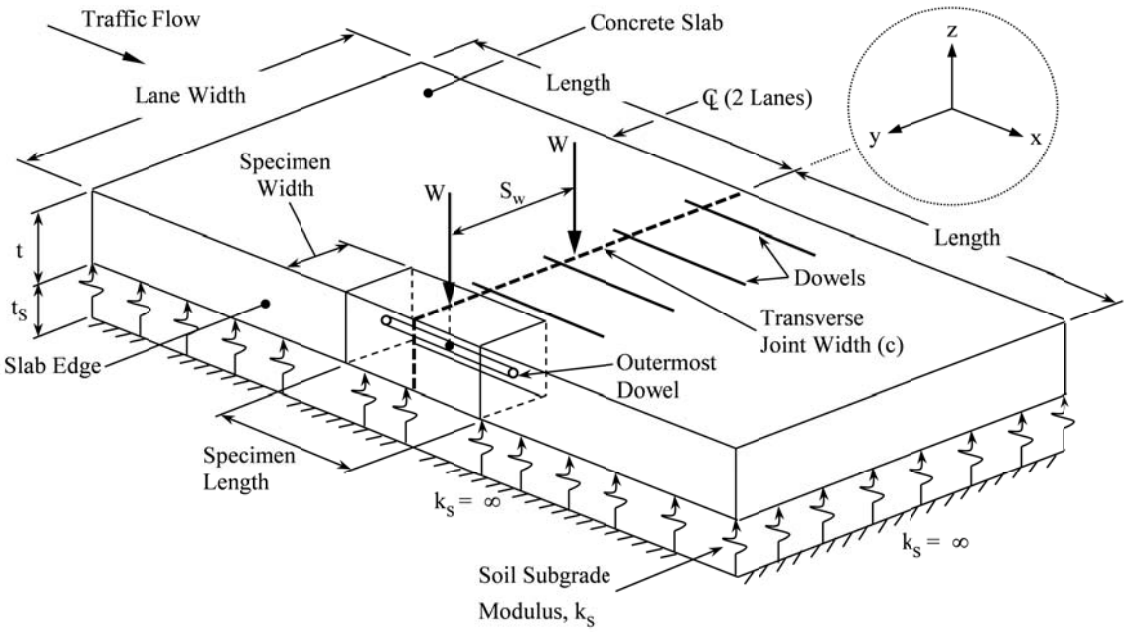

Figure 4-1 Concrete pavement sections (slabs)

portion of both wheel loads (Yoder, et al. 1975) is distributed laterally to the dowels (Friberg 1940). This assumed transverse-linear distribution distributes 50 percent of each wheel load to the dowels considering the modulus of subgrade reaction (k_s) and the radius of relative influence (L_r) as given in Section 2.6. For highway and airport pavements, the resulting direct shear (V) is applied to a specified dowel in the center of the joint width. This loading assumes that an inflection point (IP) occurs in the dowel at the joint center.

The slab is in equilibrium by removing the wheel loads, separating the slab sections at the dowel IP and applying their corresponding shear load to each effective dowel spaced along the transverse joint. The sum of these dowel shear loads (along the separated joint) is equal to 50 percent of the wheel loads (Yoder, et al. 1975). The subgrade carries the remaining portion of the wheel loads.

The shear load is generally different for each dowel, and the wheel loads positioned along the transverse joint in Figure 4-1 give the largest shear load on the outermost dowel. This position of the wheel loads (with one wheel load over the outermost dowel) will result in the largest shear load for any dowel when compared to every other wheel load position along the transverse joint. An equation for the shear load (V) in this outermost dowel was developed at Iowa State University (ISU) and given by Equation 4-1. A closer dowel spacing (s) can be selected to reduce this shear load and limit the maximum bearing stress (see Chapter 3).

$$V = \frac{1}{2}W\cdot\left[\begin{array}{l}\left[\sum_{i=0}^{Nod-1} if\left[\begin{array}{l}1.8\cdot L_r \ldots \\ +-s\cdot(i)\end{array} < 0,0,\frac{1.8\cdot L_r - s\cdot(i)}{1.8\cdot L_r}\right]\right]^{-1} \ldots \\ \hline + if\left[\begin{array}{l}1.8\cdot L_r \ldots \\ +-S_w\end{array} \le 0,0,\left[\sum_{i=0}^{Nod-1} if\left[\begin{array}{l}1.8\cdot L_r \ldots \\ +-\left|S_w - s\cdot(i)\right|\end{array} < 0,0,\frac{1.8\cdot L_r - \left|S_w - s\cdot(i)\right|}{1.8\cdot L_r - S_w}\right]\right]^{-1}\right]\end{array}\right] \quad (4\text{-}1)$$

Where:
V = shear load on the outermost dowel, lb. (kN)
W = wheel load, lb. (kN)
Nod = number of dowels
L_r = radius of relative influence, in. (mm)
s = dowel spacing, in. (mm)
S_w = wheel spacing, in. (mm)

4.2.2 Test Specimen Considerations

As shown in Figure 4-1, a test specimen (presented later in this paper) can be visualized for the dowel and the surrounding concrete. Specimens are cast under laboratory conditions using one of the three aforementioned test methods to determine the dowel's deflected shape within the concrete. The specimen thickness should be the same as the pavement thickness (t). The dowel's embedment length within the concrete is

given as L_e in this paper. The test specimens are generally as wide as the dowel spacing but not less than 12 inches (305 mm) to include the Boussinesq stress distribution for a single dowel (Granholm 1929). The Boussinesq theory assumes an infinite medium below the dowel. Interrupting these bulb-shaped stress distributions, as presented by Spangler (1951), either by width or depth discontinuities, may increase the resulting stress below the dowel.

Transitioning from full-scale slabs (Ingram Thesis 2004) to individual test specimens may have an effect on the k value (contact modulus). Multiple dowels in a row in full-scale slabs, with similar loading in the same direction, may have a reduced k when compared to a single loaded dowel (Granholm 1929). This reduction occurs due to overlapping of Boussinesq bulb-shaped stress distributions below adjacent dowels in a row (Granholm 1929). As the dowel spacing is reduced, this effect may be more apparent. A reduced k results in greater dowel deflections experienced in full-scale slabs. Therefore, testing specimens with two (Porter, et al. 2008) or more dowels in a row is required to verify this anomaly and possibly add a correction to k (Granholm 1929).

4.2.3 Load Transfer across a Transverse Joint

The problem of load transfer across a transverse joint (see Figure 4-2) includes the dowel supported by a concrete elastic foundation plus the doweled-slab joint supported by a soil elastic foundation. The transverse joint is a weak plane with reduced flexural rigidity. The soil-supported joint has relative deflection, joint deflection and joint rotation (γ_e in Figure 4-2) when compared to the uncracked slab section. Relative deflection, as given in Porter, et al. (2001), defines the difference in elevation of two adjacent slabs on either side of the joint. The assembled stiffness matrices for the

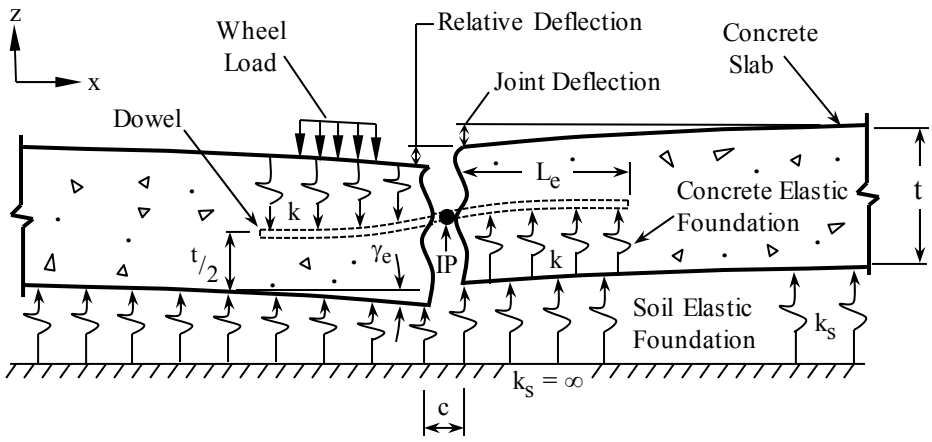

Figure 4-2 Full-scale pavement joint

laboratory test methods include shear deflection for the dowel spanning the transverse joint and can be used to determine the relative deflection.

Further compaction of the soil subgrade (beyond initial preparation) may occur at the transverse joint due to this joint deflection and rotation. Therefore, bearing stress between the dowel and concrete (see Chapter 3) and between the slab and subgrade are factors limiting the magnitude of the wheel loads that cross the transverse joint. Bearing stress is considered in place of Load Transfer Efficiency (AASHTO 1993).

4.2.4 Dynamic Effects on Dowel Loading

As a vehicle travels along the pavement, the concrete deflects below the wheel loads and the vehicle is continuously driving uphill even on perfectly level pavement. This vehicle (wheels, suspension, etc.), through its motion, propagates a short wave outward through the slab and downward into the subgrade, and the resulting dynamic momentary stresses may be greater than the static stress (Bhattacharya 2000). An open joint would effectively stop this wave (with the exception of the waves propagated through the subgrade) and transfer a portion of the waves across the joint through the dowels.

With the introduction of overweight vehicles on highway and airport pavements, non-linear behavior at the dowel-concrete interface will produce cracks (Bhattacharya 2000) that essentially void linear-elastic analysis. Dynamic loading (Kukreti, et al. 1992) on dowels in a concrete pavement will lead to three-dimensional loading – bending about both axes and torsion about the dowel's longitudinal axis – resulting in multi-directional stress-strain analysis.

The elliptical-shaped dowel, due to dynamic loading in full-scale slabs joints, may have a torsional moment due to its shape as well as a lateral load and a shear load (V). The laboratory test methods, as mentioned previously, can incorporate shear load, lateral load and torsional moment by using several hydraulic rams simultaneously.

4.2.5 Temperature Effects on the Transverse Joint Width

At least one half of the embedded dowel, in a pavement joint, is prevented from bonding to the surrounding concrete which allows the joint to open. This non-bonding is accomplished by use of a bondbreaker or a sleeve (Farny 2001). The joint width (c) is dependent on temperature and shrinkage changes and contraction of adjacent slabs on either side of the joint. Closer joint spacing may be warranted where construction joints are used.

Typical construction occurs during warmer conditions where more drying shrinkage is prevalent. The joint opens during colder temperatures in addition to drying shrinkage (ignoring plastic shrinkage) and closes during warmer temperatures. Generally, the concrete's expansion due to heat (temperatures less than 100^{o}F ($38\ ^{o}$C) as determined by the equation in this section) offsets the amount of drying shrinkage for continuous concrete construction (straight segments) such as highway or airport

pavements. Cold weather construction may result in less drying shrinkage and smaller joint widths than for slabs constructed during warmer temperatures. The smaller joint widths would allow for less expansion due to heat.

Locations where the pavement changes direction, where the pavement's expansion is impeded, where a change in subgrade roughness occurs, where the pavement is constructed under colder conditions, or where very warm conditions prevail (greater than 100^{o}F (38 ^{o}C)) may warrant expansion joints. This paper, however, does not determine the width of expansion joints.

The analytical results shown in this paper consider a one-eighth-inch (3.2-mm) joint width for construction or contraction joints. The recommended standard joint width, however, should be greater for test specimen construction. The following procedure determines the standard transverse joint width (c) for use in laboratory test methods.

A pavement's drying shrinkage is assumed to be slightly less than for an elevated slab, but greater than for building floor slabs. The joint spacing (L_j) was based on the pavement thickness, concrete slump and maximum coarse aggregate size (Farny 2001). For a concrete slump of four to six inches (100 to 150 mm) and a maximum coarse aggregate size less than three-quarter inch (19 mm), the joint spacing in feet was assumed to be two times the pavement thickness in inches (Farny 2001). For a 12-inch (305-mm) pavement thickness, a value of 24 feet (7.3 meters) was determined. With either a lower slump or a larger coarse aggregate size, joint spacing could be increased (Farny 2001).

Equation 4-2 can be used to determine the standard joint width. Applying the joint spacing as mentioned above in conjunction with Equation 4-2 yields a joint width of three-eighth inch (9.5 mm) for a 12-inch (305-mm) pavement thickness.

$$c = \left(\Delta T \cdot \varepsilon + \varepsilon_s\right) \cdot L_j \tag{4-2}$$

Where:
c = standard joint width, in. (mm)
ΔT = change in temperature (100°F (37.8°C))
ε = coefficient of thermal expansion (5.5 x 10^{-6} in./in./°F or 10 x 10^{-6} mm/mm/°C)
ε_s = drying shrinkage (0.00060 in./in. or mm/mm)
L_j = assumed joint spacing in. (mm)

4.3 Dowel-Concrete Contact

The analysis methods presented herein assume a "perfect" specimen without construction, testing or material variables. The specimens used for testing have the potential to develop poor contact between the dowel and the concrete (see Section 2.5). Laboratory tests are subject to various concerns that may be present during casting and testing. Most of these concerns are typical of (or inherent to) concrete construction and may cause theoretical models (based on linear-elastic analysis) to inappropriately predict the contact modulus (k).

For example, theoretical analysis (see Table 2-1) produces larger k values (with less dowel deflection within the supporting medium) when compared to experimentally determined values (see Table 2-3). Therefore, this paper closes the gap between theory and experiment by analyzing the test specimens with the stiffness method (Weaver, et al. 1990 and Melerski 2000).

The difference in results necessitates the improvement of existing test methods. For example, casting the elemental shear test specimens on their side would ensure positive concrete contact between the top and bottom of the dowel when the specimen is rotated and tested. The cantilever test can be cast-on-end resulting in good concrete contact around the entire dowel.

These items of concern are, in fact, present during concrete construction. Outside the laboratory, these experimental k values would already be real-world values. Refining tests to match theoretical results, however, is required for model validation. Researchers must know how theoretically derived k values should be adjusted for application in the field.

In addition to casting variables, non-symmetrical loading may also change the location of the dowel inflection point within the joint. The cantilever test (as explained next) was developed to eliminate the problem associated with non-symmetrical loading.

4.4 Laboratory Test Methods to Verify Elastic Constants

Two elemental shear test methods have been used at ISU to verify the contact modulus (k) as explained in this section. The contact modulus is equivalent to $k_o d$, where d is the dowel's major axis and k_o is the modulus of foundation. An alternative cantilever test to verify k was also introduced. The elemental shear tests and the cantilever test are loaded statically when solving for k values. This static load on the dowel should result in bearing stress which is less than the elastic-limit stress for the concrete (see Section 3.2.3). Once k is established, these test methods can be used for cyclic or variable cyclic loading and dynamic loading to determine the long-term effects of dowels embedded in concrete.

The purpose of the elemental shear tests is to determine the relative deflection across a doweled joint. From this relative deflection, the deflection of the dowel within the concrete at the transverse joint was determined (Porter, et al. 2001). With instrumentation extending from the concrete surface to the dowel, along the embedment length, other dowel deflections within the concrete can be determined.

The Iosipescu elemental shear test, as presented by Walrath, et al. (1983), is illustrated in Figure 4-3. Walrath's test was extended to dowel behavior in transverse pavement joints due to the similarity in loading.

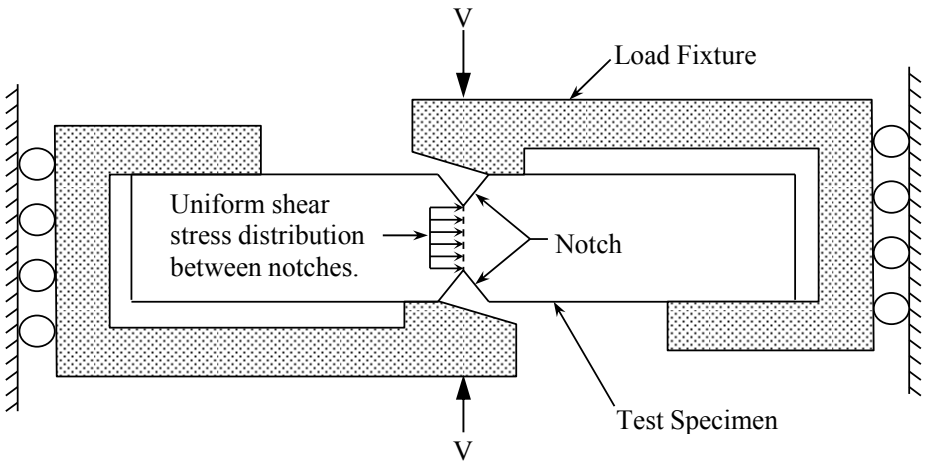

Figure 4-3 Schematic of Walrath's Iosipescu test frame (1983)

The dimensions in the following figures assume a one-eighth-inch (3.2-mm) joint width and an 18-inch (457-mm) dowel length. The joint width and dowel length can vary, and certain dimensions within these figures will vary accordingly.

The Iosipescu Shear test specimen which was used for dowel investigations is shown in Figure 4-4. The Iosipescu Shear test has been used previously at ISU (Porter, et al. 1992, Porter, et al. 1993 and Porter, et al. 1999) to determine k. This test assumes that an inflection point (IP) or point of zero moment occurs at the center of the joint (within the dowel), and the shear remains constant along the dowel throughout this joint width. The moment at the joint face is related directly to the shear, and the moment and the rotational stiffness at each face is assumed to be equal. An IP will occur in the joint center if casting variables are minimized and if both blocks are prevented from rotating in Figure 4-4.

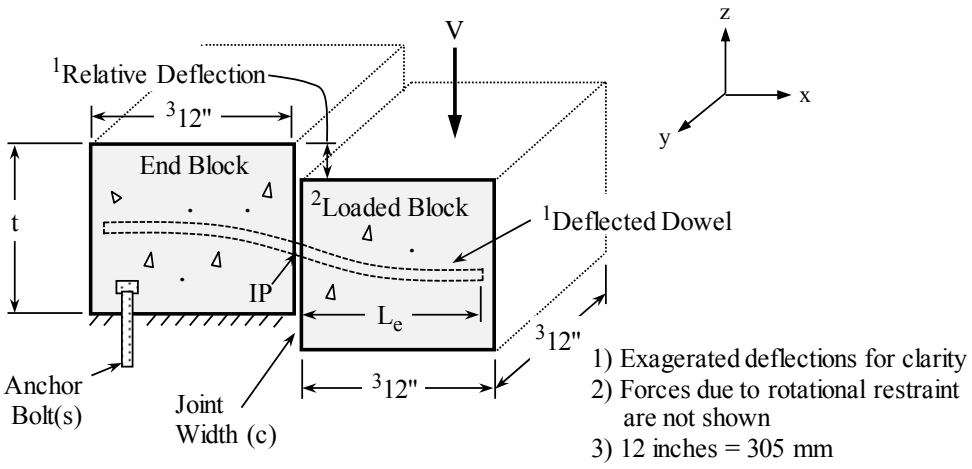

Figure 4-4 Iosipescu schematic (elemental shear test)

The American Association of State Highway and Transportation Officials (AASHTO) T253 (AASHTO 1996) elemental shear test (see Figure 4-5) is being investigated to determine its ability to verify k for the one-parameter model. An inflection point will occur in the dowel in the center of the joint width if the end blocks are prevented from rotating, if the casting variables are minimized, and if the center span is loaded symmetrically. The rotational stiffness at each face - in the joint - will be the same provided the above mentioned criteria are satisfied.

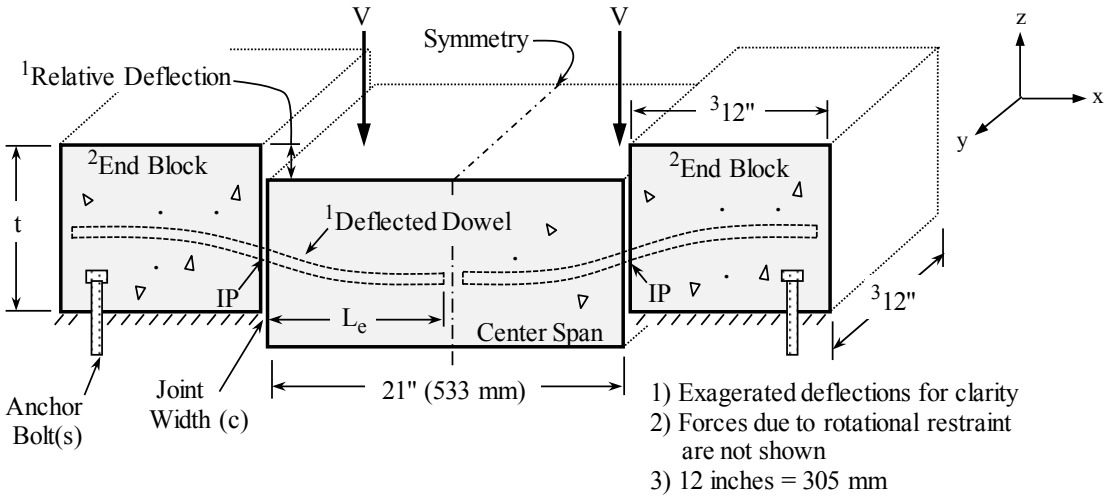

Figure 4-5 AASHTO T253 schematic (elemental shear test)

The fundamental assumption of the AASHTO T253 test is that the dowel's moment at each face within the joint will average V(c)/2 and the shear remains constant along the dowel within the joint. A difference in moments indicates a slight shift in the inflection point in the dowel within the joint as the shear loads are moved towards the line of symmetry. The average moments allow the shear load (V) to be located anywhere along the center span without affecting the final result, as long as the center span is loaded symmetrically. The difference in moment at each face is very minor and may be ignored for shear loads which result in stresses not exceeding the concrete's elastic-limit stress (see Section 3.2.3).

The AASHTO specification (AASHTO 1996) stipulates uniform loading along the center-span portion (or section). Deflection of the center span at the midpoint limits the contact for uniform loading. Therefore, two shear loads, applied symmetrically, have been proposed. Problems with non-symmetrical loading, however, as explained earlier, may occur with two shear loads (V). Loading a single shear load (2V) through the line of symmetry may avoid non-symmetrical loading. This line of symmetry makes the AASHTO T253 test theoretically equivalent to the Iosipescu Shear test, although no restraint against rotation is required for the center span (only the end blocks).

The cantilever test, as shown in Figure 4-6, allows for the measurement of deflections within the concrete along the dowel's embedment length (with proper instrumentation) and is used to verify elastic constants for both foundation models. Application of the direct-shear load to the dowel at a distance c/2 from the face of the concrete is theoretically equivalent to the elemental shear tests. A shear load (V) applied at c/2 assumes an inflection point at that location, and the deflected shape of the

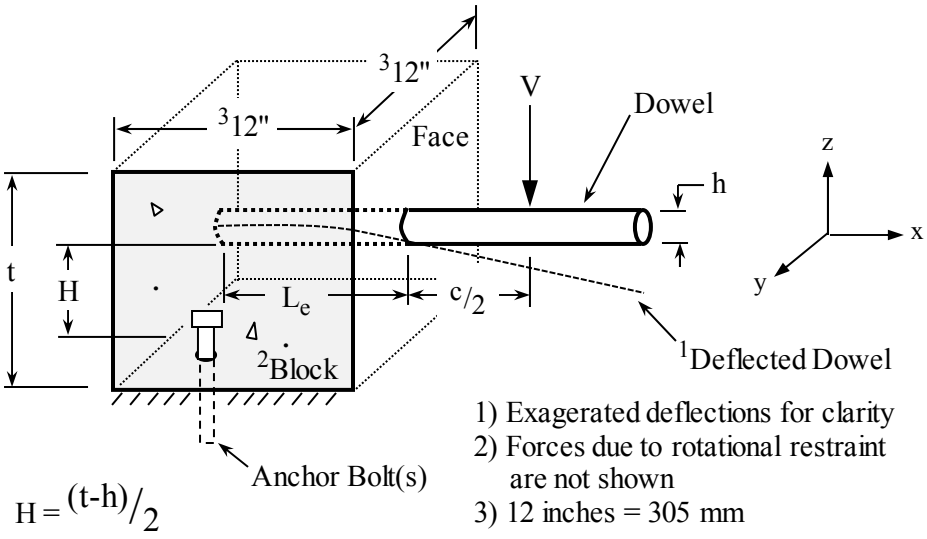

Figure 4-6 Cantilever test schematic

embedded dowel would be the same as in the elemental shear tests. Due to a small joint width, however, the test load location must be further from the concrete face.

The distance c/2 is too small in most cases to apply an experimental load, but a reduced shear load can be applied further from the concrete face. This shear load will result in a greater moment and a greater dowel slope at the concrete face. If the reduced shear load produces the same dowel deflection within the concrete at the joint face as the shear load applied at c/2, then the bearing stress (see Chapter 3) will be the same in both cases.

Due to the slightly more complex development of the two-parameter model (see Section 2.10) and because of the cantilever test's simplicity, the cantilever test is modeled with two foundation models (the one- and two-parameter models using k, and k_a and k_b, respectively). Both elemental shear tests are modeled using the one-parameter model (using the contact modulus k, or modulus of foundation k_o).

The cantilever test has been considered due to its simplicity. There are four advantages to using the cantilever test, and they are given as follows:

- Observation of the dowel-concrete interface at the transverse joint or peak stress region prior to and following testing to check for oblonging around the dowel,
- Advantage to a reduced specimen size when modeling with Finite Element Analysis (Murrison, et al. 2002) by using a finer mesh around the dowel-concrete interface,
- Placing strain gages on the concrete around the dowel to verify theoretically derived stress distribution, and
- Visual inspection of the initial failure modes or crack patterns in the concrete specimens under static loading at impending concrete failure.

The ability to understand dowel behavior in highway or airport pavements, under accelerated or cyclic loading, relies upon knowledge developed through static testing of individual dowels and verification of theoretical models as follows. These models use differential equations which were developed for this paper and are provided with an analytical solution.

4.5 Modeling Laboratory Test Methods

The differential equations for a layered system (two beams and two separate foundations) were introduced by Hetenyi (1950 and 1961). One foundation separated the top and bottom beams, while the second foundation supported the bottom beam. Using this system, the element stiffness matrix (for the dowel's embedment length) was developed and used for the center-span portion of the AASHTO T253 test and the loaded-block portion of the Iosipescu Shear test as follows.

The concrete surrounding the dowel was idealized as a beam, connected to the dowel (or top beam) with springs, and further supported by an elastic medium. The springs connecting the dowel to the concrete were represented by the modulus of foundation (k_o) and the supporting medium was represented by modulus of subgrade reaction (k_s). These foundation moduli were given in Sections 2.9.6 and 2.6, respectively.

4.5.1 Two Beams Connected by Springs

A new set of differential equations was developed at ISU by removing the supporting medium. This resulted in two beams connected by springs as illustrated in Figure 4-7. Four nodes with two degrees of freedom per node in Figure 4-7 define the two-beam element with length L_e. This figure illustrates composite action between the dowel and concrete within the elastic range and can be used for other composite members idealized as two separate beams. Deflections in the positive z direction and counterclockwise rotations are considered positive displacements.

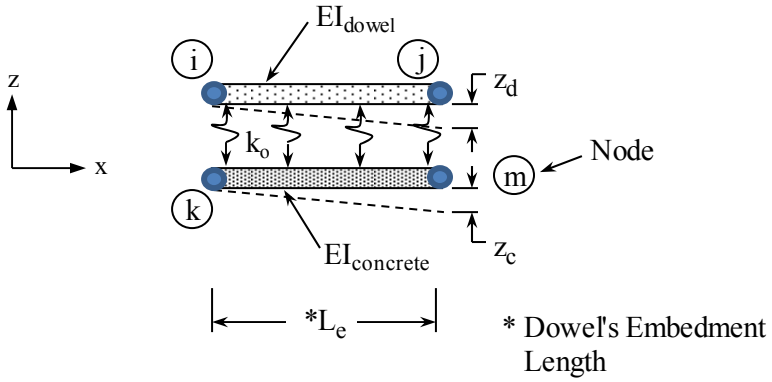

Figure 4-7 Two beams connected by springs

Equations 4-3a and 4-3b, with eight constants per equation, are the general solution to the differential equations for two beams connected by springs. Using substitution values (see Section 2.9.1) in Equations 4-3a and 4-3b and differentiating these equations, the slope (θ), moment (M), shear (V), and reaction or load (q) can be determined for both the dowel and the concrete, respectively. The following matrix formulation using [A] and [B] matrices was developed from Melerski (2000).

$$z_d(x) = C_1 + C_2 \cdot x + C_3 \cdot x^2 + C_4 \cdot x^3 \ldots + R \cdot \left(C_5 \cdot n_1(x) + C_6 \cdot n_2(x) + C_7 \cdot n_3(x) + C_8 \cdot n_4(x) \right) \quad (4\text{-}3a)$$

$$z_c(x) = C_1 + C_2 \cdot x + C_3 \cdot x^2 + C_4 \cdot x^3 \ldots + C_5 \cdot n_1(x) + C_6 \cdot n_2(x) + C_7 \cdot n_3(x) + C_8 \cdot n_4(x) \quad (4\text{-}3b)$$

Substituting:

$$n_1(x) = e^{\lambda \cdot x} \cdot cos(\lambda \cdot x) \qquad n_3(x) = e^{-\lambda \cdot x} \cdot cos(\lambda \cdot x)$$

$$n_2(x) = e^{\lambda \cdot x} \cdot sin(\lambda \cdot x) \qquad n_4(x) = e^{-\lambda \cdot x} \cdot sin(\lambda \cdot x)$$

Where:

$C_1, C_2 \ldots C_8$ = constants

x = distance along the dowel, in. (mm)

k_o = modulus of foundation, pci (MPa/m)

d = dowel's major axis, in. (mm)

E_c = concrete's elastic modulus, psi (MPa)

I_c = moment of inertia for the concrete block, in^4 (mm^4)

E = dowel's elastic modulus, psi (MPa)

I = moment of inertia for the dowel, in^4 (mm^4)

$$\lambda = \sqrt[4]{\frac{k_o \cdot d}{4} \cdot \left(\frac{1}{E_c \cdot I_c} + \frac{1}{E \cdot I} \right)} \qquad R = -\frac{E_c \cdot I_c}{E \cdot I}$$

The matrices are stacked to form the final [A] and [B] matrices and multiplied (as shown by Equation 4-4) to form the 8 x 8 element stiffness matrix [k_e] for two beams

$$k_e = \begin{pmatrix} B_d \\ B_c \end{pmatrix} \cdot \begin{pmatrix} A_d \\ A_c \end{pmatrix}^{-1} \tag{4-4}$$

connected by springs. The [A] and [B] matrices are shown below as $[A_d]$ and $[B_d]$ by Equations 4-5a and 4-5b for the dowel, and as $[A_c]$ and $[B_c]$ by Equations 4-6a and 4-6b for the concrete. The constants (C_1 through C_8) are determined by the procedure outlined in Section 2.9.4. The constants can be found by the expression $\{C\} = [A]^{-1}\{D\}$ where $\{C\}$ is the vector of constants, $[A]$ is the stacked matrix and $\{D\}$ is the corresponding joint displacement vector.

Joint displacements (deflections and rotations) are determined using the expression $[K_e]\{D\} = \{F\} - \{F_o\}$, where $\{D\}$ is the joint displacement vector, $\{F\}$ is the joint load vector, $\{F_o\}$ is vector of fixed-end forces (FEF), and $[K_e]$ is the assembled stiffness matrix for the test specimen. The fixed-end reactions were $wL_e/2$, and the fixed-end moments were $wL_e^2/12$ applied to the nodes of the concrete beam. These FEF are used for beam analysis using the stiffness method (Weaver, et al. 1990) but are appropriate for two beams connected by springs which have a shorter embedment length (L_e). The embedment length should be greater than about 9 inches (229 mm). The shear load (V) was applied to the concrete at the transverse joint face for both elemental shear tests. This loading point corresponds to the fifth degree of freedom at Node k in Figure 4-7. The actual deflection of the dowel along its embedment length (L_e in Figure 4-7) can be determined from the relative deflection of the dowel within the concrete as given by the expression $z_c(x) - z_d(x)$.

$$A_d = \begin{bmatrix} 1 & 0 & 0 & 0 & R\cdot n_1(0) & R\cdot n_2(0) & R\cdot n_3(0) & R\cdot n_4(0) \\ 0 & 1 & 0 & 0 & \lambda\cdot R\cdot(n_1(0) - n_2(0)) & \lambda\cdot R\cdot(n_2(0) + n_1(0)) & -\lambda\cdot R\cdot(n_3(0) + n_4(0)) & \lambda\cdot R\cdot(-n_4(0) + n_3(0)) \\ 1 & L_e & L_e^2 & L_e^3 & R\cdot n_1(L_e) & R\cdot n_2(L_e) & R\cdot n_3(L_e) & R\cdot n_4(L_e) \\ 0 & 1 & 2\cdot L_e & 3\cdot L_e^2 & \lambda\cdot R\cdot(n_1(L_e) - n_2(L_e)) & \lambda\cdot R\cdot(n_2(L_e) + n_1(L_e)) & -\lambda\cdot R\cdot(n_3(L_e) + n_4(L_e)) & \lambda\cdot R\cdot(-n_4(L_e) + n_3(L_e)) \end{bmatrix} \quad (4\text{-}5a)$$

$$B_d = E\cdot I\cdot \begin{bmatrix} 0 & 0 & 0 & 6 & -2\cdot\lambda^3\cdot R\cdot(n_2(0) + n_1(0)) & 2\cdot\lambda^3\cdot R\cdot(n_1(0) - n_2(0)) & 2\cdot\lambda^3\cdot R\cdot(-n_4(0) + n_3(0)) & 2\cdot\lambda^3\cdot R\cdot(n_3(0) + n_4(0)) \\ 0 & 0 & -2 & 0 & 2\cdot\lambda^2\cdot R\cdot n_2(0) & -2\cdot\lambda^2\cdot R\cdot n_1(0) & -2\cdot\lambda^2\cdot R\cdot n_4(0) & 2\cdot\lambda^2\cdot R\cdot n_3(0) \\ 0 & 0 & 0 & -6 & 2\cdot\lambda^3\cdot R\cdot(n_2(L_e) + n_1(L_e)) & -2\cdot\lambda^3\cdot R\cdot(n_1(L_e) - n_2(L_e)) & -2\cdot\lambda^3\cdot R\cdot(-n_4(L_e) + n_3(L_e)) & -2\cdot\lambda^3\cdot R\cdot(n_3(L_e) + n_4(L_e)) \\ 0 & 0 & 2 & 6\cdot L_e & -2\cdot\lambda^2\cdot R\cdot n_2(L_e) & 2\cdot\lambda^2\cdot R\cdot n_1(L_e) & 2\cdot\lambda^2\cdot R\cdot n_4(L_e) & -2\cdot\lambda^2\cdot R\cdot n_3(L_e) \end{bmatrix} \quad (4\text{-}5b)$$

$$A_c = \begin{bmatrix} 1 & 0 & 0 & 0 & n_1(0) & n_2(0) & n_3(0) & n_4(0) \\ 0 & 1 & 0 & 0 & \lambda\cdot(n_1(0) - n_2(0)) & \lambda\cdot(n_2(0) + n_1(0)) & -\lambda\cdot(n_3(0) + n_4(0)) & \lambda\cdot(-n_4(0) + n_3(0)) \\ 1 & L_e & L_e^2 & L_e^3 & n_1(L_e) & n_2(L_e) & n_3(L_e) & n_4(L_e) \\ 0 & 1 & 2\cdot L_e & 3\cdot L_e^2 & \lambda\cdot(n_1(L_e) - n_2(L_e)) & \lambda\cdot(n_2(L_e) + n_1(L_e)) & -\lambda\cdot(n_3(L_e) + n_4(L_e)) & \lambda\cdot(-n_4(L_e) + n_3(L_e)) \end{bmatrix} \quad (4\text{-}6a)$$

$$B_c = E_c\cdot I_c\cdot \begin{bmatrix} 0 & 0 & 0 & 6 & -2\cdot\lambda^3\cdot(n_2(0) + n_1(0)) & 2\cdot\lambda^3\cdot(n_1(0) - n_2(0)) & 2\cdot\lambda^3\cdot(-n_4(0) + n_3(0)) & 2\cdot\lambda^3\cdot(n_3(0) + n_4(0)) \\ 0 & 0 & -2 & 0 & 2\cdot\lambda^2\cdot n_2(0) & -2\cdot\lambda^2\cdot n_1(0) & -2\cdot\lambda^2\cdot n_4(0) & 2\cdot\lambda^2\cdot n_3(0) \\ 0 & 0 & 0 & -6 & 2\cdot\lambda^3\cdot(n_2(L_e) + n_1(L_e)) & -2\cdot\lambda^3\cdot(n_1(L_e) - n_2(L_e)) & -2\cdot\lambda^3\cdot(-n_4(L_e) + n_3(L_e)) & -2\cdot\lambda^3\cdot(n_3(L_e) + n_4(L_e)) \\ 0 & 0 & 2 & 6\cdot L_e & -2\cdot\lambda^2\cdot n_2(L_e) & 2\cdot\lambda^2\cdot n_1(L_e) & 2\cdot\lambda^2\cdot n_4(L_e) & -2\cdot\lambda^2\cdot n_3(L_e) \end{bmatrix} \quad (4\text{-}6b)$$

The development of the element stiffness matrix involved stacking to form the 8 x 8 matrices. Knowledge of how to develop the assembled stiffness matrix (for the entire test) determines which matrix, $[A_d]$ or $[A_c]$ and $[B_d]$ or $[B_c]$, will be on the top in Equation 4-4. Equation 4-4 assumes that the element stiffness matrix $[k_e]$ connects to the dowel on the left and to the concrete on the right. As another example, if the element stiffness matrix was connected to the concrete beam on the left and to the dowel on the right, then $[A_d]$ and $[A_c]$ and $[B_d]$ and $[B_c]$ would be switched in the formulation of Equation 4-4.

4.5.2 Assembling the Stiffness Matrix K_e

Each element stiffness matrix is used to develop the assembled stiffness matrix $[K_e]$. The element stiffness matrix for each element is joined at a common node between two adjoining elements. The number of rows and columns within the element stiffness matrix that overlap (by summing stiffness coefficients) is based on the number of degrees of freedom at that particular node. This paper considers only two-dimensional loading with no movement in the x direction, and therefore two degrees of freedom are common at each node.

4.5.3 Iosipescu Elemental Shear Test Model

For the dowel in the end-block portion of Figure 4-4, the element stiffness matrix was developed using the one-parameter model for a beam on elastic foundation. This solution uses Friberg's semi-infinite beam theory (Friberg 1940) instead of Timoshenko's finite beam theory (Timoshenko 1925 and 1976). See Section 2.9.5 for the stiffness matrix from the semi-infinite beam theory. The dowel spanning the open joint was modeled as a beam where the beam's stiffness matrix included shear deflection. The

loaded-block portion, for the dowel embedment length, was modeled as two beams (the concrete block and the dowel) connected by series of linear-elastic springs. The equation to determine the elemental stiffness matrix [k_e] was introduced earlier. The concrete from the embedded end of the dowel to the end of the specimen (from Nodes n to o in Figure 4-8) was modeled as a concrete beam. Theoretically, this concrete segment is not required in the stiffness matrix. This segment was included for comparison with the AASHTO T253 test, for applying loaded-block weight (w) and for modeling the loaded block with elastic support as presented later.

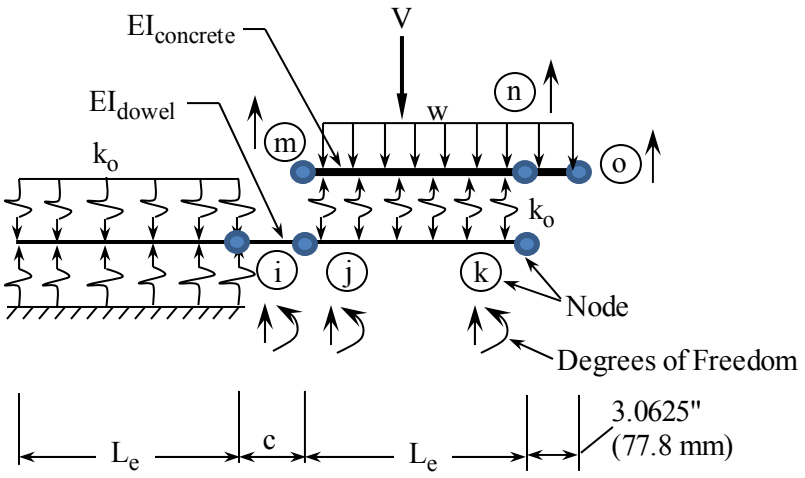

Figure 4-8 Iosipescu shear test idealization with degrees of freedom

An idealization of the Iosipescu Shear test consisted of beams and springs as shown in Figure 4-8. The weight of the concrete (for the load block) is distributed over the concrete portion and shown as w. Adding this weight assumes the test frame does not connect to the load block, and the test frame is oriented vertically (z direction in Figure 4-4). Figure 4-8 shows the degrees of freedom for the Iosipescu Shear test where six nodes with two degrees of freedom for Nodes i through k and one degree of freedom for Nodes m through o constitute the test.

The loaded block was prevented from rotating (theoretically) by imposing boundary conditions which removed rotational degrees of freedom at specified nodes. Rows and columns were removed in the stiffness matrix which corresponded to the rotations at Nodes m through o along the concrete load block and theoretically prevented rotation. The deflections at Nodes m through o will be the same.

4.5.4 AASHTO T253 Elemental Shear Test Model

A model of the AASHTO T253 test was developed at ISU using the stiffness method. This model was inclusive of the end blocks, joint widths and center span shown in Figure 4-5. For the dowel in the end block, the stiffness matrix was developed using the one-parameter model for a beam on elastic foundation. The assembled stiffness matrix incorporates the stiffness matrix from Friberg's semi-infinite beam theory given in Section 2.9.5 instead of Timoshenko's finite beam theory. The dowel spanning the open joint was modeled as a beam where the beam's stiffness matrix included shear deflection. The center-span was separated at the line of symmetry. The portion along the dowel's embedment length was modeled as two beams (the concrete block and the dowel) connected by series of linear-elastic springs such that the number of springs exceeded four per half wave (Cook, et al. 1985).

This criterion is satisfied by the differential equation for two beams connected by springs, but would apply to approximate methods which connect the dowel to the concrete with individual springs. Finally, the stiffness matrix was included for the concrete beam segment from the embedded end of the dowel to the line of symmetry (shown as Nodes n to o in Figure 4-9).

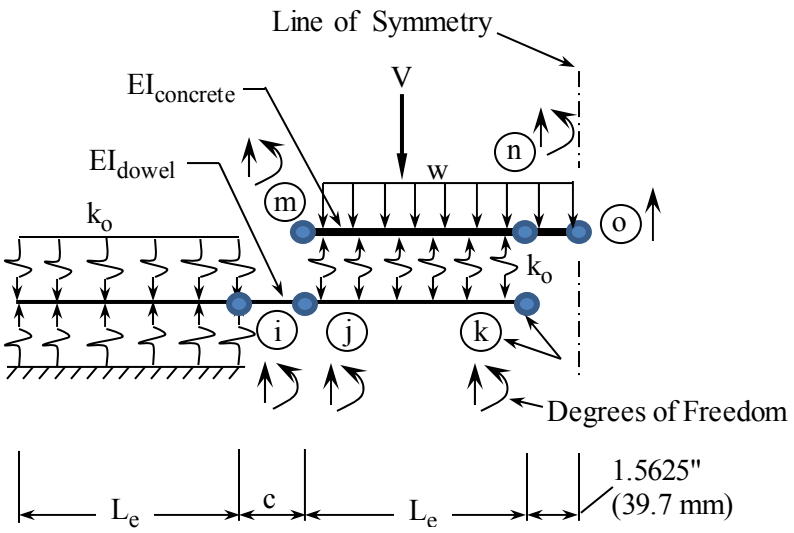

Figure 4-9 AASHTO T253 test idealization with degrees of freedom

Figure 4-9 shows the degrees of freedom (DOF) for the AASHTO T253 test. The line of symmetry reduced the number of DOF required to analyze the structure and accordingly reduced the size of the assembled stiffness matrix. At the line of symmetry, the structure is assumed to be at a point of maximum deflection, and the rotation at that point is then zero. In Figure 4-9, the maximum concrete deflection (at Node o) occurs in the center-span portion of the test, and the rotations (at Nodes m and n) are nearly zero making the AASHTO T253 test theoretically equivalent to the Iosipescu Shear test.

4.5.5 Cantilever Test Model

Figure 4-10 shows an idealization of the cantilever test with a theoretical load assumed to be located at c/2 which was the joint center. As mentioned earlier, the load application point would be greater than c/2 during experimental testing.

The assembled stiffness matrix [K_e] for the cantilever test was developed as follows. The embedded dowel in the concrete block was modeled as a beam on elastic

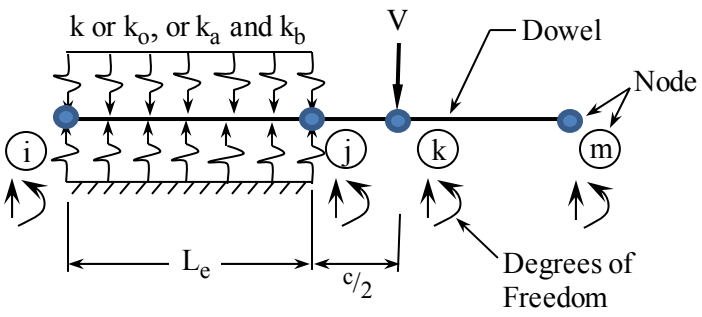

Figure 4-10 Cantilever test idealization with degrees of freedom

foundation. This solution uses the stiffness matrix from the two-parameter model given in Section 2.10. The two-parameter equations can be used for: 1) the two-parameter model with k_a and k_b, 2) the one-parameter model letting k_b equal zero and k_a equal k, and 3) the investigation of shear effect (shear deflection along the dowel's embedment length) for the one parameter model. The dowel was modeled as two beams which were separated by Node k in Figure 4-10. The beam's stiffness matrix from Nodes j to k included shear deflection. The dowel from Nodes k to m is not required in the analysis. As noted in Section 2.10.2 the parameter k_a is the Winkler constant and the parameter k_b is the load-spreading constant for the two-parameter foundation.

The block weight may have to be added to the shear load in Figure 4-10 (depending on the testing configuration) as either one half of the center span portion in the AASHTO T253 test or the loaded-block portion in the Iosipescu Shear test. This extra weight is added to the shear (V) and applied at a distance c/2 from the concrete face. The deflection (z), slope (θ), moment (M), shear (V) and reaction (q) results for the embedded dowel from the all three test methods will be the same when considering the one-parameter model.

4.6 Soil Modeling

The pavement spreads the vehicle loads over a broader area and reduces the pressure and deformation experienced by the subgrade. The load may be spread over a smaller area for overloaded vehicles, though. In reality, the soil does not rebound to its original or reference state immediately but is delayed due to internal soil friction (Zaretskii 1972). Theoretically, the soil will rebound fully at time equals infinity. Due to repeat loading, the soil will not have time to completely recover and soil compaction (or inelastic set) is immanent. This behavior (time-dependent elastic strain recovery) is typical of a viscoelastic medium. The soil has both elastic and viscous properties modeled with springs and a dashpot, respectively. The soil may also include shearing resistance or coupling between springs (Bowles 1996). The theory of rheology (Keedwell 1984) or Kelvin-Voigt hypothesis (Zaretskii 1972), when applied to properties of a soil medium, describes deformations due to external loads by summing elastic and viscous effects. Static loading would consider the elastic behavior of the supporting medium; whereas, repetitive loading would consider both elastic and viscous behavior of the supporting medium.

Past dowel research has used either steel beams (Porter, et al. 1993) or large steel springs (Eddie, et al. 2001) to simulate the subgrade in full-scale slab tests. Steel beams and springs are linear elastic over a large range of stress levels, provide only partial support below the specimen and do not account for delayed recovery. A more appropriate elastic support under the elemental shear tests or full-scale slab test specimens would be sheets of gum rubber, expansion joint material, or neoprene with

known Poisson's ratio (μ_r) and modulus of elasticity (E_r) in compression (ASTM D 395-98, D 575-91, D 6048-96, and D 6049-96).

The properties of the rubber subgrade are used to determine the modulus of subgrade reaction (k_s) from the equation outlined in Section 2.6. The rubber properties (E_r and μ_r) are substituted for the soil properties in that equation, which is shown by Equation 4-7 considering the elastic behavior of rubber.

$$k_S = \frac{0.91}{t} \cdot \sqrt[3]{\frac{E_r \cdot \left(1 - \mu_c^{\,2}\right)}{E_c \cdot \left(1 - \mu_r^{\,2}\right)}} \cdot \frac{E_r}{\left(1 - \mu_r^{\,2}\right)} \qquad (4\text{-}7)$$

Where:

k_s = modulus of subgrade reaction, pci (MPa/m)
E_c = concrete pavement's modulus of elasticity, psi (GPa)
E_r = rubber's modulus of elasticity, psi (MPa)
t = thickness of the concrete slab or specimen, in. (mm)
μ_c = concrete Poisson's ratio
μ_r = rubber Poisson's ratio

Rubber is a viscoelastic material that also exhibits inelastic deformations typical of soil. Multiple layers of rubber material can be used and should have sufficient thickness to eliminate confinement errors. Poisson's ratio and elastic modulus will be varied to model subgrades with different properties and modulus of subgrade reaction k_s (see Equation 4-7). Rubber will provide continuous elastic support below the test specimens and would be more representative of the soil-pavement interaction.

4.7 Modeling Laboratory Tests with Elastic Support

4.7.1 Hetenyi Model

A viscoelastic medium can be placed under the loaded-block portion of the Iosipescu test and the center span portion of the AASHTO T253 test. The embedded dowel in each of these portions was modeled by two beams (the dowel and the concrete) connected by linear-elastic springs where the spring stiffness was represented by the modulus of foundation (k_o). The concrete beam was further supported by a soil elastic foundation where the spring stiffness was represented by the modulus of subgrade reaction (k_s).

Hetenyi (1950 and 1961) defined this layered system with three parameters which were given by the two foundation moduli and the flexural rigidity of the second (or bottom) concrete beam. The following equations were modified from those presented by Hetenyi to include the elastic modulus for both beams.

4.7.2 Three-Parameter Model

The three-parameter model (Avramidis, et al. 2006 and Morfidis 2007) is shown in Figure 4-11. Four nodes with two degrees of freedom per node in Figure 4-11 define the two-beam element supported by an elastic medium with length L_e. Deflections in the positive z direction and counterclockwise rotations are considered positive displacements.

The general solution (as slightly modified from Hetenyi (1950 and 1961)) is given by Equation 4-8a for the dowel and Equation 4-8b for the concrete. When k_s is unity or less (but greater than zero), Equations 4-8a and 4-8b can be used for two-beams connected by springs.

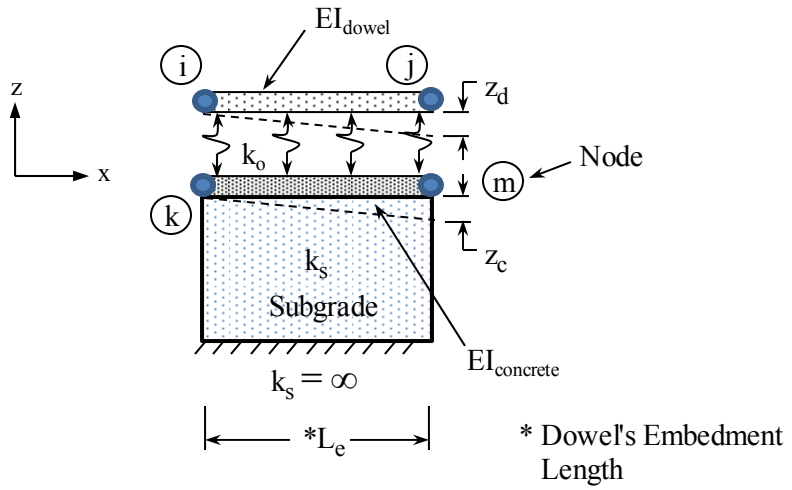

Figure 4-11 Three-parameter model

$$z_d(x) = C_1 \cdot n_1(x) + C_2 \cdot n_2(x) + C_3 \cdot n_3(x) + C_4 \cdot n_4(x) \ \ldots \\ + C_5 \cdot n_5(x) + C_6 \cdot n_6(x) + C_7 \cdot n_7(x) + C_8 \cdot n_8(x) \tag{4-8a}$$

$$z_c(x) = R_a \cdot \left(C_1 \cdot n_1(x) + C_2 \cdot n_2(x) + C_3 \cdot n_3(x) + C_4 \cdot n_4(x)\right) \ \ldots \\ + R_b \cdot \left(C_5 \cdot n_5(x) + C_6 \cdot n_6(x) + C_7 \cdot n_7(x) + C_8 \cdot n_8(x)\right) \tag{4-8b}$$

Substituting:

$$n_1(x) = e^{\lambda_a \cdot x} \cdot \cos\left(\lambda_a \cdot x\right) \qquad n_5(x) = e^{\lambda_b \cdot x} \cdot \cos\left(\lambda_b \cdot x\right)$$

$$n_2(x) = e^{\lambda_a \cdot x} \cdot \sin\left(\lambda_a \cdot x\right) \qquad n_6(x) = e^{\lambda_b \cdot x} \cdot \sin\left(\lambda_b \cdot x\right)$$

$$n_3(x) = e^{-\lambda_a \cdot x} \cdot \cos\left(\lambda_a \cdot x\right) \qquad n_7(x) = e^{-\lambda_b \cdot x} \cdot \cos\left(\lambda_b \cdot x\right)$$

$$n_4(x) = e^{-\lambda_a \cdot x} \cdot \sin\left(\lambda_a \cdot x\right) \qquad n_8(x) = e^{-\lambda_b \cdot x} \cdot \sin\left(\lambda_b \cdot x\right)$$

Where:

C_1, C_2 …C_8 = constants

x = distance along the dowel, in. (mm)

w_s = specimen width supported by the soil, in. (mm)

k_s = modulus of subgrade reaction, pci (MPa/m)

$$R_a = 1 - (S + T) \cdot \frac{E \cdot I}{k_o \cdot d} \qquad R_b = 1 - (S - T) \cdot \frac{E \cdot I}{k_o \cdot d}$$

$$N = \frac{k_o \cdot d \cdot \left(E \cdot I + E_c \cdot I_c\right) + k_s \cdot w_s \cdot (E \cdot I)}{E \cdot I \cdot \left(E_c \cdot I_c\right)} \qquad O = \frac{k_o \cdot d}{E \cdot I} \cdot \left(\frac{k_s \cdot w_s}{E_c \cdot I_c}\right)$$

$$S = \frac{N}{2} \qquad T = \sqrt{\left(\frac{N^2}{4} - O\right)}$$

$$\lambda_{.a} = \sqrt[4]{\frac{S + T}{4}} \qquad \lambda_b = \sqrt[4]{\frac{S - T}{4}}$$

The [A] and [B] matrices are given as $[A_d]$ and $[B_d]$ by Equations 4-9a and 4-9b for the dowel and as $[A_c]$ and $[B_c]$ by Equations 4-10a and 4-10b for the concrete. The element stiffness matrix was developed using the same procedure (see Equation 4-4) as in the previous section for two beams connected by springs. The assembled stiffness matrix $[K_e]$ was developed in the same manner as for the elemental shear tests given previously with exception of the following.

The three-parameter equations were used for the embedded dowel in the loaded-block and the center-span portions of the Iosipescu Shear test and AASHTO T253 test, respectively. The concrete portion from the embedded end of the dowel to the end of specimen in the Iosipescu Shear test (and to the line of symmetry in the AASHTO T253 test) was modeled as a concrete beam on elastic foundation.

$$A_d = \begin{bmatrix} n_1(0) & n_2(0) & n_3(0) & n_4(0) & n_5(0) & n_6(0) & n_7(0) & n_8(0) \\ \lambda_a \cdot \begin{pmatrix} n_1(0) \dots \\ +-n_2(0) \end{pmatrix} & \lambda_a \cdot \begin{pmatrix} n_1(0) \dots \\ +n_2(0) \end{pmatrix} & -\lambda_a \cdot \begin{pmatrix} n_3(0) \dots \\ +n_4(0) \end{pmatrix} & \lambda_a \cdot \begin{pmatrix} n_3(0) \dots \\ +-n_4(0) \end{pmatrix} & \lambda_b \cdot \begin{pmatrix} n_5(0) \dots \\ +-n_6(0) \end{pmatrix} & \lambda_b \cdot \begin{pmatrix} n_5(0) \dots \\ +n_6(0) \end{pmatrix} & -\lambda_b \cdot \begin{pmatrix} n_7(0) \dots \\ +n_8(0) \end{pmatrix} & \lambda_b \cdot \begin{pmatrix} n_7(0) \dots \\ +-n_8(0) \end{pmatrix} \\ n_1(L_e) & n_2(L_e) & n_3(L_e) & n_4(L_e) & n_5(L_e) & n_6(L_e) & n_7(L_e) & n_8(L_e) \\ \lambda_a \cdot \begin{pmatrix} n_1(L_e) \dots \\ +-n_2(L_e) \end{pmatrix} & \lambda_a \cdot \begin{pmatrix} n_1(L_e) \dots \\ +n_2(L_e) \end{pmatrix} & -\lambda_a \cdot \begin{pmatrix} n_3(L_e) \dots \\ +n_4(L_e) \end{pmatrix} & \lambda_a \cdot \begin{pmatrix} n_3(L_e) \dots \\ +-n_4(L_e) \end{pmatrix} & \lambda_b \cdot \begin{pmatrix} n_5(L_e) \dots \\ +-n_6(L_e) \end{pmatrix} & \lambda_b \cdot \begin{pmatrix} n_5(L_e) \dots \\ +n_6(L_e) \end{pmatrix} & -\lambda_b \cdot \begin{pmatrix} n_7(L_e) \dots \\ +n_8(L_e) \end{pmatrix} & \lambda_b \cdot \begin{pmatrix} n_7(L_e) \dots \\ +-n_8(L_e) \end{pmatrix} \end{bmatrix} \quad (4\text{-}9a)$$

$$B_d = 2 \cdot E \cdot I \cdot \begin{bmatrix} -\lambda_a^3 \cdot \begin{pmatrix} n_1(0) \dots \\ +n_2(0) \end{pmatrix} & \lambda_a^3 \cdot \begin{pmatrix} n_1(0) \dots \\ +-n_2(0) \end{pmatrix} & \lambda_a^3 \cdot \begin{pmatrix} n_3(0) \dots \\ +-n_4(0) \end{pmatrix} & \lambda_a^3 \cdot \begin{pmatrix} n_3(0) \dots \\ +n_4(0) \end{pmatrix} & -\lambda_b^3 \cdot \begin{pmatrix} n_5(0) \dots \\ +n_6(0) \end{pmatrix} & \lambda_b^3 \cdot \begin{pmatrix} n_5(0) \dots \\ +-n_6(0) \end{pmatrix} & \lambda_b^3 \cdot \begin{pmatrix} n_7(0) \dots \\ +-n_8(0) \end{pmatrix} & \lambda_b^3 \cdot \begin{pmatrix} n_7(0) \dots \\ +n_8(0) \end{pmatrix} \\ \lambda_a^2 \cdot n_2(0) & -\lambda_a^2 \cdot n_1(0) & -\lambda_a^2 \cdot n_4(0) & \lambda_a^2 \cdot n_3(0) & \lambda_b^2 \cdot n_6(0) & -\lambda_b^2 \cdot n_5(0) & -\lambda_b^2 \cdot n_8(0) & \lambda_b^2 \cdot n_7(0) \\ \lambda_a^3 \cdot \begin{pmatrix} n_1(L_e) \dots \\ +n_2(L_e) \end{pmatrix} & -\lambda_a^3 \cdot \begin{pmatrix} n_1(L_e) \dots \\ +-n_2(L_e) \end{pmatrix} & -\lambda_a^3 \cdot \begin{pmatrix} n_3(L_e) \dots \\ +-n_4(L_e) \end{pmatrix} & -\lambda_a^3 \cdot \begin{pmatrix} n_3(L_e) \dots \\ +n_4(L_e) \end{pmatrix} & \lambda_b^3 \cdot \begin{pmatrix} n_5(L_e) \dots \\ +n_6(L_e) \end{pmatrix} & -\lambda_b^3 \cdot \begin{pmatrix} n_5(L_e) \dots \\ +-n_6(L_e) \end{pmatrix} & -\lambda_b^3 \cdot \begin{pmatrix} n_7(L_e) \dots \\ +-n_8(L_e) \end{pmatrix} & -\lambda_b^3 \cdot \begin{pmatrix} n_7(L_e) \dots \\ +n_8(L_e) \end{pmatrix} \\ -\lambda_a^2 \cdot n_2(L_e) & \lambda_a^2 \cdot n_1(L_e) & \lambda_a^2 \cdot n_4(L_e) & -\lambda_a^2 \cdot n_3(L_e) & -\lambda_b^2 \cdot n_6(L_e) & \lambda_b^2 \cdot n_5(L_e) & \lambda_b^2 \cdot n_8(L_e) & -\lambda_b^2 \cdot n_7(L_e) \end{bmatrix} \quad (4\text{-}9b)$$

$$A_c = \begin{bmatrix} R_a \cdot n_1(0) & R_a \cdot n_2(0) & R_a \cdot n_3(0) & R_a \cdot n_4(0) & R_b \cdot n_5(0) & R_b \cdot n_6(0) & R_b \cdot n_7(0) & R_b \cdot n_8(0) \\ R_a \cdot \lambda_a \cdot \begin{pmatrix} n_1(0) \dots \\ +-n_2(0) \end{pmatrix} & R_a \cdot \lambda_a \cdot \begin{pmatrix} n_1(0) \dots \\ +n_2(0) \end{pmatrix} & -R_a \cdot \lambda_a \cdot \begin{pmatrix} n_3(0) \dots \\ +n_4(0) \end{pmatrix} & R_a \cdot \lambda_a \cdot \begin{pmatrix} n_3(0) \dots \\ +-n_4(0) \end{pmatrix} & R_b \cdot \lambda_b \cdot \begin{pmatrix} n_5(0) \dots \\ +-n_6(0) \end{pmatrix} & R_b \cdot \lambda_b \cdot \begin{pmatrix} n_5(0) \dots \\ +n_6(0) \end{pmatrix} & -R_b \cdot \lambda_b \cdot \begin{pmatrix} n_7(0) \dots \\ +n_8(0) \end{pmatrix} & R_b \cdot \lambda_b \cdot \begin{pmatrix} n_7(0) \dots \\ +-n_8(0) \end{pmatrix} \\ R_a \cdot n_1(L_e) & R_a \cdot n_2(L_e) & R_a \cdot n_3(L_e) & R_a \cdot n_4(L_e) & R_b \cdot n_5(L_e) & R_b \cdot n_6(L_e) & R_b \cdot n_7(L_e) & R_b \cdot n_8(L_e) \\ R_a \cdot \lambda_a \cdot \begin{pmatrix} n_1(L_e) \dots \\ +-n_2(L_e) \end{pmatrix} & R_a \cdot \lambda_a \cdot \begin{pmatrix} n_1(L_e) \dots \\ +n_2(L_e) \end{pmatrix} & -R_a \cdot \lambda_a \cdot \begin{pmatrix} n_3(L_e) \dots \\ +n_4(L_e) \end{pmatrix} & R_a \cdot \lambda_a \cdot \begin{pmatrix} n_3(L_e) \dots \\ +-n_4(L_e) \end{pmatrix} & R_b \cdot \lambda_b \cdot \begin{pmatrix} n_5(L_e) \dots \\ +-n_6(L_e) \end{pmatrix} & R_b \cdot \lambda_b \cdot \begin{pmatrix} n_5(L_e) \dots \\ +n_6(L_e) \end{pmatrix} & -R_b \cdot \lambda_b \cdot \begin{pmatrix} n_7(L_e) \dots \\ +n_8(L_e) \end{pmatrix} & R_b \cdot \lambda_b \cdot \begin{pmatrix} n_7(L_e) \dots \\ +-n_8(L_e) \end{pmatrix} \end{bmatrix} \quad (4\text{-}10a)$$

$$B_c = 2 \cdot E_c \cdot I_c \cdot \begin{bmatrix} -R_a \cdot \lambda_a^3 \cdot \begin{pmatrix} n_1(0) \dots \\ +n_2(0) \end{pmatrix} & R_a \cdot \lambda_a^3 \cdot \begin{pmatrix} n_1(0) \dots \\ +-n_2(0) \end{pmatrix} & R_a \cdot \lambda_a^3 \cdot \begin{pmatrix} n_3(0) \dots \\ +-n_4(0) \end{pmatrix} & R_a \cdot \lambda_a^3 \cdot \begin{pmatrix} n_3(0) \dots \\ +n_4(0) \end{pmatrix} & -R_b \cdot \lambda_b^3 \cdot \begin{pmatrix} n_5(0) \dots \\ +n_6(0) \end{pmatrix} & R_b \cdot \lambda_b^3 \cdot \begin{pmatrix} n_5(0) \dots \\ +-n_6(0) \end{pmatrix} & R_b \cdot \lambda_b^3 \cdot \begin{pmatrix} n_7(0) \dots \\ +-n_8(0) \end{pmatrix} & R_b \cdot \lambda_b^3 \cdot \begin{pmatrix} n_7(0) \dots \\ +n_8(0) \end{pmatrix} \\ R_a \cdot \lambda_a^2 \cdot n_2(0) & -R_a \cdot \lambda_a^2 \cdot n_1(0) & -R_a \cdot \lambda_a^2 \cdot n_4(0) & R_a \cdot \lambda_a^2 \cdot n_3(0) & R_b \cdot \lambda_b^2 \cdot n_6(0) & -R_b \cdot \lambda_b^2 \cdot n_5(0) & -R_b \cdot \lambda_b^2 \cdot n_8(0) & R_b \cdot \lambda_b^2 \cdot n_7(0) \\ R_a \cdot \lambda_a^3 \cdot \begin{pmatrix} n_1(L_e) \dots \\ +n_2(L_e) \end{pmatrix} & -R_a \cdot \lambda_a^3 \cdot \begin{pmatrix} n_1(L_e) \dots \\ +-n_2(L_e) \end{pmatrix} & -R_a \cdot \lambda_a^3 \cdot \begin{pmatrix} n_3(L_e) \dots \\ +-n_4(L_e) \end{pmatrix} & -R_a \cdot \lambda_a^3 \cdot \begin{pmatrix} n_3(L_e) \dots \\ +n_4(L_e) \end{pmatrix} & R_b \cdot \lambda_b^3 \cdot \begin{pmatrix} n_5(L_e) \dots \\ +n_6(L_e) \end{pmatrix} & -R_b \cdot \lambda_b^3 \cdot \begin{pmatrix} n_5(L_e) \dots \\ +-n_6(L_e) \end{pmatrix} & -R_b \cdot \lambda_b^3 \cdot \begin{pmatrix} n_7(L_e) \dots \\ +-n_8(L_e) \end{pmatrix} & -R_b \cdot \lambda_b^3 \cdot \begin{pmatrix} n_7(L_e) \dots \\ +n_8(L_e) \end{pmatrix} \\ -R_a \cdot \lambda_a^2 \cdot n_2(L_e) & R_a \cdot \lambda_a^2 \cdot n_1(L_e) & R_a \cdot \lambda_a^2 \cdot n_4(L_e) & -R_a \cdot \lambda_a^2 \cdot n_3(L_e) & -R_b \cdot \lambda_b^2 \cdot n_6(L_e) & R_b \cdot \lambda_b^2 \cdot n_5(L_e) & R_b \cdot \lambda_b^2 \cdot n_8(L_e) & -R_b \cdot \lambda_b^2 \cdot n_7(L_e) \end{bmatrix} \quad (4\text{-}10b)$$

4.8 Results

Table 4-1 was developed theoretically from the stiffness matrix that modeled the AASHTO T253 test with an elastic support under the center-span portion. This elastic support was represented using the modulus of subgrade reaction (k_s). When the k_s value is one or less (but greater than zero) the resulting deflections will be the same as given in Table 2-1. The lower k_s value was compared to a k_s value of 400 pci (109 MPa/m) in Table 2-1. This comparison showed that only a small reduction in deflections resulted from a larger k_s value.

The following properties were used to develop the table, and these properties were from the American Highway Technology (AHT) report (Porter, et al. 2001).

Table Properties *(Porter, et al. 2001)*
E = 29,000,000 psi (200 GPa) Modulus of elasticity for steel dowels
μ = 0.29 Poisson's ratio for steel dowels
f_c' = 6,000 psi (41.37 MPa) Concrete compressive strength
E_c = 4,415,201 psi (30.4 GPa) Concrete modulus of elasticity
μ_c = 0.18 Poisson's ratio (concrete)
V = -2,000 lb. (-8.90 kN) Shear
L_e = 8.9375 in. (227 mm) Dowel embedment length
c = 1/8 in. (3.2 mm) Transverse joint width
w = 12.08 lb/in. (2.12 kN/m) Distributed concrete weight
w_s = 12 in. (305 mm) Specimen width
t = 12 in. (305 mm) Specimen thickness

Table 4-1 AASHTO T253 with elastic support (theoretical)

Dowel Description h x d, in (mm)	Relative Deflection*, $z_c - z_d$, in. (mm)	
	k_s = 1 pci (0.27 MPa/m)	k_s = 400 pci (109 MPa/m)
1.00 x 1.00 (25.40 x 25.40)	-0.0010 (-0.0259)	-0.0010 (-0.0253)
0.88 x 1.41 (22.35 x 35.81)	-0.0009 (-0.0240)	-0.0009 (-0.0229)
1.25 x 1.25 (31.75 x 31.75)	-0.0008 (-0.0205)	-0.0008 (-0.0197)
1.13 x 1.66 (28.70 x 42.16)	-0.0008 (-0.0192)	-0.0007 (-0.0185)
1.50 x 1.50 (38.10 x 38.10)	-0.0007 (-0.0170)	-0.0006 (-0.0164)
1.34 x 1.98 (34.04 x 50.29)	-0.0006 (-0.0160)	-0.0006 (-0.0152)

* Relative deflections at the transverse joint face.

4.9 Summary, Conclusions and Recommendations

4.9.1 Summary

Three laboratory test methods (two elemental shear test methods and a cantilever test method) were modeled using the stiffness method of structural analysis. These experimental tests determine the deflection of the dowel within the concrete at the transverse joint face. With proper instrumentation, the deflections of the dowel within the concrete along the dowel's embedment length can be determined. The model of each laboratory test method was used to verify these deflections and explain each test method. Also, the elemental shear test models were used to investigate soil-pavement interaction by incorporating an elastic support under a portion of the test specimen. Equations for the three-parameter model (as presented by Hetenyi (1950 and 1961)) were used in this elastic support analysis.

The concrete surrounding the dowel is represented by either of two different elastic foundation models – the one- or the two-parameter model. Deflections within the concrete are given by $z_1(x)$ and $z_2(x)$ for the one- and two-parameter models, respectively. The deflections are determined in each model using elastic constants (or parameters) given by k (contact modulus) or k_o (modulus of foundation) for the one-parameter model, and k_a (Winkler constant) and k_b (load-spreading constant) for the two-parameter model. Laboratory test methods are used to verify these elastic constants.

4.9.2 Conclusions

The following conclusions have been drawn from this paper:

- The deflections within the concrete, in Table 4-1 for the AASHTO T253 test with elastic support, change only slightly with the introduction of an elastic medium supporting the slab or specimen. Therefore, dowel deflections within the concrete at the joint face or $z_1(0)$ (see Equation 2-5) can be used for dowel deflections in full-scale slabs.
- Modeling the laboratory tests using the stiffness method has shown that the dowels in a doweled concrete joint can be accurately represented using these laboratory tests.

Changing the value of the modulus of subgrade reaction (k_s) and using the three-parameter model the following conclusions were drawn:

- The deflections along the dowel within the concrete do not change with an increase in the subgrade modulus.

- The bearing stress as presented in Chapter 3 may increase with an increase in the subgrade modulus regardless of the deflection values. This increase may be apparent for test specimens supported by a rigid test stand.

4.9.3 Recommendations

The following recommendations were determined from this research project:

- This paper recommends a standard joint width (c) of three-eighths inch (9.5 mm) for the elemental shear test and the full-scale slab specimens with a concrete thickness (t) of 12 inches (305 mm).
- The cantilever test is recommended, as shown in Figure 4-12, to verify the k_o (modulus of foundation) or k_a (Winkler constant) and k_b (load-spreading constant) for the one- or the two-parameter model, respectively.

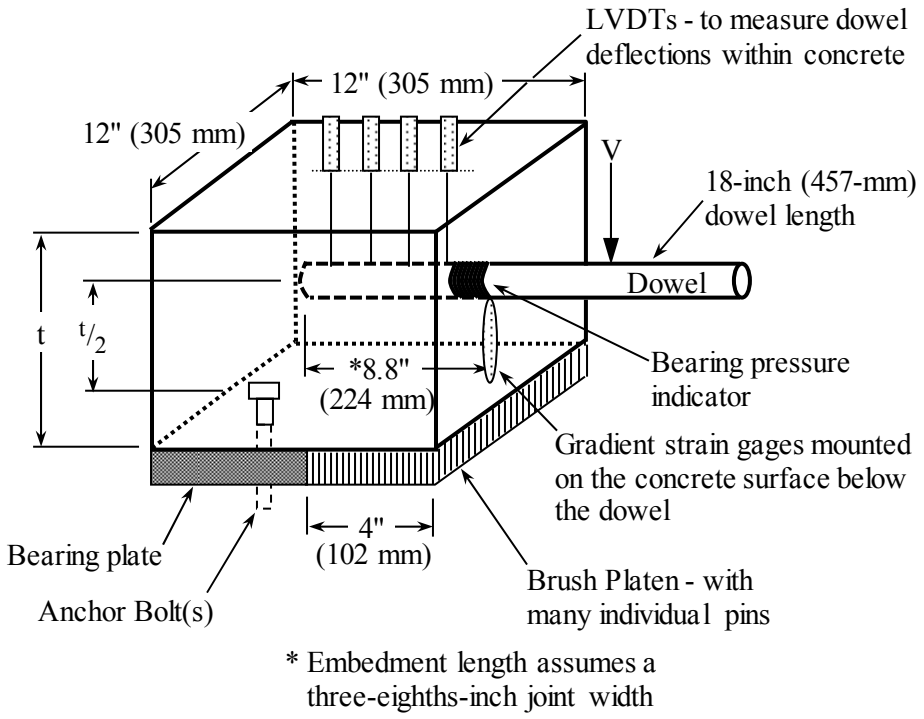

Figure 4-12 Recommended cantilever test setup

- The AASHTO T253 test method was modeled using the stiffness method to verify load application points, correct testing configuration and specimen dimensions. The test specification should be revised from its present form to include these previously listed items.

4.10 References

AASHTO, 1993. *AASHTO Guide for Design of Pavement Structures*, American Association of State Highway and Transportation Official, Washington D.C., 624.

AASHTO, 1996. *Standard Method of Test for Coated Dowel Bars*, Designation: T253, American Association of State Highway and Transportation Officials, Washington D.C.

ASTM D 395-98, Test Standard Test Methods for Rubber Property – Compression Set, *American Society for Testing Materials Vol. 9.01*, West Conshohocken, PA.

ASTM D 575-91 (Reapproved 1996), Standard Test Methods for Rubber Properties in Compression, *American Society for Testing and Materials Vol. 9.01*, West Conshohocken, PA.

ASTM D 6048-96, Standard Practice for Stress Relaxation Testing of Raw Rubber, Unvulcanized Rubber Compounds, and Thermoplastic Elastomers, *American Society for Testing and Materials Vol. 9.01*, West Conshohocken, PA.

ASTM D 6049-96, Standard Test Method for Rubber Property-Measurement of the Viscous and Elastic Behavior of Unvulcanized Raw Rubbers and Rubber Compounds by Compression Between Parallel Plates, *American Society for Testing and Materials Vol. 9.01*, West Conshohocken, PA.

Avramidis, E.I., and Morfidis, K., 2006. Bending of Beams on a Three-Parameter Elastic Foundation, *International Journal of Solids and Structures*, 43, 357-375.

Bowles, J.E., 1996. *Foundation Analysis and Design*, 5th Edition, McGraw-Hill International Edition.

Bhattacharya, K., 2000. Nonlinear Response of Transverse Joints of Airfield Pavements, *Journal of Transportation Engineering, American Society of Civil Engineers*, 126(2), 168-177.

Cook, R.D., and Young, W.C., 1985. *Advanced Mechanics of Materials*, Macmillan Publishing Company, New York, NY.

Eddie, D., Shalaby, A., and Riskalla, S., 2000. Glass Fiber-Reinforced Polymer Dowels for Concrete Pavements, *ACI Structural Journal*, 98(2), 201-206.

Farny, J.A., 2001. *Concrete Floors on Ground*, EB075, Portland Cement Association, Skokie, Illinois, U.S.A., 136 pages.

Friberg, B.F., 1940. Design of Dowels in Transverse Joints of Concrete Pavements, *Proceedings, American Society of Civil Engineers*, 105, 1076-1116.

Granholm, H., 1929. On the Elastic Stability of Piles Surrounded by a Supporting Medium, Ingeniorsvetenskapsakademiens, Handlingar NR 89, Stockholm, Sweden.

Harrington, J.F., 2006. *Comparison of Alternative Dowel Bar Testing Procedures*, Master's Thesis, Iowa State University.

Hetenyi, M., 1950. A General Solution for the Bending of Beams on an Elastic Foundation of Arbitrary Continuity. *Journal of Applied Physics*, 1, 55-58.

Hetenyi, M., 1961. *Beams on Elastic Foundations*. The University of Michigan Press, Ann Arbor, Michigan.

Ingram, D.N.J., 2004. *The Effects of the Dowel Bar Shape and Spacing in Portland Cement Concrete Pavements on the Load Transfer Efficiency of the Transverse Joint*, Master's Thesis, Iowa State University.

Keedwell, M.J., 1984. *Rheology and Soil Mechanics*, Elsevier Applied Science Publishers LTD, London, England and New York, N.Y.

Kukreti, A.R., and Taheri, M.R., 1992. Dynamic Analysis of Rigid Airport Pavements with Discontinuities, *Journal of Transportation Engineering, American Society of Civil Engineers*, 118(3), 341-360.

Melerski, E.S., 2000. *Design Analysis of Beams, Circular Plates and Cylindrical Tanks on Elastic Foundations*, Balkema, Netherlands.

Morfidis, K., 2007. Exact matrices for Beams on Three-Parameter Elastic Foundation, *Computers and Structures*, 85, 1243-1256.

Murison, S., Shalaby, A., and Mufti, A.A., 2002. Modeling of Concrete Pavement Dowel-Slab Interaction. *4th Transportation Specialty Conference of the Canadian Society for Civil Engineering*, Montreal, Quebec, Canada.

Porter, M.L., Albertson, M., Barnes, B., Lorenz, E.A., and Viswanath, K.P., 1992. *Thermoset Composite Concrete Reinforcement*. Report HR-325. Iowa Department of Transportation and Iowa Highway Research Board, Ames, Iowa.

Porter, M.L., Hughes, B.W., Barnes, B.A., and Viswanath, K.P., 1993. *NonCorrosive Tie Reinforcing and Dowel Bars for Highway Pavement Slabs*. Submitted to Highway Division of the Iowa Department of Transportation and Iowa Highway Research Board, Project No. HR 343.

Porter, M.L., Davis, D., and Rohner, J., 1999. *Investigation of Glass Fiber Composite Dowel Bars for Highway Pavement Slabs.* Progress Report TR-408. Iowa Department of Transportation and Iowa Highway Research Board, Ames, Iowa.

Porter, M.L., Guinn, R.J., and Lundy, A.L., 2001. *Dowel Bar Optimization: Phase I and II, Final Report*, American Highway Technology (AHT), Center for Transportation Research and Education, Iowa State University.

Porter, M.L., Peterson, S., and Lorenz, E.A., 2008. *Determination of the Performance of Concrete Slab Dowels,* Department of Civil, Construction and Environmental Engineering, Iowa State University.

Timoshenko, S., and Lessels, J.M., 1925. *Applied Elasticity*, Westinghouse Technical Night School Press, East Pittsburgh, Pennsylvania.

Timoshenko, S., 1976. *Strength of Materials – Part II*, 3rd Edition, Robert E. Krieger Publishing Company, Huntington, New York.

Walrath, D.E., and Adams, D.F., March 1983. The Iosipescu Shear Test as Applied to Composite Materials, *Experimental Mechanics*, 105-110.

Weaver, W., and Gere, J.M., 1990. *Matrix Analysis of Framed Structures*, 3rd Edition, Von Nostrand Reinhold International Company.

Yoder, E.G., and Witczak, M.W., 1975. *Principles of Pavement Design*, 2nd Edition, John Wiley & Sons, Inc., New York, NY.

Zaretskii, Y.K., 1972. *Theory of Soil Consolidation*, (Translated from Russian), Israel Program for Scientific Translations, U.S. Department of the Interior and the National Science Foundation, Washington, D.C.

CHAPTER 5. GENERAL CONCLUSIONS

The elliptical shape was compared to the circular shape for dowels embedded in concrete. Both the one- and two-parameter models were used to represent the concrete surrounding the dowels. The following conclusions were drawn from this shape comparison:

- For a given load, and compared to the circular shape with equivalent flexural rigidity, the elliptical shape is an improved alternative for steel dowels used in concrete slab joints based on deflection,
- The elliptical shape results in less bearing stress than the circular shape with equivalent flexural rigidity. This shape improvement was determined by both the one- and two-parameter foundation models,
- The elliptical shape resulted in lower deflections at the transverse joint face than a comparable circular shape with equivalent flexural rigidity. This lower deflection means the elliptical shape would potentially cause less oblonging of the hole in the concrete surrounding the dowel's cross section,
- Based on a reduced bearing stress, the elliptical-shaped dowel reduces tensile field splitting below the dowel,
- Deflections at the transverse joint face from the first companion paper (see Chapter 2) are used to determine the maximum bearing stress for the one-parameter model (either finite beam or semi-infinite beam theories as a function of x) and the two-parameter model. For the semi-infinite beam theory, a simplified equation for q_o (reaction at the transverse joint face when x is zero) is used to find the maximum bearing stress without deflection values.

A comparison was made between the one- and two-parameter foundation models which represented the concrete around the dowels. The deflected shape of the embedded dowel, through laboratory testing, is required to determine which elastic foundation model is more appropriate for a particular dowel size, shape and material. This research project did not include experimental deflection data along the embedded dowel. Maximum deflections within the concrete at the transverse joint face, however, were measured for each dowel based on the relative deflection across the transverse joint. These maximum deflections were used to conclude the following:

- Based on the maximum deflection of all dowel sizes in this research project, the one-parameter model is a good alternative and compares favorably to the two-parameter model.

The following conclusion was determined based on the one- and the two-parameter model using a 12-inch (305-mm) thick specimen:

- The maximum deflection at the transverse joint face is used to determine the maximum bearing stress. As the deflections increase, as for a larger shear load, the bearing stress will increase.

The previous conclusion is modified based on a reduction in concrete depth below the dowel:

- For the dowel sizes in this research project embedded in an eight-inch (305-mm) thick specimen, as the medium depth below the dowel is reduced, the dowel deflections within this medium were smaller,
- As the medium depth below the dowel is reduced, an increase in bearing stress will result.

Laboratory testing of dowels embedded in concrete resulted in the following conclusions:

- The dowel is a separate entity within the concrete and transfers shear load across the transverse joint. Modeling the laboratory tests using the stiffness method has shown that the dowels in a doweled concrete joint can be accurately represented by these laboratory tests,
- The AASHTO T253 test method was modeled using the stiffness method to verify load application points, correct testing configuration and specimen dimensions. The test specification should be revised from its present form to include these previously listed items.

APPENDIX: DERIVATIVE FUNCTIONS FOR BOTH FOUNDATION MODELS

The derivative functions (in vector form) for the one-parameter model are given below. These equations are in terms of $n_1(x)$ through $n_4(x)$ as given by Equation 2-6.

$$N_1'(x) = \beta \cdot \begin{pmatrix} n_1(x) - n_2(x) \\ n_1(x) + n_2(x) \\ -n_3(x) - n_4(x) \\ n_3(x) - n_4(x) \end{pmatrix}$$

$$N_1''(x) = 2 \cdot \beta^2 \cdot \begin{pmatrix} -n_2(x) \\ n_1(x) \\ n_4(x) \\ -n_3(x) \end{pmatrix}$$

$$N_1'''(x) = 2 \cdot \beta^3 \cdot \begin{pmatrix} -n_1(x) - n_2(x) \\ n_1(x) - n_2(x) \\ n_3(x) - n_4(x) \\ n_3(x) + n_4(x) \end{pmatrix}$$

$$N_1''''(x) = 4 \cdot \beta^4 \cdot \begin{pmatrix} -n_1(x) \\ -n_2(x) \\ -n_3(x) \\ -n_4(x) \end{pmatrix}$$

The derivative functions (in vector form) for the two-parameter model are given below. These equations are in terms of $n_1(x)$ through $n_4(x)$ as given by Equation 2-16.

$$N_2'(x) = L\cdot\begin{pmatrix} -\alpha\cdot n_3(x) + \lambda\cdot n_2(x) \\ -\alpha\cdot n_4(x) + \lambda\cdot n_1(x) \\ \alpha\cdot n_1(x) + \lambda\cdot n_4(x) \\ \alpha\cdot n_2(x) + \lambda\cdot n_3(x) \end{pmatrix}$$

$$N_2''(x) = L^2\cdot\begin{bmatrix} \left(\lambda^2 - \alpha^2\right)\cdot n_1(x) + (-2\cdot\alpha\cdot\lambda)\cdot n_4(x) \\ \left(\lambda^2 - \alpha^2\right)\cdot n_2(x) + (-2\cdot\alpha\cdot\lambda)\cdot n_3(x) \\ \left(\lambda^2 - \alpha^2\right)\cdot n_3(x) + (2\cdot\alpha\cdot\lambda)\cdot n_2(x) \\ \left(\lambda^2 - \alpha^2\right)\cdot n_4(x) + (2\cdot\alpha\cdot\lambda)\cdot n_1(x) \end{bmatrix}$$

$$N_2'''(x) = L^3\cdot\begin{bmatrix} \left(\alpha^3 - 3\cdot\alpha\cdot\lambda^2\right)\cdot n_3(x) + \left(\lambda^3 - 3\cdot\alpha^2\cdot\lambda\right)\cdot n_2(x) \\ \left(\alpha^3 - 3\cdot\alpha\cdot\lambda^2\right)\cdot n_4(x) + \left(\lambda^3 - 3\cdot\alpha^2\cdot\lambda\right)\cdot n_1(x) \\ \left(3\cdot\alpha\cdot\lambda^2 - \alpha^3\right)\cdot n_1(x) + \left(\lambda^3 - 3\cdot\alpha^2\cdot\lambda\right)\cdot n_4(x) \\ \left(3\cdot\alpha\cdot\lambda^2 - \alpha^3\right)\cdot n_2(x) + \left(\lambda^3 - 3\cdot\alpha^2\cdot\lambda\right)\cdot n_3(x) \end{bmatrix}$$

$$N_2''''(x) = L^4\cdot\begin{bmatrix} \left(\alpha^4 - 6\cdot\alpha^2\cdot\lambda^2 + \lambda^4\right)\cdot n_1(x) + \left(4\cdot\alpha^3\cdot\lambda - 4\cdot\alpha\cdot\lambda^3\right)\cdot n_4(x) \\ \left(\alpha^4 - 6\cdot\alpha^2\cdot\lambda^2 + \lambda^4\right)\cdot n_2(x) + \left(4\cdot\alpha^3\cdot\lambda - 4\cdot\alpha\cdot\lambda^3\right)\cdot n_3(x) \\ \left(\alpha^4 - 6\cdot\alpha^2\cdot\lambda^2 + \lambda^4\right)\cdot n_3(x) + \left(4\cdot\alpha\cdot\lambda^3 - 4\cdot\alpha^3\cdot\lambda\right)\cdot n_2(x) \\ \left(\alpha^4 - 6\cdot\alpha^2\cdot\lambda^2 + \lambda^4\right)\cdot n_4(x) + \left(4\cdot\alpha\cdot\lambda^3 - 4\cdot\alpha^3\cdot\lambda\right)\cdot n_1(x) \end{bmatrix}$$